

*Commenced Publication in 1973*

Founding and Former Series Editors:

Gerhard Goos, Juris Hartmanis, and Jan van Leeuwen

## Editorial Board

David Hutchison

*Lancaster University, UK*

Takeo Kanade

*Carnegie Mellon University, Pittsburgh, PA, USA*

Josef Kittler

*University of Surrey, Guildford, UK*

Jon M. Kleinberg

*Cornell University, Ithaca, NY, USA*

Alfred Kobsa

*University of California, Irvine, CA, USA*

Friedemann Mattern

*ETH Zurich, Switzerland*

John C. Mitchell

*Stanford University, CA, USA*

Moni Naor

*Weizmann Institute of Science, Rehovot, Israel*

Oscar Nierstrasz

*University of Bern, Switzerland*

C. Pandu Rangan

*Indian Institute of Technology, Madras, India*

Bernhard Steffen

*University of Dortmund, Germany*

Madhu Sudan

*Microsoft Research, Cambridge, MA, USA*

Demetri Terzopoulos

*University of California, Los Angeles, CA, USA*

Doug Tygar

*University of California, Berkeley, CA, USA*

Gerhard Weikum

*Max-Planck Institute of Computer Science, Saarbruecken, Germany*

Shlomi Dolev Mihai Oltean (Eds.)

# Optical Supercomputing

Second International Workshop, OSC 2009  
Bertinoro, Italy, November 18-20, 2009  
Proceedings

Volume Editors

Shlomi Dolev

Department of Computer Science, Ben Gurion University of the Negev

Beer-Sheva, Israel

E-mail: dolev@cs.bgu.ac.il

Mihai Oltean

Department of Computer Science, Babeş-Bolyai University

Cluj-Napoca, Romania

E-mail: moltean@cs.ubbcluj.ro

Library of Congress Control Number: 2009938819

CR Subject Classification (1998): F.1, B.4.3, C.5.1

LNCS Sublibrary: SL 1 – Theoretical Computer Science and General Issues

ISSN 0302-9743

ISBN-10 3-642-10441-X Springer Berlin Heidelberg New York

ISBN-13 978-3-642-10441-1 Springer Berlin Heidelberg New York

This work is subject to copyright. All rights are reserved, whether the whole or part of the material is concerned, specifically the rights of translation, reprinting, re-use of illustrations, recitation, broadcasting, reproduction on microfilms or in any other way, and storage in data banks. Duplication of this publication or parts thereof is permitted only under the provisions of the German Copyright Law of September 9, 1965, in its current version, and permission for use must always be obtained from Springer. Violations are liable to prosecution under the German Copyright Law.

springer.com

© Springer-Verlag Berlin Heidelberg 2009

Printed in Germany

Typesetting: Camera-ready by author, data conversion by Scientific Publishing Services, Chennai, India

Printed on acid-free paper SPIN: 12793952 06/3180 5 4 3 2 1 0

# Preface

OSC, the International Workshop on Optical SuperComputing, is a new annual forum for research presentations on all facets of optical computing for solving hard computation tasks. Optical computing devices have the potential to be the next computing infrastructure. Despite the frequency limitations and cross-talk phenomena, as well as soft-errors of electronic devices the natural parallelism of optical computing devices, along with the advance in fiber optics and optical switches make optical computing commercial-able. The workshop focuses on in research on the theory, design, specification, analysis, implementation, or application of optical supercomputers. Topics of interest include, but are not limited to: designs or demonstrations of optical computing devices and systems; algorithmics and complexity issues of optical computing; computation representation by photons and holograms; neural and brain inspired architectures; electro-optic devices for interacting with optical computing devices; practical implementations; analysis of existing devices and case studies; optical photonics and laser switching technologies; optical and photonic memories; optical signal processing subsystems; optical networks for high-performance computing; optical interconnections; quantum optical systems; applications and algorithms for optical devices; alpha particles, X-rays and nano-technologies for optical computing. The second OSC workshop was held during November 18–20, 2009, in Bertinoro International Center for Informatics, Bici, Italy.

This volume contains 19 contributions selected by the Program Committee. All submitted papers were read and evaluated by the Program Committee members. We are grateful to the EasyChair system in assisting the reviewing process.

OSC 2009 was organized in cooperation with SPIE and OSA. The support of Bertinoro International Center for Informatics, Ben-Gurion University and Babeş-Bolyai University are also gratefully acknowledged.

September 2009

Shlomi Dolev  
Mihai Oltean

# Organization

OSC, the International Workshop on Optical SuperComputing, is an annual forum for research presentations on all facets of optical computing. OSC 2009 was organized in cooperation with the SPIE and OSA.

## Steering Committee

H. John Caulfield	Fisk University, USA
Shlomi Dolev	Ben-Gurion University of the Negev, Israel
Yeshaiahu Fainman	University of California, San-Diego, USA
Tobias Haist	Stuttgart Universität, Germany
Mihai Oltean	Babeş-Bolyai University, Romania

## Organizing Committee

Program Chair	Shlomi Dolev, Ben-Gurion University of the Negev, Israel
---------------	--

## Program Committee

Aharon Agranat	Hebrew University, Israel
George Barbastathis	MIT, USA
Antonella Bogoni	CNIT
H. John Caulfield	Fisk University, USA
Ernesto Ciaramella	SSSUP
Cristian Calude	University of Auckland, New Zealand
Shlomi Dolev (Chair)	Ben-Gurion University, Israel
Yeshaiahu Fainman	UCSD
Dietmar Fey	Erlangen-Nuremberg University, Germany
William Green	IBM
Tobias Haist	Stuttgart Universität, Germany
Jürgen Jahns	FU Hagen, Germany
Efstratios Kehayas	NTUA
Shimon Levit	Weizmann Institute of Science, Israel
Michal Lipson	Cornell University, USA
David Miller	Stanford University, USA
Thomas Naughton	NUIM and University of Oulu, Finland
Kouichi Nitta	Kobe University, Japan
Jeremy L. Obrien	University of Bristol, UK
Mihai Oltean	Babeş-Bolyai University, Romania
Wolfgang Osten	Stuttgart Universität, Germany

VIII Organization

Haldun Ozaktas

Joseph Rosen

Yunlong Sheng

Natan T. Shaked

Joseph Shamir

Dan Tamir

Kristof Vandoorne

Damien Woods

Toyohiko Yatagai

Zeev Zalevsky

Xinliang Zhang

Bilkent University, Turkey

Ben-Gurion University, Israel

Laval University, Canada

Duke University, USA

Technion, Israel

Texas State University, USA

Universiteit Gent, Belgium

University of Seville, Spain

Utsunomiya University, Japan

Bar-Ilan University, Israel

Huazhong University, China

# Table of Contents

Invited Talk: What Can We Learn from an Image? . . . . .	1
<i>H. John Caulfield</i>	
Nanophotonics for Information Systems . . . . .	2
<i>Yeshaiahu Fainman, Kazuhiro Ikeda, and D.T.H. Tan</i>	
All-Optical Clocked Flip-Flops Exploiting SOA-Based SR Latches and Logic Gates . . . . .	5
<i>Jing Wang, Gianluca Meloni, Gianluca Berrettini, Luca Potì, and Antonella Bogoni</i>	
All-Optical Logic Gates Based on Semiconductor Optical Amplifiers and Tunable Filters . . . . .	19
<i>Xinliang Zhang, Jing Xu, Jianji Dong, and Dexiu Huang</i>	
Zero-Energy Optical Logic: Can It Be Practical? . . . . .	30
<i>H. John Caulfield</i>	
On Attributes and Limitations of Linear Optics in Computing . . . . .	37
<i>Joseph Shamir</i>	
Optical Designs for Non-deterministic Turing Machines (Extended Abstract) . . . . .	47
<i>Shlomi Dolev and Yuval Nir</i>	
Evolutionary Design of Graph-Based Structures for Optical Computing . . . . .	56
<i>Mihai Oltean and Oana Muntean</i>	
Computing a Solution for the Subset Sum Problem with a Light Based Device . . . . .	70
<i>Md. Raqibul Hasan and M. Sohel Rahman</i>	
An Optical Wavelength-Based Solution to the 3-SAT Problem . . . . .	77
<i>Sama Goliaei and Saeed Jalili</i>	
Incoherent Optical Spatial Image Processing . . . . .	86
<i>Melania Paturzo, Pietro Ferraro, Alexander Zlotnik, and Zeev Zalevsky</i>	
A Scheme for SIMD Processing in Two Dimensional Binary Images and Its Applications . . . . .	95
<i>Kowichi Nitta and Osamu Matoba</i>	

Proposal for Secure Key Distribution Using Classical Optics . . . . .	99
<i>Tobias Haist and Wolfgang Osten</i>	
Analyze the Discrete Photo-Induced Current Pulses of the Photorefractive Spatial Light Modulator . . . . .	102
<i>Xiujian Li, Xiaoguang Hou, Yongming Nie, Wenhua Hu, Jiankun Yang, and Junbo Yang</i>	
Optical Multiplexing Techniques for Photonic Clos Networks in High Performance Computing Architectures . . . . .	110
<i>Dietmar Fey, Max Schneider, Jürgen Jahns, and Hans Knuppertz</i>	
Improvement of a System for Prime Factorization Based on Optical Interferometer . . . . .	124
<i>Kouichi Nitta, Nobuto Katsuta, and Osamu Matoba</i>	
Combinatorial Optimization Using Electro-Optical Vector by Matrix Multiplication Architecture . . . . .	130
<i>Dan E. Tamir, Natan T. Shaked, Wilhelmus J. Geerts, and Shlomi Dolev</i>	
Dynamic Optical Circuit Switching Applied to Storage Area Networks . . . . .	144
<i>Aharon J. Agranat, Noam Sapiens, and Larry Rudolph</i>	
Optical Correlator for Star Identification and Tracking . . . . .	145
<i>Jia Hui, Yang Jiankun, Li Xiujian, Hu Wenhua, Yang Juncai, Fan Qingchun, and Hao Yuncai</i>	
<b>Author Index . . . . .</b>	<b>155</b>



# Invited Talk: What Can We Learn from an Image?

H. John Caulfield

Fisk University  
1000 17th Ave., N.  
Nashville, TN 37308  
hjc@fisk.edu

**Abstract.** Depending on the task, there are huge differences in the difficulties of parallel image processing. The recipe we apply to many images is as follows. Use Artificial Color to either recognize the target or recognize and remove the background, we then use edge-preserving smoothing on the resulting image, use our "nonlinear discrimination Fourier processing method" to identify and locate the target in the scene, and finally, use the subset that found the target to provide a prototype that suggests the targets' pose and scale. In this paper, I will illustrate each step.

# Nanophotonics for Information Systems

Yeshaiahu Fainman, Kazuhiro Ikeda, and D.T.H. Tan

Dept. of Electrical and Computer Engineering, University of California, San Diego  
9500 Gilman Drive, La Jolla, California, 92093-0407  
fainman@ece.ucsd.edu

**Abstract.** The field of photonics finds applications in information technology, health care, lighting, and sensing. This paper explores the role of nanotechnology with focus on nanophotonics in dielectric and inhomogeneous metamaterials for optical communications, information and signal processing in data centers.

**Keywords:** Information optics, nanophotonics, metamaterials, optoelectronics.

## 1 Introduction

Optics has the potential to solve some of the most exciting problems in computing hardware. It promises crosstalk-free interconnects with essentially unlimited bandwidth, long-distance data transmission without skew and without power- and time-consuming regeneration, miniaturization, parallelism, and efficient implementation of important algorithms such as Fourier transforms. Numerous information processing systems and concepts in space and time have been studied during the past decades. Yet, optical computing and processing in space and time has so far failed to move out of the lab. The free-space and guided-wave devices are costly, bulky, and fragile in their alignment. They are also difficult to integrate with electronic systems, both in terms of the fabrication process and in terms of delivery and retrieval of the massive volumes of data the optical elements can process. Our most recent work emphasizes the construction of optical subsystems directly on-chip, with the same lithographic tools as the surrounding electronics. This has been made possible by the advances in these tools, which can now create features significantly smaller than the optical wavelength; experts predict lithographic resolution as fine as 16nm by year 2020. Arranged in a regular pattern, subwavelength features act as a metamaterial whose optical properties are controlled by the density and geometry of the pattern and its constituents [1-5]. Lenses, polarizers, chromatic dispersers, diffraction gratings, and other optical processing devices can now be implemented on-chip using metamaterials wherever natural materials with similar properties either do not exist, or (more frequently) would not be compatible with lithographic fabrication.

## 2 Nanophotonics Process

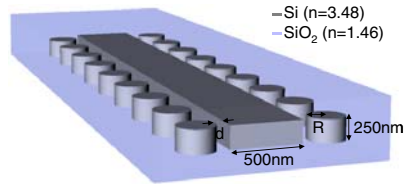
To advance this technology, investigations of nanostructures and their interaction with electromagnetic field are critical. Engineers also need appropriate modeling and

design tools, new fabrication recipes, and test instruments capable of characterizing on-chip components. The design of integrated photonic systems is a challenging task as it not only involves the accurate solution of electromagnetic equations, but also the need to incorporate the material and quantum physics equations to enable the investigation and analysis of near field interactions. These studies need to be integrated with device fabrication and characterization to verify device concepts and optimize device designs. In this talk, we discuss some of the CMOS-compatible Silicon-on-insulator metamaterials and devices recently demonstrated in our lab. These include graded-index lenses, birefringent elements that utilize a combination of geometry and material properties to separate light into orthogonal polarizations, frequency-selective resonators and Bragg gratings, and metal-dielectric nanostructures that can achieve extremely tight field confinement. Characterization tools, including our Heterodyne Near Field Optical Microscope, will also be discussed. This microscope uses a fiber probe tapered to 200nm diameter and brought close enough to the nanostructure under test to pick up its evanescent electromagnetic fields. Subsequent heterodyne detection permits simultaneous measurement of both amplitude and phase of the evanescent fields, while also providing an amplification to boost the weak signal. The mapping of evanescent fields has proven to be a powerful aid in understanding the performance of nano-optical elements.

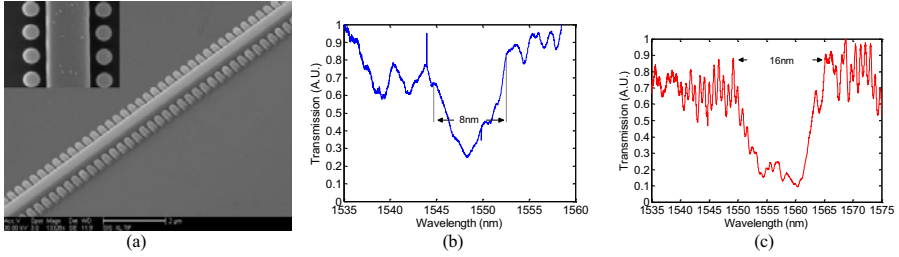
### 3 Example: Cladding-Modulated Resonant Quantum Wires

Bragg structures are fundamental in implementing various optical devices for switching, wavelength division multiplexing (WDM) and sensing applications. We have previously demonstrated on-chip sidewall modulated Bragg grating (SMBG) realized using single-step lithography [6]. The strength of the coupling coefficient in SMBG is determined by the modulation amplitude which in turn is limited by the resolution of electron beams used to pattern these structures. Narrow bandwidth WDM components require Bragg gratings which have weak coupling coefficients and which can be easily controlled. To address these issues, we introduce a novel cladding-modulated Bragg grating (CMBG) implemented with silicon on insulator (SOI) material platform. The proposed CMBG is shown to overcome the limitations inherent to SMBG in fabricating devices that require high resolution, wide dynamic range and high precision control of the coupling strength.

Our CMBG consists of a single mode waveguide at 1.55 $\mu\text{m}$  with the Bragg effect arising from placements of silicon cylinders with period,  $A_B$  a distance,  $d$  away from the silicon waveguide (see Fig. 1). The cylinder radius,  $R$  is chosen to be 100nm to avoid supporting any resonant modes. Since the field amplitude of the propagating mode decays exponentially outside the waveguide boundaries, the extent of the evanescent tails residing in the silicon cylinders and hence the strength of mode coupling



**Fig. 1.** CMBG schematic. Waveguide radius,  $R=100\text{nm}$ .



**Fig. 2.** (a) SEM Micrographs of fabricated devices. Measured transmission spectra of (b) device A ( $L=100\mu\text{m}$ ,  $d=200\text{nm}$ ) and (c) device B ( $L=70\mu\text{m}$ ,  $d=50\text{nm}$ ).

can be varied by adjusting the distance  $d$ . We first calculate the CMBG coupling coefficient,  $\kappa$  of the CMBG as a function of  $d$  using coupled mode theory (CMT).

The device is fabricated using electron-beam lithography followed by reactive ion etching and plasma enhanced chemical vapor deposition of the  $\text{SiO}_2$  overcladding. The spectral response of two fabricated devices (A & B) measured using an optical spectrum analyzer is shown in Fig. 2. Even though the length of the device B was  $L=70\mu\text{m}$ , the value of  $\kappa.L \gg \pi$  indicating that  $\kappa$  is the dominant in contributing to  $\Delta\lambda$ . The values of  $\Delta\lambda$  measured for devices A and B are 8nm and 16nm respectively, close to the expected values of 7nm and 13nm respectively from our 2D FDTD results.

## 4 Conclusion

It is evident that nanophotonics and metamaterials are important technologies for future information processing systems. The research exploiting near field optical phenomena will be key in achieving new functionalities in materials properties (birefringence, dispersion, nonlinearities) as well as unique device functionalities such as adaptation, generation, modulation, transport and detection of light.

**Acknowledgments.** This work was supported by the NSF, DARPA, and the NSF CIAN ERC.

## References

- [1] Richter, I., Sun, P.C., Xu, F., Fainman, Y.: Appl. Opt., 34, 2421–2429 (1995)
- [2] Tyan, R., Sun, P.C., Scherer, A., Fainman, Y.: Opt. Lett. 21, 761–763 (1996)
- [3] Nakagawa, W., Sun, P.C., Chen, C.H., Fainman, Y.: Optics Letters 27, 191–193 (2002)
- [4] Levy, U., Tsai, C.H., Pang, L., Fainman, Y.: Opt. Lett. 29, 1718–1720 (2004)
- [5] Rokitski, R., Tetz, K., Fainman, Y.: PRL 95(17), 177401–1–4 (2005)
- [6] Ikeda, K., Nezhad, M., Fainman, Y.: 92, 20, 201111 (2008)

# All-Optical Clocked Flip-Flops Exploiting SOA-Based SR Latches and Logic Gates

Jing Wang<sup>1</sup>, Gianluca Meloni<sup>2</sup>, Gianluca Berrettini<sup>3</sup>, Luca Potì<sup>2</sup>,  
and Antonella Bogoni<sup>2</sup>

<sup>1</sup> Department of Electronic Engineering, Tsinghua University, Beijing, 100084, China  
jwang1983@gmail.com

<sup>2</sup> National Laboratory of Photonic Networks, CNIT, via Moruzzi 1, Pisa, 56124, Italy

<sup>3</sup> Scuola Superiore Sant'Anna-CEIICP, via Moruzzi 1, Pisa, 56124, Italy

**Abstract.** All-optical flip-flops are key components of photonic digital processing in next generation optical network and computing. In most digital applications, signal synchronization with a reference clock is a basic feature. In this paper, an entire set of all-optical clocked flip-flops, including SR, D, T, and JK types is proposed and demonstrated, each employing a single SR latch and optical logic gates previously introduced in literature. The bi-stable element is based on gain quenching mechanism between SOAs of two coupled fiber ring lasers. Three logic gates are carried out by exploiting four wave mixing (FWM) and cross gain modulation (XGM) nonlinear effects in SOA. Different flip-flop functionalities are obtained by adding one of the logic gates, or a combination of them, to the latch scheme. Performance evaluation in terms of extinction ratio demonstrates the effectiveness of proposed schemes. Speed limitation of flip-flop operation is also investigated and photonic integration is identified as a feasible solution to increase the operation speed beyond GHz.

**Keywords:** optical flip-flop, optical logic gate, optical signal processing, semiconductor optical amplifier (SOA).

## 1 Introduction

In order to meet the ever-increasing demand of data communication for future optical networks, high-speed digital processing is required. Photonics signal elaboration at the optical layer is attractive to perform various computational functionalities as packet buffering, bit-length conversions, header processing, switching, retiming, re-shaping, and time-division multi/demultiplexing. In recent years a lot of effort has been spent in these fields and all-optical digital processing seems to be one of the most promising technologies to bring increased capacity, flexibility, and scalability to the next generation systems in the optical domain.

Due to their great potential in optical computation, several all-optical digital devices have been proposed as building elements for more complex subsystems, including optical threshold function [1], logic gates [2-5], optical buffer [6], flip-flops [1, 7] and shift register [8]. In particular, optical flip-flop has attracted special interest since it can work as a finite state machine in an optical computer. Moreover, it serves as a

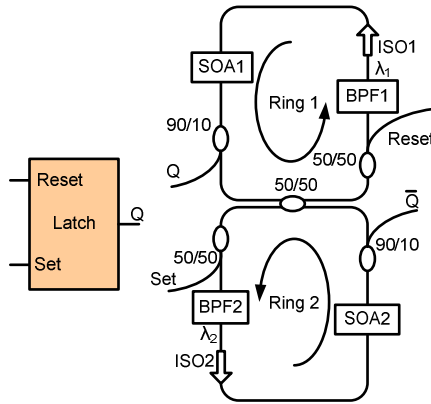
key component in optical packet switching networks, in which the routing, the buffering, and the forwarding of optical packets are all carried out in the optical domain, bringing together the wide fiber bandwidth and the high routers forwarding capacity [1, 9]. By now, several schemes of all-optical flip-flops have been demonstrated, including coupled fiber ring lasers [1], coupled laser diodes [10-11], nonlinear polarization switches [12], and coupled Mach-Zehnder interferometers [7].

However, in these proposed scenarios, the optical flip-flops work in asynchronous way since the outputs states are controlled by set/reset signals without any clock input. These kinds of flip-flops are also referred as optical set-reset (SR) latches. In optical computing, one of the most significant features is the signal synchronization, in which all operations are triggered by clock signal. In addition, in several applications a clocked optical flip-flop can also take memory of the past input signals and process them with current inputs. To the best of our knowledge, there are no works in literature about clocked all-optical flip-flops.

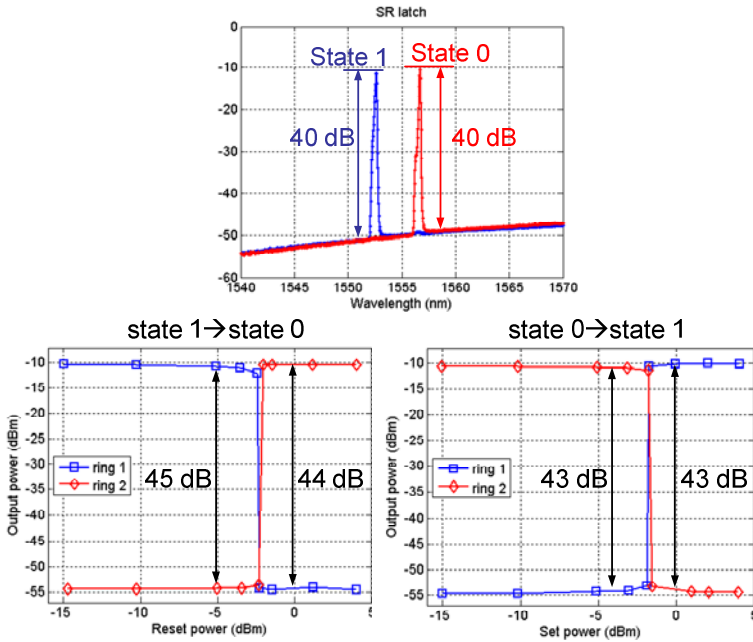
In this paper, clocked all-optical SR, D, T, and JK type flip-flops, whose state switching is triggered by a pulsed clock, are proposed and demonstrated. The core component of all presented flip-flops is a bi-stable SR latch proposed in [1], which is based on two coupled fiber ring lasers exploiting a semiconductor optical amplifier (SOA) as active element. The use of three different logic gates (or a combination of them) enables us to carry out SR, D, T, and JK type flip-flop functionalities.  $A \cap B$ ,  $A \cap \bar{B}$ , and  $A \cap B \cap \bar{C}$  logic functions between input clock and control signals are carried out by exploiting four wave mixing (FWM) and cross gain modulation (XGM) nonlinear effects in SOA. All flip-flop configurations are suitable for photonic integration and due to the broad bandwidth of SOA, the input signals can be tuned in the whole C-band. The effectiveness of proposed schemes is demonstrated by performance evaluation in terms of extinction ratio. The limitation of the flip-flop switching time is also investigated, identifying photonic integration as a feasible solution to increase the flip-flop speed beyond GHz. This paper is organized as follows. In section 2 the core elements of clocked flip-flops, including the SOA based SR latch and optical AND logic gates will be introduced; in section 3 SR, D, T and JK types of clocked flip-flops will be proposed and demonstrated, and we conclude with a discussion about speed limitation of flip-flop operation.

## 2 SOA Based SR Latch and Optical AND Logic Gates

All flip-flop configurations described in the follow are based on an all-optical SR latch [1] shown in Fig.1. It consists of two SOA-based ring lasers. The two fiber cavities, coupled together by an optical coupler, are operating at  $\lambda_1$  and  $\lambda_2$  respectively. The SR latch has two output states defined by the lasing of only one ring. In “state 1”, only ring 1 is lasing whereas ring 2 is suppressed. The output light of SOA 1 is coupled into ring 2, depleting the carriers of SOA 2 and suppressing the ring 2 lasing. The ring 1 outputs a CW light at  $\lambda_1$  ( $Q = 1$ ) and ring 2 outputs a low optical power of ASE noise ( $\bar{Q} = 0$ ). Similarly, only ring 2 is lasing in “state 0”. In this case, the output light of SOA 2, coupled into ring 1, depletes the carriers of SOA 1 and suppresses ring 1. The ring 2 outputs a CW light at  $\lambda_2$  ( $\bar{Q} = 1$ ), and ring 1 outputs low power ASE noise ( $Q = 0$ ).



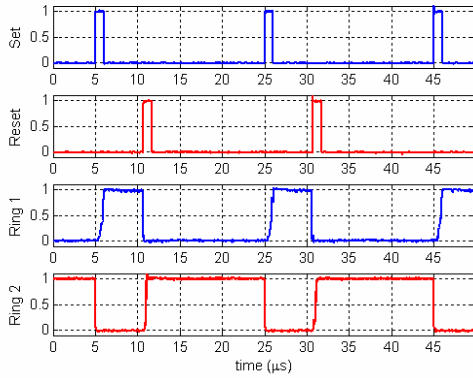
**Fig. 1.** All-optical SR latch. SOA: semiconductor optical amplifier; BPF: band pass filter; ISO: isolator.



**Fig. 2.** Optical spectra of two latch states (top) and the output power of two ring lasers with set/reset powers (bottom)

Set and reset control signals are injected into the two fiber ring lasers in order to change the latch state. The insertion of optical power with a wavelength different by  $\lambda_1$  and  $\lambda_2$  into the dominant ring, switches off its lasing. Subsequently, the lasing in the other ring is switched on. In Fig.2, the output optical spectra of both the latch states are reported. An extinction ratio for each state of 40 dB is measured. In addition, the

output power of both ring lasers is plotted as a function of the set/reset optical power. An on-off ratio more than 40 dB is evaluated for each state, in agreement with the value measured by the optical spectra. By injecting set and reset pulses into the two rings alternatively, SR latch dynamic state toggling operation is demonstrated. Experimental results using signals with 50 KHz repetition rate are shown in Fig.3. By simply tuning the cavities optical filter it is possible to change the latch output wavelengths in whole SOA band (1530-1565-nm). Since the optical output of proposed flip-flops are defined by the SR latch state and is almost independent by other parts of the scheme, their performances can be evaluated by considering the extinction ratio measurements reported in Fig. 2. In order to implement different types of clocked flip-flops, three all-optical AND logic gates are included in the experimental setups.



**Fig. 3.** State toggling operation at a repetition rate of 50 kHz

$A \cap B$ ,  $A \cap \bar{B}$ , and  $A \cap B \cap \bar{C}$  logic functions are carried out by exploiting FWM and XGM nonlinear effects in SOA. The effectiveness of these optical logic gates was previously demonstrated in [2], showing a power penalty lower than 0.5 dB. In proposed schemes, the outputs of these logic gates are used as the control signals of SR latches and do not affect the flip-flop output performance significantly. For each logic gate, there is only one semiconductor device used, reducing cost and complexity of the schemes. In our applications, A is used as an input clock pulse, whereas B and C are external control signals.

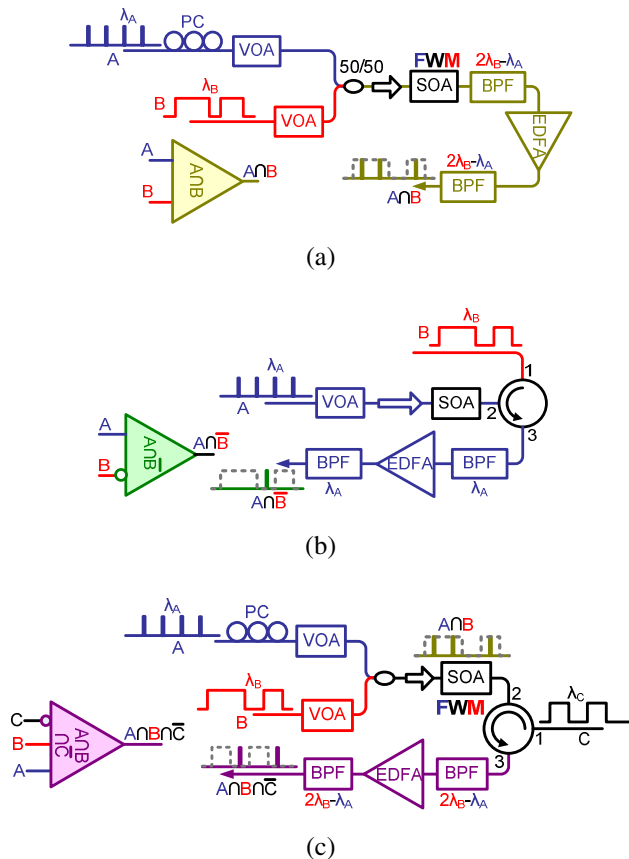
The experimental setup of the  $A \cap B$  gate is shown in Fig. 4 (a). The logic function is performed by filtering out the FWM signal ( $\lambda_{\text{FWM}}=2\lambda_B-\lambda_A$ ) between A and B. When a clock pulse A comes and the control signal B=1, a pulse at  $\lambda_{\text{FWM}}$  is generated. If B=0, there is no FWM generation, and no pulse is present at the gate output. The truth table of  $A \cap B$  gate is shown in Table 1. Variable optical attenuators (VOA) and polarization controllers (PC) are used to adjust the input optical power and the polarization state, in order to maximize the FWM efficiency in SOA. However, the polarization dependence of this  $A \cap B$  gate can also be eliminated by polarization diversity technique.

The experimental setup of  $A \cap \bar{B}$  gate is shown in Fig. 4 (b). The logic function is carried out between clock pulse A and inverted control signal B by exploiting XGM



in SOA. When  $B=1$  the carriers of SOA are depleted, so the input clock  $A$  can not be amplified. On the contrary, if  $B=0$ , signal  $A$  passes through the gate with amplification. In Table 1 the truth table of  $A \cap B$  gate is also reported.

Finally, the setup of  $A \cap B \cap \bar{C}$  gate is shown in Fig. 4 (c). The logic function is carried out between the clock  $A$ , control signal  $B$  and inverted control signal  $C$ . The proposed gate can be considered as a combination of nonlinear effects described previously. In particular,  $A \cap B$  is carried out by exploiting FWM between  $A$  and  $B$ , whereas XGM is exploited to include the AND function with the inverted  $C$ . If  $B=0$  there is no FWM generated between  $A$  and  $B$ , and the gate output is 0. In case of  $B=1$  and  $C=1$ , the FWM component generated between  $A$  and  $B$  is strongly suppressed by the saturation effect of SOA, and the gate only outputs low power ASE noise. Only when  $B=1$  and  $C=0$ , FWM is filtered out at the gate output with amplification. The truth table of  $A \cap B \cap \bar{C}$  gate is also shown in Table 1.



**Fig. 4.** SOA-based optical logic gates; (a)  $A \cap B$  gate; (b)  $A \cap \bar{B}$  gate; (c)  $A \cap B \cap \bar{C}$  gate; SOA: semiconductor optical amplifier; BPF: band pass filter; VOA: variable optical attenuator; PC: polarization controller; EDFA: erbium doped fiber amplifier

**Table 1.** Truth tables of  $A \cap B$ ,  $A \cap \bar{B}$ ,  $A \cap B \cap \bar{C}$  gates

$A \cap B$ (FWM)				$A \cap \bar{B}$ (XGM)			
A	B	OUT	Comment	A	B	OUT	Comment
0	0	0	no FWM	0	0	0	no input
0	1	0	no FWM	0	1	0	no input
1	0	0	no FWM	1	0	1	amplification
1	1	1	FWM	1	1	0	gain saturation

$A \cap B \cap \bar{C}$ (FWM+XGM)				
A	B	C	OUT	Comment
0	0	0	0	no FWM
0	1	0	0	no FWM
1	0	0	0	no FWM
1	1	0	1	FWM + amplification
0	0	1	0	no FWM + gain saturation
0	1	1	0	no FWM + gain saturation
1	0	1	0	no FWM + gain saturation
1	1	1	0	FWM + gain saturation

### 3 Clocked SR, D, T, and JK Flip-Flops Based on SR Latch and Logic Gates

In this section SR, D, T and JK types of all-optical clocked flip-flops are proposed and demonstrated. Each scheme exploits the aforementioned SR latch and logic gates.

#### 3.1 SR Flip-Flop

The clocked SR flip-flop setup is shown in Fig. 5 (a). It consists of two  $A \cap B$  gates and one SR latch. “AND 1” gate performs AND function between the clock signal (CLK) and set signal (S). “AND 2” gate performs AND function between the clock and reset signal (R). The outputs of “AND 1” and “AND 2” are connected to the “Set” and “Reset” ports of the latch, respectively.

The truth table of SR flip-flop is shown in Table 2. The flip-flop changes its state only when a clock pulse comes, according to the S and R values at that time, but the S and R values at any other time are ignored and the flip-flop will not change its states accordingly. Therefore the flip-flop is clocked. In particular, if  $S=R=0$  the flip-flop maintains its previous state; if  $S=1$   $R=0$ , it is set to the “state 1”; If  $S=0$   $R=1$ , the flip-flop is set to “state 0”. The condition  $S=R=1$  is forbidden for SR flip-flop since the latch is unstable. In this case, it is statistically not known which ring laser will lase.

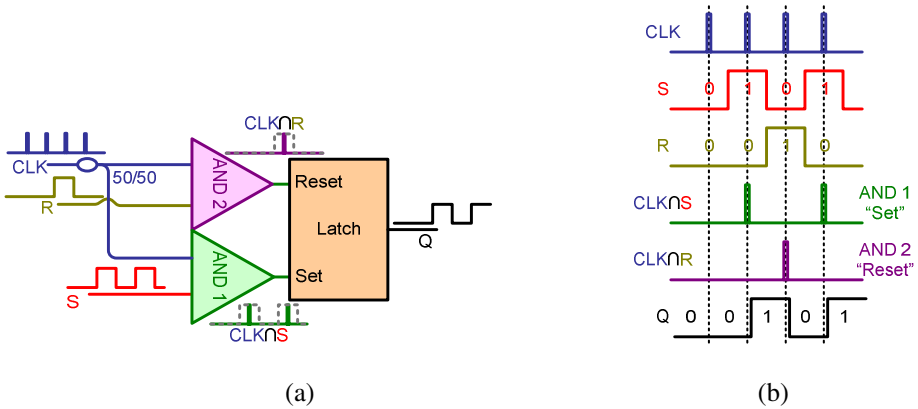


Fig. 5. Clocked SR flip-flop: (a) logic circuits; (b) working principle

Table 2. Truth table of SR flip-flop

CLK	S	R	$Q_{next}$	Comment
	0	0	Q	hold previous state
	1	0	1	Set
	0	1	0	Reset
	1	1	N/A	Forbidden
	X	X	Q	hold previous state

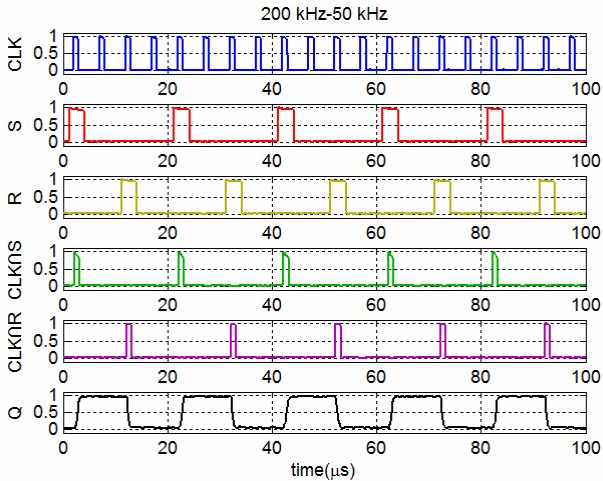


Fig. 6. Clocked all-optical SR flip-flop operation

In Fig.5 (b) the SR flip-flop working principle is reported. When a clock pulse comes in, if  $S=R=0$  there is no output coming from “AND 1” and “AND 2” gate. In this condition, neither “Set” nor “Reset” receive a pulse, so the flip-flop maintains its previous state ( $Q_{next} = Q$ ). If  $S=1 R=0$ , only “AND 1” output is high. The “Set” port receives a pulse so the flip-flop is set to “state 1” ( $Q_{next}=1$ ). Similarly, if  $S=0 R=1$ , only “Reset” port receives a pulse and the flip-flop is set to “state 0” ( $Q_{next}=0$ ). If  $S=R=1$ , both “AND 1” and “AND 2” outputs are high, getting into the forbidden condition.

All-optical clocked SR flip-flop operation is experimentally demonstrated in Fig. 6. The clock pulse has a repetition rate of 200 kHz with a pulse-width of 1  $\mu$ s. S and R have a pulse-width of 3  $\mu$ s with a repetition rate of 50 kHz, opportunely synchronized with the clock. The different repetition rates and pulse-widths of clock and control signals are intentionally used to obtain all possible logical input combinations. Good agreement between experimental results and Fig. 5 (b) can be observed.

### 3.2 D Flip-Flop

The setup of clocked D flip-flop is reported in Fig.7 (a). “AND 1” gate performs the AND function between the clock and input signal D; whereas “AND 2”, an  $A \cap \bar{B}$  gate, carries out AND function between the clock and inverted D.

The truth table of D flip-flop is shown in Table 3. The flip-flop synchronous operation is verified since it only responds to D values when a clock pulse comes, but ignores D at any other time. If  $D=0$ , the flip-flop is set to “state 0”; otherwise set to “state 1”.

The working principle of D flip-flop is shown in Fig.7 (b). If  $D=1$  “AND 1” gate and “AND 2” gate output high level and low level respectively.

So only the “Set” port receives a pulse and the flip-flop is set to “state 1”. On the contrary, if  $D=0$  the flip flop is set to “state 0”. Clocked D type flip-flop operation is experimentally demonstrated in Fig. 8.

The clock pulse has a repetition rate of 60 kHz and pulse-width of 1  $\mu$ s, while the input signal D has a repetition rate of 100 kHz with pulse-width of 6  $\mu$ s. In this case, a good agreement can also be obtained between experimental results and Fig. 7 (b).

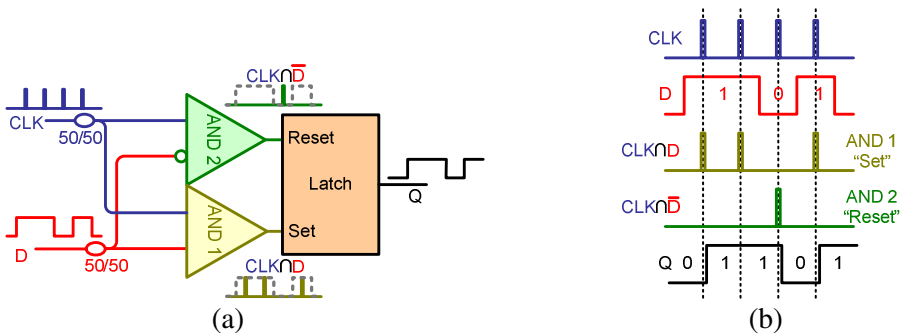



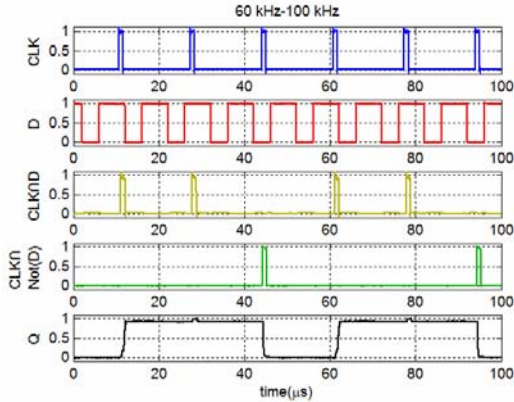


Fig. 7. Clocked D flip-flop; (a) logic circuits; (b) working principle

**Table 3.** Truth table of D flip-flop




CLK	D	$Q_{next}$	Comment
	0	0	Reset
	1	1	Set
	X	Q	hold previous state

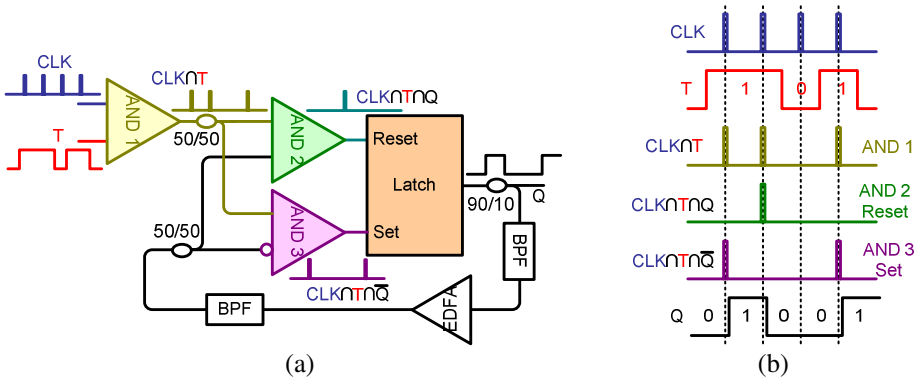
**Fig. 8.** Clocked D flip-flop operation

### 3.3 T Flip-Flop

The truth table of T flip-flop is shown in Table 4. The flip-flop also works in a synchronous way, only responding to the T values when a clock pulse comes. In particular, if  $T=0$  the flip-flop holds its previous state, whereas if  $T=1$  the flip-flop toggles its state. For this behavior it is referred as toggling (T) flip-flop. The experimental setup is shown in Fig. 9 (a), consisting of three logic gates and one SR latch. Unlike previously described SR and D flip-flops, the next state of T flip-flop ( $Q_{next}$ ) is not only determined by external control signals, but also depends on the previous state due to the toggling property. For this reason, a feedback of the output  $Q$  is used in Fig. 9 (a). “AND 1” gate carried out AND function between the clock and T signal, whereas “AND 2” performs AND function between the output of “AND 1” ( $CLK \cap T$ ) and the feedback  $Q$ . The other logic gate, “AND 3”, performs AND function between  $CLK \cap T$  and inverted  $Q$ .

**Table 4.** Truth table of T flip-flop

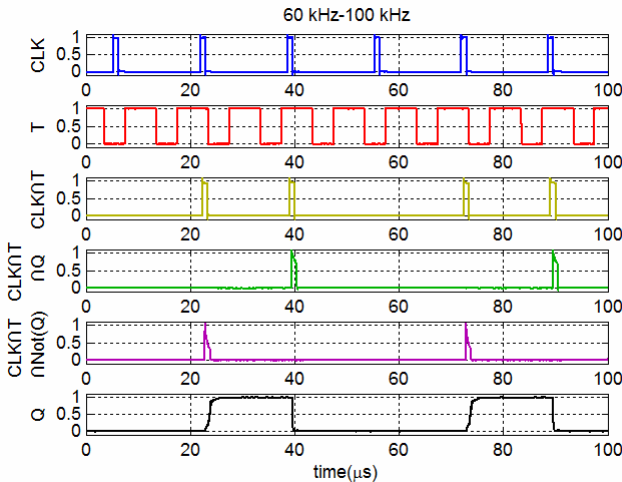
CLK	T	$Q_{next}$	Comment
	0	$\overline{Q}$	hold previous state
	1	$\overline{Q}$	toggle
	X	Q	hold previous state



**Fig. 9.** Clocked T flip-flop; (a) logic circuits; (b) working principle

The working principle of T flip-flop is shown in Fig.9 (b). When a clock pulse comes, if  $T=0$  there is no FWM signal at the output of “AND 1”. In this condition both “AND 2” and “AND 3” have at least one input at low level, and independently to the Q value “AND 2” and “AND 3” has no output, so the latch holds its previous state. On the other hand, if  $T=1$  FWM signal between T and clock is filtered out at “AND 1” output, and two different cases should be considered. If  $Q=1$  “AND 2” output is at high level and “AND 3” output is at low level. In this way the “Reset” port receives a pulse and the flip-flop toggles its state to “state 0”. In the other case, if  $Q=0$  only the “Set” port receives a pulse from “AND 3” and the flip-flop toggles its state to “state 1”.

The clocked T flip-flop operation is demonstrated in Fig.10. The clock pulse has a repetition rate of 60 kHz with a pulse-width of 1  $\mu\text{s}$ , whereas the signal T has a repetition rate of 100 kHz and a pulse-width of 6  $\mu\text{s}$ . Oscilloscope traces shown a good agreement with Fig. 9 (b).



**Fig. 10.** Clocked T flip-flop operation

### 3.4 JK Flip-Flop

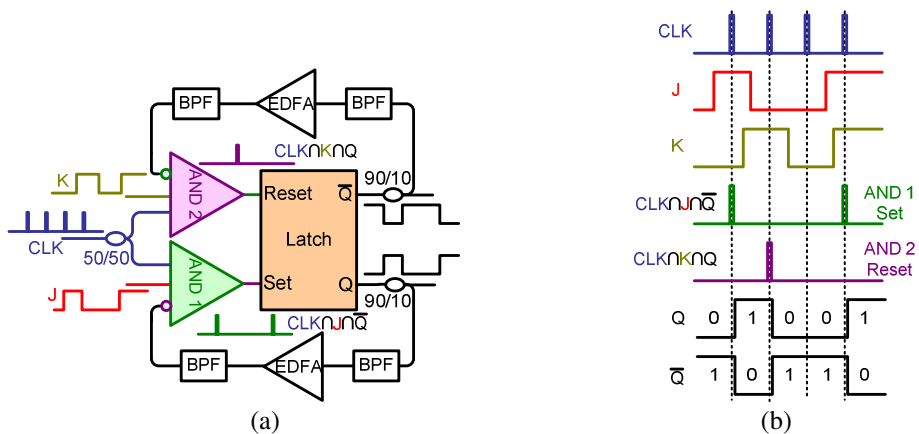
The JK flip-flop truth table is shown in Table 5. This flip-flop can be considered as a combination of the previously described SR flip-flop and T flip-flop. In cases of  $J=K=0$ ,  $J=1$   $K=0$ , and  $J=0$   $K=1$ , the JK flip-flop works as an SR flip-flop, where J and K signals are used as “Set” and “Reset” signals. However, unlike the SR flip-flop, the condition of  $J=K=1$  is not forbidden and under this condition the flip-flop toggle its state like a T flip-flop.

The setup of the JK flip-flop is reported in Fig. 11 (a). It consists of two logic gates and one SR latch. The two complementary outputs of two fiber ring lasers in SR latch are used as Q and  $\bar{Q}$  respectively. “AND 1” gate performs AND function between the clock, J, and inverted Q; whereas “AND 2” gate performs AND function between the clock, K, and Q. The functions of  $CLK \cap J$  and  $CLK \cap K$  are carried out in two AND gates respectively, but the feedback of Q is also taken into account like a T flip-flop.

The working principle of the JK flip-flop is shown in Fig. 11 (b). In case of  $J=K=0$  FWM signal is not generated neither in “AND 1” nor in “AND 2”, so both “Set” and “Reset” ports receive no pulse. The flip-flop holds its previous state. If  $J=1$   $K=0$  “AND 2” output is at low level, while “AND 1” output depends on the Q value at that time. If  $Q=1$  “AND 1” outputs low level and the flip-flop holds its state. On the other hand, if  $Q=0$  “AND 1” outputs high level and the flip-flop is set to “state 1”. Therefore, the final state of the flip-flop is “state 1” in both cases.

**Table 5.** Truth table of JK flip-flop

CLK	J	K	$Q_{next}$	Comment
	0	0	Q	hold previous state
	1	0	1	set
	0	1	0	reset
	1	1	$\bar{Q}$	toggle
	X	X	Q	hold previous state



**Fig. 11.** Clocked JK flip-flop; (a) logic circuits; (b) working principle

In the same way, if  $J=0$   $K=1$  the final state of the flip-flop is “state 0”. Finally, for  $J=K=1$  it is also necessary to consider the two cases of  $Q$  value. If  $Q=1$  only “AND 2” gate generates FWM signal and the flip-flop is set to “state 0” ( $Q_{\text{next}}=0$ ). On the contrary, if  $Q=0$  the flip-flop is set to “state 1” ( $Q_{\text{next}}=1$ ). In both cases the flip-flop toggles its state.

The JK flip-flop experimental results are shown in Fig.12. The clock pulse has a repetition rate of 200 kHz and a pulse-width of 1  $\mu\text{s}$ . In order to realize all the possible input combinations according to Table 5,  $J$  and  $K$  have a particular stream, with a repetition rate of 100 kHz and a pulse-width of 3  $\mu\text{s}$ . Experimental results have a good agreement with Fig. 11 (b).

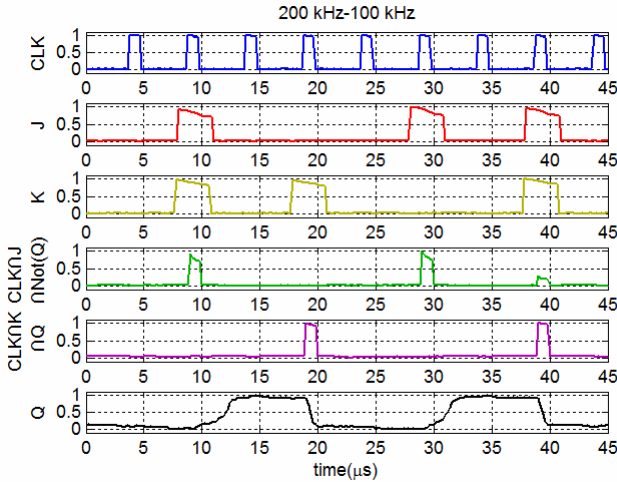


Fig. 12. Clocked JK flip-flop operation

### 3.5 Speed Limitation of Clocked Flip-Flops

In the experimental implementation, the flip-flop operation speed of clocked SR, D, T, and JK type flip-flops are all limited to hundreds of KHz. Since  $A\cap B$ ,  $A\cap\bar{B}$ , and  $A\cap B\cap\bar{C}$  logic gates are based on very fast nonlinear effects in SOAs, the flip-flop operation speed is mainly limited by the state-switching time of the SR latch. Since the SR latch is based on gain quenching effect between the two fiber ring lasers, the state-switching time consists of two parts: the switching-off time (fall time) of formerly lasing ring and the switching-on time (rise time) of formerly suppressed ring. As shown in Fig.13, it can be observed that the fall time is about 5 ns, equal to the edge time of the injected pulses, whereas the building-up process of lasing in the suppressed ring, takes place step by step, with each step corresponding to one round-trip time of the ring cavity. Therefore, the rise time depends on the ring cavity length and the number of roundtrips the light needs to circulate before reaching stable lasing condition. Due to the discrete fiber pigtailed experimental implementation, each ring laser of the SR latch has a cavity length of about 40 m, corresponding to a roundtrip time of 0.2  $\mu\text{s}$ . The building-up process takes 5-6 steps, so the rise time is  $\sim 1$   $\mu\text{s}$ .



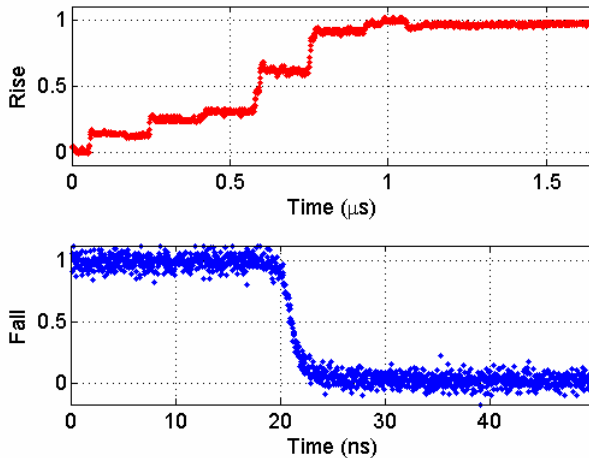


Fig. 13. Transition time of the SR latch

However, since all the proposed flip-flop setups are SOA-based, in [13] it is demonstrated that photonic integration can reduce the cavity length to millimeters. This way it is possible to reduce the rise time to less than 100 ps, thus making GHz flip-flop operation possible.

## 4 Conclusion

An entire set of all-optical clocked flip-flops including SR, D, T, and JK types is proposed. All schemes use an external clock for synchronous operations and are tunable in C-band. The core element, common for each configuration, is an already known all-optical SR latch used as a bi-stable memory element. The latch is based on two coupled ring lasers in which a SOA is employed as active element. Several logic functionalities are obtained by exploiting three different optical gates (or a combination of them) based on FWM and XGM nonlinear effects in SOAs. Clocked SR, D, T, and JK flip-flops are experimentally demonstrated. Flip-flops performances are directly related to the SR latch outputs and are almost independent by the rest of the scheme. Extinction ratios higher than 40 dB confirm the effectiveness of all proposed configurations. Flip-flops speed limitation is also investigated, pointing out in the photonic integration a feasible solution to increase the operation rate beyond GHz.

**Acknowledgments.** This work has been partially supported by the European Commission through EUROFOS, and by the Italian ministry through the POET project.

## References

1. Dorren, H.J.S., Hill, M.T., Liu, Y., Calabretta, N., Srivatsa, A., Huijskens, F.M., de Waardt, H., Khoe, G.D.: Optical packet switching and buffering by using all-optical signal processing methods. *Journal of Lightwave Technology* 21, 2–12 (2003)

2. Berrettini, G., Simi, A., Malacarne, A., Bogoni, A.: Poti: Ultrafast integrable and reconfigurable XNOR, AND, NOR, and NOT photonic logic gate. *IEEE, Photonics Technology Letters* 18, 917–919 (2006)
3. Bogoni, A., Wu, X., Fazal, I.: Willner: All-optical 160Gb/s half-addition half-subtraction and AND/OR function exploiting pump depletion and nonlinearities in a PPLN waveguide. In: 34th European Conference on Optical Communication, 2008. ECOC 2008, pp. 1–2 (2008)
4. Lee, J.H., Nagashima, T., Hasegawa, T., Ohara, S., Sugimoto, N., Kikuchi, K.: 40 Gbit/s XOR and AND gates using polarisation switching within 1 m-long bismuth oxide-based nonlinear fibre. *Electronics Letters* 41, 1074–1075 (2005)
5. Adonis, B., Pantelis, V.: Dimitris: Numerical Investigation of a 160-Gb/s Reconfigurable Photonic Logic Gate Based on Cross-Phase Modulation in Fibers. *IEEE, Photonics Technology Letters* 19, 402–404 (2007)
6. Changyong, T., Chongqing, W., Zhengyong, L.: Ning: Dual-Wavelength Packets Buffering in Dual-Loop Optical Buffer. *IEEE, Photonics Technology Letters* 20, 578–580 (2008)
7. Hill, M.T., de Waardt, H., Dorren, J.S.: Fast all optical flip-flop using coupled Mach-Zehnder interferometers. In: Technical Digest. Summaries of papers presented at the Conference on Lasers and Electro-Optics, 2001. CLEO 2001, vol. 188 (2001)
8. Zhang, S., Li, Z., Liu, Y., Geldenhuys, R., Ju, H., Lenstra, D., Khoe, G.D., Dorren, J.S.: Optical shift register based on an optical flip-flop memory with a single active element. In: 31st European Conference on Optical Communication, 2005. ECOC 2005, vol. 232, pp. 233–234 (2005)
9. Liu, Y., Tangdiongga, E., Hill, M.T., van Zantvoort, J.H.C., Smalbrugge, E., de Vries, T., Binsma, H., Oei, Y.S., Leijtens, X.J.M., Smit, M.K., Khoe, G.D., Dorren, J.S.: All-optical switching of 80 Gb/s data packets using a wavelength converter controlled by a monolithically integrated optical flip-flop. In: 31st European Conference on Optical Communication, 2005. ECOC 2005, vol. 26, pp. 27–28 (2005)
10. Kawaguchi, H.: Bistable laser diodes and their applications: state of the art. *IEEE Journal of Selected Topics in Quantum Electronics* 3, 1254–1270 (1997)
11. Hill, M.T., de Waardt, H., Khoe, G.D., Dorren, J.S.: All-optical flip-flop based on coupled laser diodes. *IEEE Journal of Quantum Electronics* 37, 405–413 (2001)
12. Liu, Y., Hill, M.T., de Waardt, H., Khoe, G.D., Lenstra, D., Dorren, J.S.: All-optical flip-flop memory based on two coupled polarisation switches. *Electronics Letters* 38, 904–906 (2002)
13. Malacarne, A., Jing, W., Yuancheng, Z., Barman, A.D., Berrettini, G., Poti, L.: Bogoni: 20 ps Transition Time All-Optical SOA-Based Flip-Flop Used for Photonic 10 Gb/s Switching Operation Without Any Bit Loss. *IEEE Journal of Selected Topics in Quantum Electronics* 14, 808–815 (2008)

# All-Optical Logic Gates Based on Semiconductor Optical Amplifiers and Tunable Filters

Xinliang Zhang, Jing Xu, Jianji Dong, and Dexiu Huang

Wuhan National Laboratory for Optoelectronics, Huazhong University of Science and Technology, Wuhan, 430074, P.R. China  
xlzhang@mail.hust.edu.cn

**Abstract.** All-optical logic gates based on semiconductor optical amplifiers (SOAs) and tunable filters are investigated in this paper. Based on single SOA and different filter detuning, five different logic gates at 40Gb/s were demonstrated and all-optical digital 2-4 encoder was also realized. All-optical generation of minterms for two input signals and three input signals are also demonstrated based on comb filters and SOAs. Advantages such as powerful function, flexible operational principle and possible integrated could help these schemes to have potential applications in optical computing and optical networks.

**Keywords:** all-optical logic gates; semiconductor optical amplifiers (SOAs); delay interferometer; bandpass filter.

## 1 Introduction

All-optical signal processing has been receiving more and more attention in past twenty years for their potential applications in high-speed optical networks and optical computing. Comparing with conventional O-E-O signal processing schemes, all-optical schemes can increase the operational speed to Tb/s and reduce the system power consumption greatly. Many different signal processing functions have been widely investigated[1-3], such as all-optical wavelength conversion, all-optical 3R regeneration, all-optical sampling, all-optical logic gates, all-optical buffer, etc. Comparatively, all-optical logic operation and all-optical buffer are two difficult problems and far away from practical applications in commercial systems. It is very urgent to find out some efficient and flexible ways to realize these two functions for next generation optical networks and optical computing.

Nonlinearities in optical fiber, periodically poled lithium niobate (PPLN)[4], Chalcogenide-based waveguide, silicon and polymer-based waveguides and semiconductor optical amplifiers (SOAs)[5-17] can all be exploited to realize all-optical logic operation function, and each scheme has its own advantages and disadvantages. SOA-based all-optical logic operation has demonstrated great potential in terms of low power consumption, small footprint, and optical integration. Furthermore, in SOAs, different nonlinearities[5-17] such as cross-gain modulation (XGM), cross-phase modulation (XPM), four-wave mixing (FWM) and some intraband ultrafast nonlinearities such as carrier heating, two-photon absorption and spectral hole burning can

all be used to realize different logic functions. Therefore, SOA-based schemes deserve to be widely and deeply investigated.

In this paper, two schemes for all-optical logic operation based on SOAs and tunable filters are presented. Based on single SOA and different filter detuning, five different logic gates at 40Gb/s were demonstrated, and based on this scheme, all-optical 2-4 encoder and comparator were also realized. Secondly, based on delay interferometer-based comb filter and SOA, all-optical generation of minterms was investigated, and based on these minterms, arbitrary logic functions could be demonstrated.

## 2 Configurable All-Optical Logic Gates Based on Single SOA and Tunable Filter

In this section, we propose and experimentally demonstrate reconfigurable all-optical logic gates based on various nonlinearities in single SOA. The operation principle of the configurable logic gates is described in Fig. 1. Data A and B are the data signals that have to be processed, whose wavelengths are  $\lambda_A$  and  $\lambda_B$ , respectively. The probe signal is a CW at wavelength  $\lambda_c$ , which will be gain- and phase-modulated by the data signals through the SOA. Thus the output optical spectrum of the probe signal will be broadened. Different logic gates can be realized at different OBF setting.

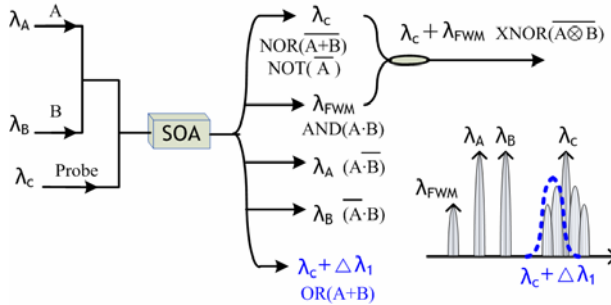
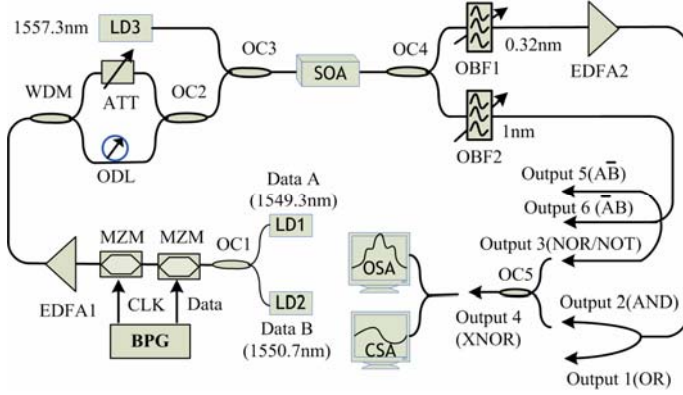


Fig. 1. Illustration of the configurable logic gates

When both data signals are present in the SOA, the conjugated light is generated due to FWM effect. It can be optically filtered out to implement AND logic. When either data A or B, or both are present, the probe signal is gain-modulated with polarity-inverted output, which is logic NOR gate. Whereas, the slow gain recovery of SOA degrades the output logic with serious pattern effects. In order to accelerate the SOA gain recovery, the blue shifted OBF with small detuning to the probe carrier is necessary. On the other hand, when the OBF is blue shifted by properly large detuning (i.e.,  $\lambda_c + \Delta\lambda_1$ ), the OBF is used to reject the probe carrier and select the blue-shifted spectrum. Either data A or B or both launched into the SOA will induce blue shifted spectrum, which fits in the OBF passband. If both data signals are absent, the OBF will block the probe carrier. Therefore the output is logic OR gate, which is

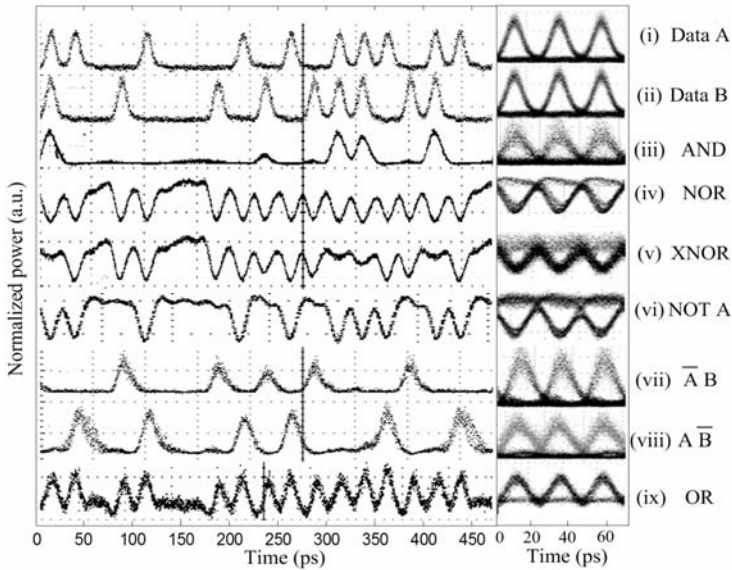


**Fig. 2.** Experimental setup of the configurable logic gates

based on the principle of SOA T-XPM. The XNOR can be obtained by coupling the AND output and NOR output with proper power equalization. The NOR logic gate can be simply changed to NOT logic, merely turning off one data signal.

The experimental setup for configurable logic gates are described in Fig. 2. The wavelengths of three CW beams generated by LD1, LD2, and LD3 are 1549.3nm ( $\lambda_A$ ), 1550.7nm ( $\lambda_B$ ), and 1557.3nm ( $\lambda_C$ ), respectively. The data signals ( $\lambda_A$  and  $\lambda_B$ ) are modulated by two Mach-Zehnder Modulators (MZMs) at 40Gb/s to form 231-1 return-to-zero (RZ) pseudo random binary sequence (PRBS) signals. The duty cycle of these RZ pulses is 33%. Two data signals will be separated by the wavelength division multiplexer (WDM) and one of them is delayed for several bits by an optical delay line (ODL), therefore, two data signals with different data pattern are obtained. The employed SOA is the same to that of Fig. 2. A tunable narrow OBF1 with 0.32nm bandwidth is used to filter the OR logic and AND logic. Another 1nm-bandwidth tunable OBF2 is used to filter the probe signal with NOR/NOT output, or filter the data A with  $\bar{A}$  output, or filter data B with  $\bar{B}$  output. Both  $\bar{A}$  and  $\bar{B}$  should be obtained with large power contrast between data A and B. EDFA2 is used to amplify the AND power, and the coupler (OC5) can combine it with NOR power to realize XNOR logic. Finally, the optical spectrum analyzer (OSA) and communication signal analyzer (CSA) are used to observe the optical spectrum and waveform of the converted signal.

The input data A and B before entering the SOA are shown in Fig. 3(i) and (ii), respectively. Both waveforms have a peak power of 2.6mW with extinction ratio (ER) over 13dB. The probe signal has a power of 0.6mW. We can see that the conjugated light appears at 1548nm at the SOA output, as shown in Fig. 4(a). The conjugated light is filtered out by OBF1 and amplified by EDFA2, then the output signal is the logic AND with good eye pattern, as shown in Fig. 3(ii). The output ER is 8.04. In fact, the input probe signal has additional function to accelerate gain recovery speed of SOA and eliminate pattern dependent distortions. When the central wavelength of OBF2 is blue-shifted by 0.1nm with respect to the probe wavelength, the output signal is NOR logic, as shown in Fig. 3(iv). The ER of NOR logic operation is 10dB. The



**Fig. 3.** Output waveforms for different logic gates, (i) and (ii) are input data signals, (iii)-(ix) are logic AND, NOR, XNOR, NOT,  $\bar{A}B$ ,  $A\bar{B}$ , and OR, respectively

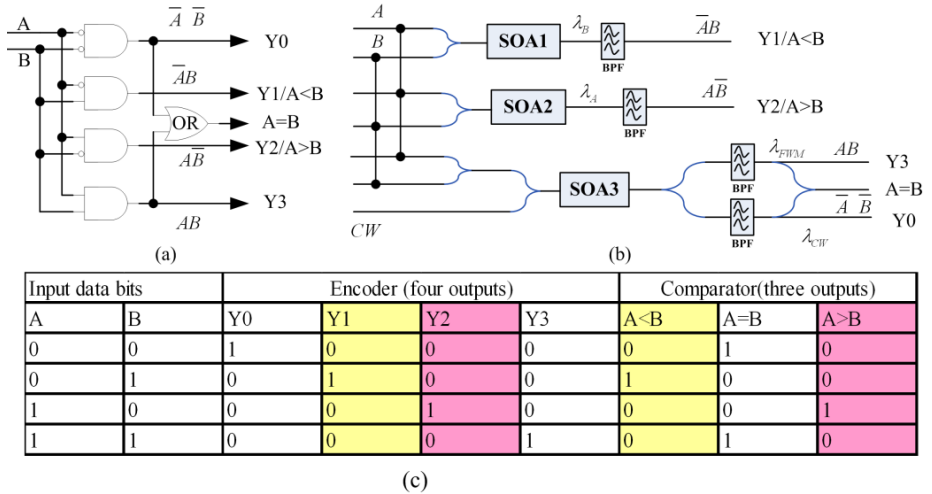
AND output has a low power level due to low conversion efficiency of FWM, while the NOR output has a high power level. With the assistance of EDFA2, the AND output and NOR output have an equal power level with peak power of 1.7mW, which are combined by optical coupler (OC5), thus the mixed signal is XNOR logic, shown in Fig. 3(v). We can observe much noise appears in level “one”, which is caused by different modulation intensity in the NOR and AND outputs. As a result, there is a small eye opening ratio with ER of 6dB. When LD2 is turned off, the NOR gate can be simply changed to the NOT gate, as shown in Fig. 3(vi). Good eye pattern can be observed and the ER reaches 11.5dB.

Based on these five logic gates, all-optical digital encoder and comparator could be demonstrated. As shown in Fig. 4(a) and Fig. 1(c), digital encoder consists of four logic outputs Y0, Y1, Y2, Y3, which are corresponding to four different input conditions. These four different outputs are achieved by four different logic gates:  $\bar{A}\cdot\bar{B}$ ,  $\bar{A}B$ ,  $A\bar{B}$  and  $AB$ , respectively. For input signal A and B with bits “00”, “01”, “10” and “11”, output bit “1” appears only at port Y0, Y1, Y2 and Y3, respectively.

For digital comparator, three logic outputs are needed to represent three results after comparing the two digital signals. When A is bit “0” and B is bit “1”, only the  $A<B$  output port is bit “1”, and this operation can be represented by  $\bar{A}B$  logic. When A and B are both bit “0” or bit “1”, only  $A=B$  output port is bit “1”, and this operation can be represented by  $A\odot B$  or XNOR logic. When A is bit “1” and B is bit “0”, only the output  $A>B$  port is bit “1”, this operation can be represented by  $A\bar{B}$  logic. From above discussions, we can find that Y1 output in digital encoder is identical

with  $A < B$  output in comparator and  $Y2$  output is identical with  $A > B$  output. In other words, all-optical digital encoder and comparator can be achieved by five different logic functions:  $\overline{A} \cdot \overline{B}$ ,  $\overline{AB}$ ,  $AB$ ,  $AB$  and  $A \odot B$ .

Fig. 4(b) shows the principle diagram of proposed scheme for all-optical digital encoder and comparator. Three SOAs are exploited in this scheme. Signal A and B are input signals with wavelength  $\lambda_A$  and  $\lambda_B$ , respectively. SOA1 is used to achieve  $\overline{AB}$  logic function at wavelength  $\lambda_B$  based on XGM effect while the optical power of signal A is much larger than signal B. Contrarily, SOA2 is used to achieve  $AB$  logic function at wavelength  $\lambda_A$  while signal B is much stronger than signal A. Signal A and B are injected into SOA3 together with a continuous wave  $\lambda_{cw}$ . FWM and XGM effects occur simultaneously in SOA3. Based on XGM effect, we can get NOR logic at wavelength  $\lambda_{cw}$ . On the other hand, we can achieve logic AND at the new generated channel based on FWM effect while the optical power of two data signals is nearly equal. Based on the output AND and NOR gates, we can get the XNOR gate by coupling the two outputs together with proper power equalization. Therefore, we can obtain five different logic gates based on XGM or FWM effects in three SOAs, which can be exploited to achieve all-optical digital encoder and comparator simultaneously.



**Fig. 4.** Concept and operation principle of digital encoder and comparator, (a) digital gate-level diagram of encoder/comparator; (b) optical implementation of encoder/comparator; (c) logical truth table for the encoder/comparator

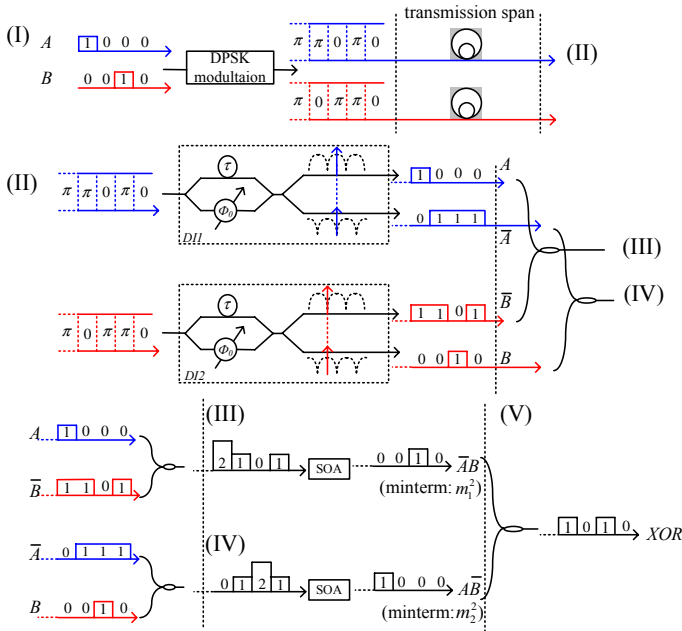
### 3 All-Optical Minterms Generation Based on Delay Interferometer and SOAs

In this section, a general scheme for reconfigurable logic gates for multi-input DPSK signals with integration possibility is proposed. Benefiting from the optical logic minterms developed by two kinds of optical devices, i.e., optical delay interferometers

and semiconductor optical amplifiers (SOAs), target logic functions can be realized by combining specific minterms together. The scheme is reconfigured by changing the phase control of the delay interferometers or the input wavelengths.

In our scheme, delay interferometers (DI) and semiconductor optical amplifiers (SOA) are used to develop NOT gates and NOR gates, respectively. A DI is a Mach-Zehnder interferometer which has a differential delay  $\tau$  in one arm and a tunable phase controller  $\Phi_0$  in the other, as shown in Fig. 5.  $\tau$  must equal the bit interval of the given bitrate in order to correctly demodulate DPSK signals while  $\Phi_0$  must be tunable to ensure accurate demodulation.

In order to explain the operation principle of the scheme, the logic evolutions of DPSK signals through the entire system is briefly described, as shown in Fig. 5. In the first stage (I), two DPSK signals are generated from two absolute binary data A and B respectively. The coding rule is assumed that ‘1’ is encoded as no phase shift between adjacent bits while ‘0’ is encoded as  $\pi$  shift. After transmission, as shown in the second stage (II), DIs are used to demodulate DPSK signals and recover the original binary data (i.e., A or B in this case). Note that either the original data or its inversion can be obtained at a certain output of the DI, depending on whether the interference at that port is constructive or destructive. This can be seen from the frequency domain by checking whether the signal wavelength is located on the transmission peak or notch of the spectrum of the concerned output. If the signal wavelength is located on the transmission notch, the spectrum will features as two main peaks with a noticeable notch at its central



**Fig. 5.** Logic evolution of two DPSK signals in the generation of optical logic gates from optical minterms based on DIs and SOAs



wavelength. On the other hand, only one main peaks is observed. Based on the illustrated locations of the signal wavelengths on the transmission spectra of the DI (as shown in the dashed box in Fig. 5), A (original data) shows up in the upper output port of DI1 and  $\bar{A}$  (inverted data) in the lower output. Oppositely, B is obtained in the lower output of DI2 and  $\bar{B}$  in the upper output. In fact, DIs offer a large degree of flexibility of the scheme besides carrying out NOT operation, as will be shown later.

The demodulated signals are combined by optical couplers before launching into the SOAs. It is well known that the cross-gain modulation (XGM) of SOA can be used to carry out NOR operation of nonreturn-to-zero (NRZ) OOK signals. Fig. 6 shows the output probe ( $\lambda_2$ ) power of the SOA versus the input pump ( $\lambda_1$ ) power. Due to the gain-saturation characteristics of the SOA, the CW probe light will be switched off at the output of the SOA if the input signal power is larger than  $P_{in, H}$ , corresponding to '0' in the output. On the other hand, CW probe light is switched on at the output of the SOA if the input pump power is smaller than  $P_{in, L}$ , corresponding to '1' in the output. For input power between  $P_{in, L}$  and  $P_{in, H}$ , error logic results will occur. Note that SOA can carry out multi-input NOR operation as well. This is because when one tributary is at ON-state, no matter what states other tributaries are, the total input power during that bit period will exceed  $P_{in, H}$  and saturate the gain of the SOA to generate '0' at the output. The case that the input DPSK signals are return-to-zero (RZ) format needs to be mentioned. Although the logic integrity is kept, the NOR logic results given by the SOAs will be in dark-RZ pulses due to the characteristics of XGM. To avoid this, other kinds of NOR gates that can process RZ signals can be utilized instead, such as logic gates based on SOAs and optical filtering. In the third stage (III), an SOA carries out NOR operation of data A and  $\bar{B}$ , creating logic result  $\overline{AB}$ . Similarly, the other SOA generates  $\overline{A\bar{B}}$  by executing NOR operation of  $\bar{A}$  and B in stage (IV). In stage (V), final logic  $\overline{AB} + \overline{A\bar{B}}$  is derived by combining the output of stage (III) and (IV) through an optical coupler which functions as an OR gate due to the fact that the probability of concurrence of '1' in different minterms is zero. Therefore, an exclusive-OR (XOR) logic result has been derived. If we change the connection of the optical couplers before stage (III) and (IV) so that the low output port of DI1 is connected to the upper output port of DI2, an XNOR logic ( $\overline{AB} + AB$ ) can be obtained. However, the same result can be achieved without changing any physical connections. This is because the DIs can provide a way to exchange the output signals between its two output ports. That is, we can adjust the location of the signal wavelength on the transmission spectra of the DIs to exchange

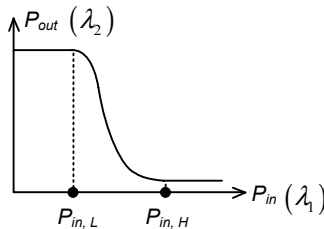


Fig. 6. Output probe power of the SOA versus the input pump power

the interference conditions of their two output ports. This can be achieved by tuning  $\Phi_0$  of the DIs or adjusting the wavelengths of the input signals. Note that unlike doing proof-of-concept experiments as what we have done, it is difficult to change the input signals in practical situations. In that case, tuning  $\Phi_0$  is the only choice.

Simplified setups are adopted in the experimental trials. That is, a single DI can perform NOT operation for several DPSK signals simultaneously if the input wavelengths can be adjusted. Fig. 7 shows the experimental setup for realizing two-input minterms. Fig. 8 shows the setup for realizing three-input minterms. To facilitate description, important measuring points, i.e., Do1, Do2, Si1, Si2, So1, So2 and So3, are marked on Fig. 7 and Fig. 8.

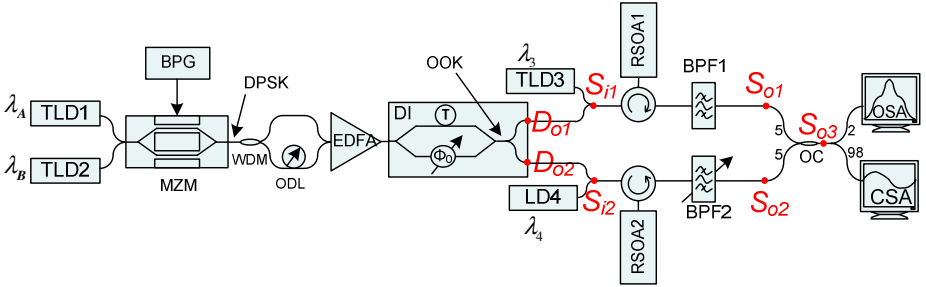


Fig. 7. Experimental setup for two-input NRZ-DPSK logic minterms or logic gates

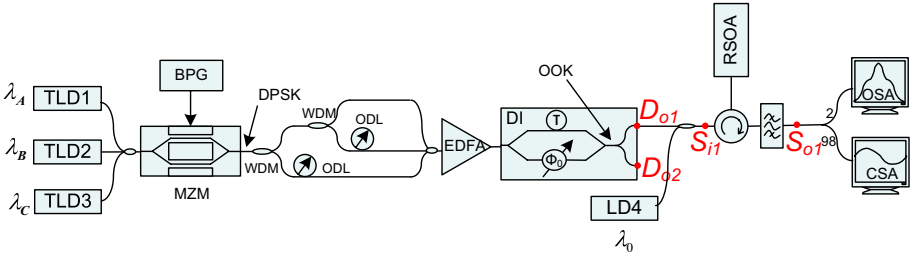
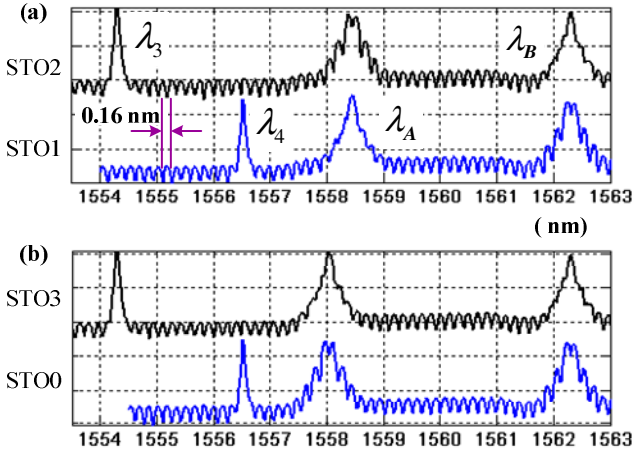


Fig. 8. Experimental setup for three-input NRZ-DPSK logic minterms

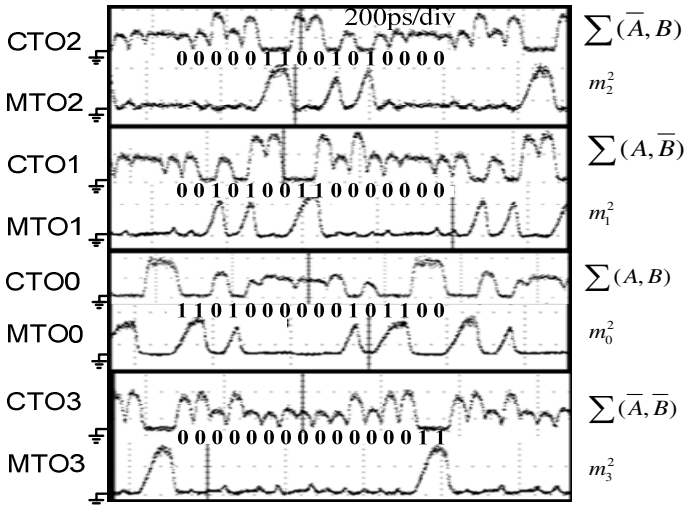
### 3.1 Two-Input Minterms

Due to energy conservation,  $m_1^2$  and  $m_2^2$  appear simultaneously and so does  $m_0^2$  and  $m_3^2$ . The signal spectra STO2 shown in Fig. 9(a) are measured at Si1 when two-input minterms  $m_2^2$  are derived at So1. Simultaneously,  $m_1^2$  are obtained at So2 and the spectrum measured at Si2 are shown by STO1. In this case, signal at  $\lambda_A$  and  $\lambda_B$  are destructively and constructively demodulated at Si1, respectively. Using the same setup but shifting  $\lambda_A$  downwards by 0.4nm, both  $\lambda_A$  and  $\lambda_B$  are constructively demodulated at Si1.  $m_0^2$  and  $m_3^2$  are derived at the same time and the spectrum measured at Si1 and Si2 are shown by STO3 and STO0 in Fig. 9(b).



**Fig. 9.** STO0~STO3: signal spectra measured at Si1 or Si2 in Fig. 7 when two-input minterms ( $m_0^2 \sim m_3^2$ ) are derived at So1 or So2

Fig. 10 shows the measured trace of  $m_0^2 \sim m_3^2$  (MTO0 ~MTO3), observed at So1 (MTO1 and MTO2) and So2 (MTO0 and MTO3), respectively. Also shown in Fig. 10 are combined traces CTO0~CTO3 measured at Do1 or Do2, corresponding to  $\sum(\bar{A}, \bar{B})$ ,  $\sum(\bar{A}, B)$ ,  $\sum(A, \bar{B})$ , and  $\sum(A, B)$ , respectively. The symbol  $\sum$  stands for power superposition. Note that  $m_0^2$  equals NOR logic and  $m_3^2$  equals AND logic. Since  $m_0^2$  and  $m_3^2$  appear at the same time, a simultaneous AND and NOR logic operation can be obtained.



**Fig. 10.** Measured  $m_0^2 \sim m_3^2$  (MTO0~MTO3) as well as the corresponding combined signal measured at Do1 or Do2 in Fig. 7 (CTO0~CTO3)

### 3.2 Three-Input Minterms

Using the set up shown in Fig.8, eight minterms for three-input DPSK signals are obtained. The temporal waveforms of  $m_0^3 \sim m_7^3$  are shown by MTE0~MTE7 in Fig. 11. The temporal waveforms of combined signals measured at Do1 when  $m_7^3$  are derived at So1 are shown by CTE7 in Fig. 10 as well. As shown by STE7,  $\sum(\overline{A}, \overline{B}, \overline{C})$  are derived at the input of the RSOA according to the properties of the demodulated spectra as described in section III, resulting in  $m_7^3$  after the NOR operation which can be verified by comparing CTE7 and MTE7 in Fig. 11. The full logic integrity of the scheme can be verified by calculating the logic results manually.

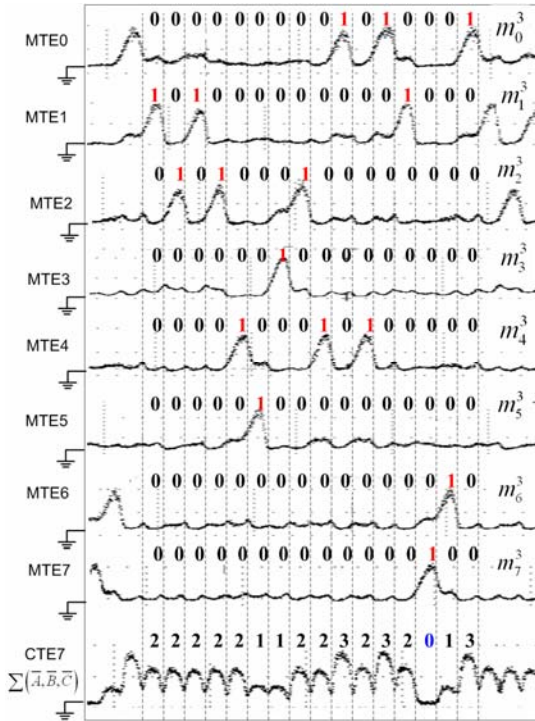


Fig. 11. MTE0~MTE7: measured temporal waveforms of  $m_{0-7}^3$

## 4 Conclusions

All-optical logic operation is very important function for all-optical signal processing in optical networks and optical supercomputing. Based on various nonlinearities in single SOA, five different logic gates were demonstrated, and all-optical digital 2-4 encoder and comparator could be realized with similar principle in three SOAs. Based on demodulation process of DPSK signals with delay interferometer and XGM effect in SOA, all-optical minterms generation for two input and three input signals were demonstrated, and these minterms could be exploited to realize

arbitrary logic functions. These two schemes are flexible and powerful functional, and possible to be integrated, therefore, these schemes are worth to be further investigated for possible practical applications in real systems.

## References

1. Houbavlis, T., Zoiros, K.E., Kalyvas, M., Theophilopoulos, G., Bintjas, C.: All-optical signal processing and applications within the esprit project DO\_ALL. *J. Lightwave Technol.* 23, 781–801 (2005)
2. Liu, Y., Tangdiongga, E., Li, Z., Zhang, S., de Waardt, H., Khoe, G.D., Dorren, H.J.S.: Error-free all-optical wavelength conversion at 160 Gb/s using a semiconductor optical amplifier and an optical bandpass filter. *J. Lightwave Technol.* 24, 230–235 (2006)
3. Liu, Y., Tangdiongga, E., Li, Z., De Waardt, H., Koonen, A.M.J., Khoe, G.D., Dorren, H.J.S., Shu, X., Bennion, L.: Error-free 320 Gb/s SOA-based wavelength conversion using optical filtering. In: PDP28, OFC 2006 (2006)
4. Kumar, S., Gurkao, D., Willner, A.E., Parameswaran, K., Fejer, M.: All-optical half adder using a PPLN waveguide and an SOA. In: OFC 2004, February, 1, pp. 23–27 (2004)
5. Zhang, X., Wang, Y., Sun, J., Liu, D., Huang, D.: All-optical AND gate at 10 Gbit/s based on cascaded single-port-couple SOAs. *Opt. Express* 12, 361–366 (2004)
6. Zhao, C., Zhang, X., Liu, H., Liu, D., Huang, D.: Tunable all-optical NOR gate at 10Gb/s based on SOA fiber ring laser. *Opt. Express* 13, 2793–2798 (2005)
7. Xu, J., Zhang, X., Liu, D., Huang, D.: Ultrafast all-optical NOR gate based on semiconductor optical amplifier and fiber delay interferometer. *Opt. Express* 14, 10708–10713 (2006)
8. Kumar, S., Willner, A.E.: Simultaneous four-wave mixing and cross-gain modulation for implementing an all-optical XNOR logic gate using a single SOA. *Opt. Express* 14, 5092–5097 (2006)
9. Xu, J., Zhang, X., Dong, J., et al.: Ultrafast all-optical AND gate based on cascaded SOAs with assistance of optical filters. *Electronics Letters* 43(10), 585–587 (2007)
10. Berretini, G., et al.: Ultrafast integrable and reconfigurable XNOR, AND, NOR, and NOT photonic logic gate. *IEEE, Photonics Technology Letters* 18, 917–919 (2006)
11. Li, Z., Li, G.: Ultrahigh-speed reconfigurable logic gates based on four-wave mixing in a semiconductor optical amplifier. *IEEE, Photonics Technology Letters* 18, 1341–1343 (2006)
12. Li, Z., et al.: All-optical logic gates using semiconductor optical amplifier assisted by optical filter. *Electronics Letters* 41, 1397–1399 (2005)
13. Son, C.W., Kim, S.H., Byun, Y.T., Jhon, Y.M., Lee, S., Woo, D.H., Kim, S.H., Yoon, T.H.: Realisation of all-optical multi-functional logic gates using semiconductor optical amplifiers. *Electronics Letters* 42, 1057–1059 (2006)
14. Deng, N., Chan, K., Chan, C.-K., Chen, L.-K.: An all-optical XOR logic gate for high-speed RZ-DPSK signals by FWM in semiconductor optical amplifier. *IEEE Journal of Selected Topics in Quantum Electronics* 12, 702–707 (2006)
15. Dong, J., Zhang, X., Fu, S., Xu, J., Shum, P., Huang, D.: Ultrafast all-optical signal processing based on single semiconductor optical amplifier and optical filtering. *Journal of Selected Topics in Quantum Electronics* 14(3), 770–778 (2008)
16. Xu, J., Zhang, X., Dong, J., Liu, D., Huang, D.: Simultaneous All-Optical and and nor Gates for NRZ Differential Phase-Shift-Keying Signals. *IEEE Photonics Technology Letters* 20(8), 596–598 (2008)
17. Wang, Y., Zhang, X.L., Dong, J.J., et al.: Simultaneous demonstration on all-optical digital encoder and comparator at 40 Gb/s with semiconductor optical amplifiers. *Optics Express* 15(23), 15080–15085 (2007)

# Zero-Energy Optical Logic: Can It Be Practical?

H. John Caulfield

Fisk University  
1000 17<sup>th</sup> Ave., N.  
Nashville, TN 37308

**Abstract.** The thermodynamic “permission” to build a device that can evaluate a sequence of logic operations that operate at zero energy has existed for about 40 years. That is, physics allows it in principle. Conceptual solutions have been explored ever since then. A great number of important concepts were developed in so doing. Over the last four years, my colleagues and I have explored the possibility of a constructive proof. And we finally succeeded. Somewhat unexpectedly, we found such a proof and found that lossless logic systems could actually be built. And, as we had anticipated, it can only be implemented by optics. That raises a new question: Might an optical zero-energy logic system actually be good enough to displace electronic versions in some cases? In this paper, I do not even try to answer that question, but I do lay out some problems now blocking practical applications and show some promising approaches to solving them. The problems addressed are speed, size, and error rate. The anticipated speed problem simply vanishes, as it was an inference from the implicit assumption that the logic would be electronic. But the other two problems are real and must be addressed if energy-free logic is to have any significant applications. Initial steps in solving the size and error rate are addressed in more detail.

## 1 Introduction

Over the last few years, my colleagues from multiple universities (Fisk, The Technion, Idaho State, Utah) and two fields (optics and logic) have worked to solve the 40-year-old problem of how to do an arbitrary sequence of logic operations without using any energy (1-3). We finally achieved that goal. References 4-7 retrace our path. We had hoped to show that zero-energy logic operations were possible, and we finally did so. That, of course, is gratifying. We accomplished that goal by showing how to build such lossless logic systems. But we had assumed that a demonstration would have an effect somewhat like the effect of Turing machine: Fundamentally significant but not something we would like to use for practical applications. We had a constructive proof that zero-energy logic is possible. Prior models such as the billiard ball computers can not be built. So the question of practical implementation never arose. But our systems can be built. So the next question is: Can we make it practical? The obvious problems are speed, accuracy (always a problem with analog operations), and size (optics is usually bigger than electronics). These are new problems, so the solutions developed here are preliminary. They are also likely to be far from final.

## 1.1 Background

Thermodynamics is a science of the possible and the impossible, but it does not give us ways to achieve the allowable. Logic operations can operate without energy consumption<sup>1</sup> if they do nothing lossy or irreversible. This was proved and examined in some detail by IBM scientists Landauer and Bennett (1-3). Since then many great computer scientists and physicists did important and clever work trying to accomplish the goal of energy-free logic (4 -7). Some while ago, my colleague Joseph Shamir and I sought to accomplish this optically, for the simple reason that, unlike electronics, optics need no push or pull to move carriers along. Light is self driving as is implicit in any periodic solution to Maxwell's equations. We learned a lot even though we failed in the goal of creating energy-free logic (8). Many years later, we secured funding to see if we could create logic operation at no cost in energy/ this time, however we would work closely with logicians. The time and the people involved turned out to be adequate to the problem. Of the papers published en route to the final solution, we list only a few here (9-11). The conventional analysis of reversible logic gates is shown in Fig. 1.

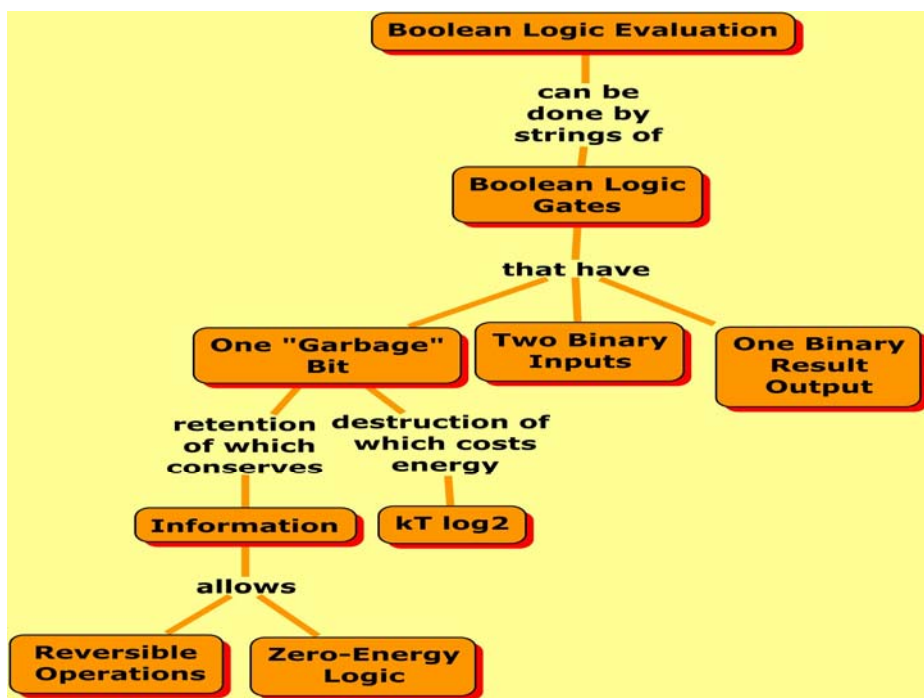


Fig. 1. Shows the situation as it was known on the 1860s and 1970s

<sup>1</sup> Zero energy logic is just that. Energy is still required to insert data and to read data. What happens between input and output is what is the subject of this 40 year effort.

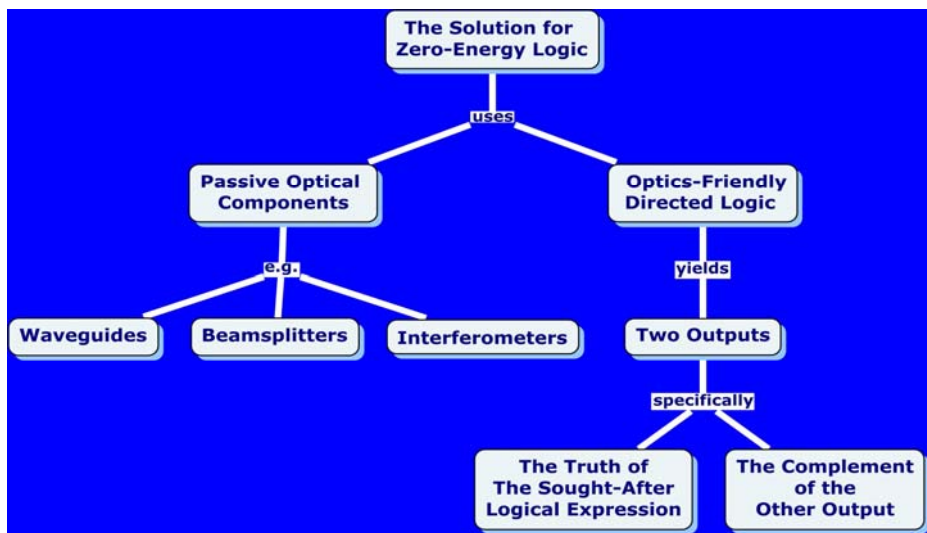
Retrospectively, some of what we did is almost obvious even though it was difficult for us as it was for the wonderful scientists who went before us, Very often, the solution to a longstanding problem results from examining implicit assumptions. Removing those assumptions took some effort. Let us tabulate the implicit assumptions usually made and note in the process how eliminating each makes solving the problem easier.

Assumption	Consequences if true	Consequences if false
Boolean logic requires some version of Boolean logic gates	We need gates that perform the Boolean function along with “garbage”	Perhaps we can find a signal flow logic more suitable for optical logic
The logic gates must be electronic	Lossless logic is precluded from the beginning	The many passive optical operators in optics offer hope
Decisions are nonlinear operations and will always need energy	The only hope would be something unheard of – linear decision making	We can view Mach-Zehnder interferometers as decision makers
Decisions must be represented by signal intensity	The intensity read says whether the logical operation is true or false	Computation can be converted from intensity to position. Where light appears carries the information

Table 1 shows some of the implicit assumptions we ignored and how eliminating them made lossless optical logic attainable.

This introduction is not intended to describe our solution in detail, but the references cited earlier do as does the graphical explanation in Fig. 2.





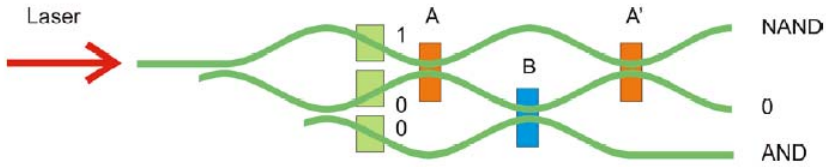
**Fig. 2.** Eventually we found a way to do lossless optical logic as suggested here

Using all of the consequences shown in the right most column of Table 1 apply, we simply note the basic elements of our solution.

- All operations are optical and thus analog by the physical structures. They are. The logic is, in a sense performed by the light not by the physical apparatus. This is arguably the most dramatic of our team's accomplishments to date. Directed Logic directs light through a sequence of optical operators that allows or directs them to do the desired operations.
- The logic implemented is what we have called Directed Logic (8). Any Boolean logic operation can be evaluated with Directed Logic. Directed Logic uses optical propagation not switches to operate. So far as I can tell, this is the first optics-friendly logic ever devised. Classical logic gates not always be imbedded in Directed Logic even though the same problems are being performed.
- Interferometers or their near neighbors do the decisions for us.
- The system has two inputs we can call A and B and two outputs C and D. Let the logical operation being performed be  $f(A, B)$ . Then one of the outputs (call it C without loss of generality) has light output if  $f(A, B)$  is true. As light must go somewhere, the other output will be  $\neg f(A, B)$ . Thus, it generates both  $f(A, B)$  and  $\neg f(A, B)$ . That is not the case in the conceptual designs of reversible logic gates.

Directed Logic is new and has been discussed elsewhere (refs). It is so different from conventional Boolean logic gate systems that we choose not to describe it in depth here.

Rather, we show a simple example that illustrates the problems that stand between the constructive proof and practical applications.



**Fig. 3.** Shows an optical embodiment of a simple logic operation. All of the problems addressed apply here.

## 2 The Speed Problem

As described in a very simple way by Feynman (9) the speed problem was expected to be fundamental and also make these lossless devices very very slow. In an electronic zero-energy system, a signal entered must wait for Brownian drift to create a signal at the output. But applying a voltage, we can improve the speed of the signal through the system. But that requires energy.

This problem does not apply in optics. As shown by Maxwell's equations, electromagnetic waves drive themselves and do so at a fixed speed. The phrase "computation at the speed of light" is often used and often meaningless. But, light does not need to be pushed or pulled through a system.

But "speed" means something else to computer scientists. It usually means allowable bandwidth. The fastest pulses in the world are optical. Pulses as short as a few wavelengths have been made. In our embodiments, we can limit the clock skew to a small fraction of a wavelength. Directed Logic maps easily onto the physical configuration suggested by Shamir and Caulfield 20 years ago (8). This allows path lengths to be equal for all signals and allows the paths to be equal to within a fraction of a wavelength. As the shortest pulses of light are many wavelengths long, clock skew will not be a problem. Device construction does not limit the bandwidth. There is a latency but it is small and the same for all paths if we use the pattern of system construction we proposed 20 years ago (8).

## 3 The Accuracy Problem

All computations are analog. Digital computers correct the 1 or 0 after each elementary operation, so the raw BER (Bit Error Rate) can be made very small. This slows down the operations but allows very accurate results are obtained. Analog operations are faster and cost less energy but are vulnerable to cumulative error as outputs of each component are not corrected before they are input to the next operation. These problems are inevitable in any zero-logic system,. But we have found a new way of reducing error that remains to be explored for optical Directed Logic. In digital computation, the predominant source of error is due to the detection of no photons at a position where a 1 is intended. As Poisson distributions are predictable, we can calculate the average number of photon detections needed to reduce this error below any given rate. For instance an expected 88 detected photons per detection period allows a  $10^{-9}$  BER.

But our devices are almost certainly better than such an operation would suggest. There are two outputs, not one as in binary Boolean logic operations. And, those outputs are complementary (light must go somewhere. If it does not go to one output, it must go to the other. We have two outputs to measure and help us find and remove errors. Just how to do that is less clear. If we get a zero in both channels, we can be quite certain that an error has occurred. If there is a single photon in one and none in the other, we declare a 1 to be present. There are many possible ways to do the error detection and correction. The contrast ratio between the two outputs seems a good thing to measure. Large contrast means probably correct results. But we have not decided how to use this extra information, but we are certain that using the information will be better than not using it.

The other thing that makes us a little less concerned about than we were at first is the accuracy problem. No one really needs computations to be correct to a  $10^{-9}$  BER. That error rate is necessary in some applications, because the computational complexity of many problems makes the result many orders of magnitude less accurate than the accuracy of the accuracy of the computer itself. The logical computations we are likely to make will not be that complex, so for many cases a much lower BER is satisfactory.

## 4 The Size Problem

There is a fundamental problem when optical logic is compared with electronic logic. The wavelength of light is much greater than the wavelength of electrons. Electronic elements can, in principle, be much smaller than optical elements. In current practice that is the case. But the UV photolithography used to make some small electronics logic can be used to make optical logic gates as well.

If we sacrifice the zero energy advantage we might use plasmonic commotions to accomplish subwavelength logic.

Also slow light reduces interaction distances and may help make smaller components.

## 5 Motivations for This Paper

It was my hope five years ago to make a significant contribution to the zero-energy-dissipation logic problem. The most important thing I did was to gather a group of physicists, electrical engineers, and logicians to work with me. My fondest expectation was that we might find a way to make such devices. It would undoubtedly be impractical as were the early concepts in the field, e.g. the billiard ball computer. To my great relief, we actually solved the problem and have reported on our solution elsewhere. But there was an even greater surprise from my viewpoint. Zero-energy logic was possible to implement and that implementation lent itself to being on chip with other optics and with electronics. Perhaps it might become useful in applications as well as in providing a manufacturability existence proof of zero-energy logic. It might even be useful in real applications.

Toward that end, I wanted to summarize the problems I saw in implementation of these systems and even offer some preliminary remarks on how each of the problems might be alleviated. This is a transparent attempt on my part to transfer further work

on this problem to some of the many others who are better equipped by background and skills in such matters. I have taken this matter as far as I can go.

## 6 Conclusions

Zero-energy-dissipation logic has now been shown possible using passive optics. It could be implemented in bulk optics but the integrated optics implantation seems closer to becoming a practical approach for on-chip implementation. This paper has shown that there are at least three problems with that implementation: speed, accuracy, and size. It is my hope that all of these problems can be solved, and I have presented preliminary thoughts on how they may be solved or at least greatly reduced. Like Moses and Martin Luther King, Jr., I have seen the Promised Land. But I may not get there. Zero-energy logic seems to me likely to be useful in some real world situations. Only others with more suitable backgrounds and skills are needed to realize that dream.

**Acknowledgments.** Solving the fundamental problem of zero energy logic required a team of hard working experts in many fields, I was fortunate enough to put such a team together. Alphabetically, they are Elizabeth Golden, James Hardy, Lei Qian, Joseph Shamir, Jonathan Westphal, and Andrey Zavalin. Without them, this paper would not have been written. The Missile Defense Agency sponsored this work for four years, so they deserve mention even though the contract was over when these considerations were made.

## References

1. Landauer, R.: Irreversibility and Heat Generation in the Computing Process. *IBM J. Res. Dev.* 5, 183 (1961)
2. Bennett, C.H., Landauer, R.: The Fundamental Physical Limits of Computation. *Scientific American* 253, 48–56 (1985)
3. Keyes, R.W.: Fundamental Limits of Silicon Technology. *Proc. IEEE* 89, 227–239 (2001)
4. Caulfield, H.J., Soref, R.A., Qian, L., Zavalin, A., Hardy, J.: Generalized optical logic elements – GOLE. *Optics Communications* 271, 365–376 (2007)
5. Qian, L., Caulfield, H.J.: What can we do with a linear optical logic gate. *Information Sciences* 176, 3370–3392 (2006)
6. Caulfield, H.J., Vikram, C.S., Zavalin, A.: Optical Logic Redux. *Optik- International Journal for Light and Electron Optics* 117, 199–209 (2006)
7. Hardy, J., Shamir, J.: Optics inspired logic. architecture *Optics Express* 15(1), 150–165 (2007)
8. Shamir, J., Caulfield, H.J., Miceli, W., Seymour, R.J.: Optical Computing and the Fredkin Gate. *Appl. Opt.* 25, 1604–1607 (1986)
9. Feynman, R.P.: Quantum mechanical computers. *Foundations of physics* 16, 507–531 (1985)

# On Attributes and Limitations of Linear Optics in Computing

Joseph Shamir

Department of Electrical Engineering  
Technion - Israel Institute of Technology, Haifa 32000, Israel  
jsh@ee.technion.ac.il

**Abstract.** Rejuvenated interest in exploiting linear optical processes within computing and signal processing architectures calls for reconsideration of its attributes and limitations. The objective of this work is a reassessment of various aspects of optics in computing in view of recent advances in computing concepts and technology. The main emphasis will be on the temporal aspects that are ignored in the majority of publications. Since the characteristics of a computing system are architecture- and application-dependent, the discussion will present various issues invoking special examples. The discussions are limited to the aspects of linear optics although a processing architecture may contain non-linear devices as well.

## 1 Introduction

Coherent optical processors introduced in the early nineteen sixties mark the beginning of the optical signal processing era. Fast development and excitement over the possibility of “computing with the speed of light” caused workers in the field to overlook both some fundamental limitations and the immaturity of the technology. In fact, some of the advantages of optical processing have not been discovered until much later. Of course this is not an unusual development for a new and promising research area. Unfortunately, frustration caused by the inability to materialize expectations caused a marked decline of interest in the field. During the years, the introduction of new technologies and concepts helped to reverse this trend with various *ups* and *downs* along the way.

To assist in keeping up a balanced outlook, this paper will elucidate some of the fundamental attributes of optics in computing, discuss physical limitations imposed on the performance of optical and electro-optical architectures and indicate some novel concepts that may help in advancing the field. The main emphasis is on the mostly ignored temporal aspect, which will be illustrated by several representative examples. There is no attempt to address *all* advantages and drawbacks of optical processors, most of which have been treated, in a scattered way, by several authors [1]-[9] but it is expected that the results here will trigger adequate interests in followup investigations.

## 2 Basic Considerations

The fundamental function of an optical field is that it solves the wave equation in the three dimensional (3D) space under a given set of boundary conditions. If we consider the boundary conditions as the input signal, the solution of the wave equation within a given architecture constitutes the required process. Thus, a huge amount of information can be processed in parallel, at the speed of light. However, by its nature this process is subject to intrinsic limitations that can be partly mitigated only at the expense of some of the advantages. Probably the most important attribute of optics is its huge parallelism, which comes about by the *non-interaction* between photons. This attribute is also the handicap that prohibits the translation to optics of electronic processes where the mutual interaction among electrons is the basis for any operation.

From a global point of view we are dealing with operations in 3D. However, in optics usually one dimension is reserved for the propagation and processing, leaving only the two other dimensions for the information input and output. In other words, given the propagation architecture (free space, optical system, set of waveguides, etc.), the whole process is uniquely determined by the boundary condition (information input) presented over a single, 2D surface (not necessarily plane). If it is desired to include information from a 3D region, such as holographic recording, this is done on the expense of the information density obtained from each surface within that 3D region of space. In other words the amount of information on a hologram is determined by the hologram material and recording process and it can store a corresponding amount of information from a single surface, or, the information can be distributed in 3D space on the expense of the available resolution from each 2D surface. Moreover, although the velocity of light is quite high, it is still finite. This finite velocity may cause information from different parts of the input space to reach a detection region at different times giving rise to a time delays and time-skew effects. This problem was realized in 1987 [2] and is the main subject of this work as well.

The manifestation of the general properties of light depends on the optical architecture and the application at hand. Sometimes they show up as attributes that make the process work while at other instances they cause impediments that must be mitigated for implementing a certain process.

Classical optical systems, such as imaging systems, are based on discrete optical components separated by sections of free space. The main attribute of such systems is the large amount of information that is transmitted in parallel. The total quantity of information that can be conveyed within a given optical system was extensively studied and is quite well understood. Considering the high velocity of light and the relatively slow detection systems employed in these classical systems, much less attention was directed toward the issue of temporal response [2]. This situation meets a significant challenge when one intends to extend the operation of these systems toward the implementation of high-speed mathematical processors.

During the 1980's much effort was directed toward the implementation of optical computing architectures. While some of those worked quite well with a

limited number of processing elements their characteristics were extrapolated to large arrays operating at high speeds. Unfortunately in many of these extrapolations the finite velocity of light was ignored until some of its implications were realized [2] and further investigated in Refs. [5] and [6]. In the following, the temporal aspects of problem will be illustrated by a few examples invoking some new insights that were not realized before. In the following sections we shall address this problem in more detail with specific examples providing some new insights.

### 3 Optical Systems Based on Free Space Propagation

As indicated above, classical optical systems are composed of sections of free space enclosed between discrete components such as lenses, spatial light modulators (SLM) and detector arrays. The outside information is introduced in one or more of these devices, the light propagating through the system performs the desired operation and the final, or intermediary results are usually detected by a detector array or recording medium. Consequently, the most frequently employed process is the propagation in a free space section. In this section we discuss this propagation from its temporal aspect as suggested in Ref. [2] from a straight forward geometrical point of view as shown in Fig. 1. In the following we shall consider, for simplicity, only one dimension out of the two input dimensions in a characteristic optical system. With some additional labor and space all results can be easily generalized for the complete 2D. Assume a section of free space of length  $L$  enclosed between an input plane,  $In$ , where, for example, an SLM or a transparency illuminated by a coherent plane wave can be placed, and an output plane,  $Out$ , which may contain a recording medium or device, or, it may be an intermediary plane followed by additional optical components. Since there is just free space between the two planes, diffraction effects, originating from the wave equation, predict that light from each point of the input plane

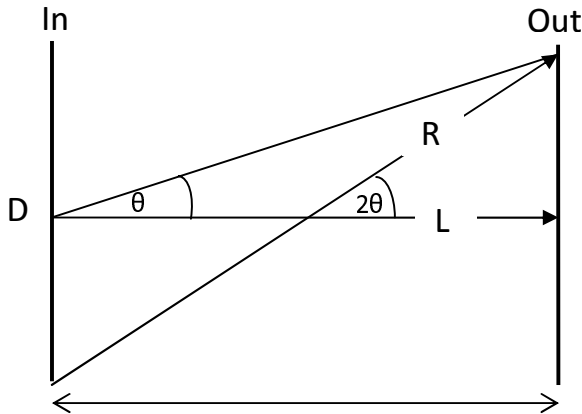


Fig. 1. Time skew in free space

reaches each point of the output plane. Thus, illustratively, there are “light rays” of various lengths between  $L$  and  $R$  that can meet over the output plane. The shortest distance between the two planes is  $L$  with the so called *pipeline delay*,  $L/c$ , with  $c$  the velocity of light. The pipeline delay is significant but usually has no damaging effects. The more destructive effect is introduced by the relative delay between  $L$  and  $R$ . If the length dimension of the effective aperture of the input plane is  $D$ , we obtain a length difference between the direct ray,  $L$ , and the most inclined ray,  $R$ ,

$$\delta = R - L = \frac{D}{\sin(2\theta)} - \frac{D}{\tan(2\theta)} = \frac{D}{\sin(2\theta)} [1 - \cos(2\theta)] = D \tan \theta \quad (1)$$

where  $\sin \theta$  may be regarded as the numerical aperture ( $NA$ ) of the system. To appreciate the implications of Eq. (1) we take a typical configuration with  $D = 1\text{cm}$  and  $NA = 0.5$  to obtain  $\delta \approx 5.8\text{mm}$ , which leads to a relative maximum time delay of  $\Delta t \approx 20\text{ps}$ . Such a figure may be quite bothering in several applications. For example, on one hand, if a coherent process is considered, such as holographic recording, the coherence time must exceed this delay. On the other hand, if high-speed digital processes are to be implemented, any short pulse length will be broadened to at least  $\Delta t$  since all time delays will be integrated from 0 to  $\Delta t$ . This becomes extremely significant when processing speeds of the order of 100 GHz are considered. We should point out that the number derived here is the maximum delay observed at the edge of the output plane and, according to the geometry of the system, the time skew will be reduced, depending on the position over the output plane and the scattering characteristics of the input function.

## 4 Fourier Transform Optical Systems

The simple geometrical arguments of Ref. [2] were generalized for more complex optical systems in Ref. [6]. Here we shall discuss, also with some new insights, optical systems containing one or two lenses. We start with the single lens Fourier transform (FT) system of Fig. 2 based on a lens with focal length  $f$ , an input plane of clear aperture with dimension  $D$  containing the input function illuminated by a coaxial plane wave and the output plane. To analyze this system we may decompose the input function into its plane wave spectrum. One component of the plane wave spectrum is shown in the figure with three associated rays. All these rays converge to the spatial frequency component represented by a point on the output plane, which in this case is the FT plane. By this process, the contribution from the whole input plane to this spectral component is integrated (superposed) at that corresponding point. Each ray has a different path length with a maximum differential value, and a corresponding time delay,

$$\delta = D \sin \theta \quad \Delta t = \delta/c \quad (2)$$

where the maximal acceptance angle,  $\theta_{max}$ , corresponds to the system  $NA$  i.e.  $\sin \theta_{max} = NA$ , and  $c$  is the velocity of light. Mathematically, this time delay



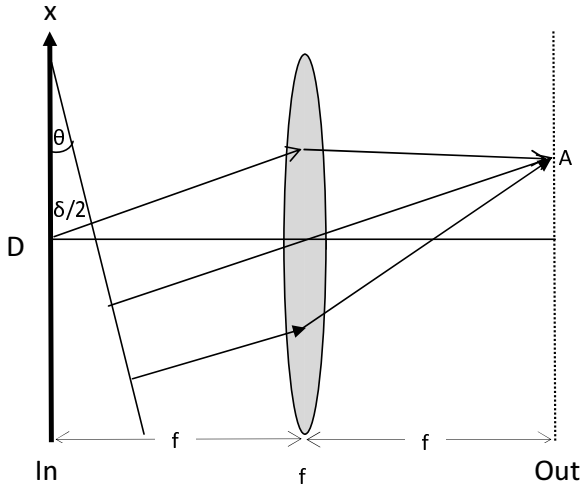
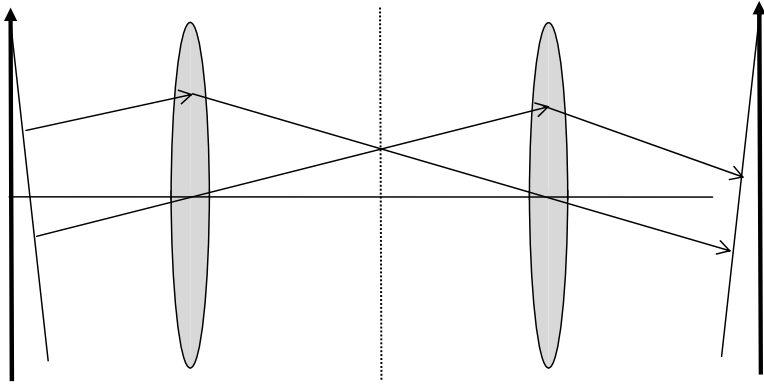


Fig. 2. Time skew in a Fourier transforming optical system

can be interpreted as a phase delay, which is represented by a linear phase factor that serves as the kernel of the FT operation. Thus, this phase delay is intrinsic to the FT operation and cannot be modified if this transformation is to be performed. The implications of this result are significant. First of all, to perform an optical FT the coherence time of the illuminating light source must exceed  $\Delta t_{max} = D \sin \theta_{max} / c$ . If the coherence time is smaller, i.e. operation with incoherent light or short pulses, a FT *will not* be performed. Also, similar to the free space operation of Fig. 1, a sub-picosecond pulse illumination will be broadened over the Fourier plane. Unlike in the free space case, the broadening is uniquely determined for each spatial frequency component which, in turn, depends on  $\theta$ .

It is interesting to note that for paraxial systems,  $\tan \theta \approx \sin \theta$  leading to similarity of the maximal time skew in free space and the FT system but the distribution of its value over the output plane is quite different. Caution should be exercised during applications of these results to non-paraxial systems where the situation is much more complicated than suggested by the above simplified derivations.

Now, suppose that we extend our optical system by a second, identical FT system as in Fig. 3. The figure indicates that the time skew is exactly compensated by the second FT system. Indeed, we know that in this case we ideally obtain a one-to-one image with no distortion. This state of affairs is fundamentally altered when we place a material object, such as a transparency or spatial light modulator, in the FT plane. In this case a point by point multiplication occurs between the FT of the original input function and the new function present on the FT plane. In principle, this is a non-linear operation which generates new spectral components contained in the field transmitted by the FT plane toward the output plane may lead to an enhancement of the time skew effect, rather

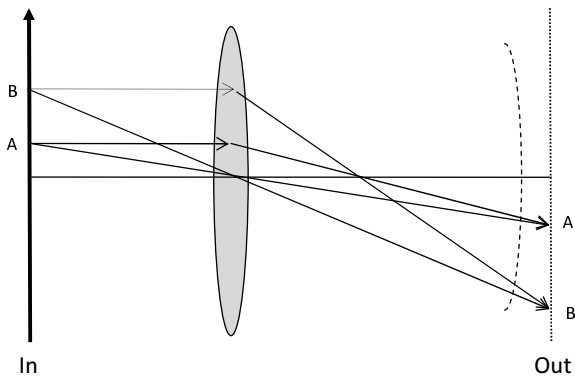


**Fig. 3.** A double Fourier transform system

than its compensation. Obviously, the degree of the skew observed over the output plane of this  $4f$  optical correlator is a strong function of the nature of both input functions and can vary between 0 and twice the amount of a single FT.

### 5 Imaging Optical Systems

The empty  $4f$  imaging system of Fig. 3 represents an ideal imaging system where the mapping of each point from the input plane onto the output plane takes exactly the same time. In Ref. [6] such a system is classified as possessing *double Fermat degeneracy*. In contrast, a single lens imaging system, such as the one in Fig. 4, contains only a *simple Fermat degeneracy* because it may take a different time to map point **A** onto **A'** than the time it takes to map point **B** onto **B'**. The reason is the presence of a quadratic phase factor associated with the single



**Fig. 4.** Single lens imaging with the spherical wave front incident on the output plane indicated by the curve line

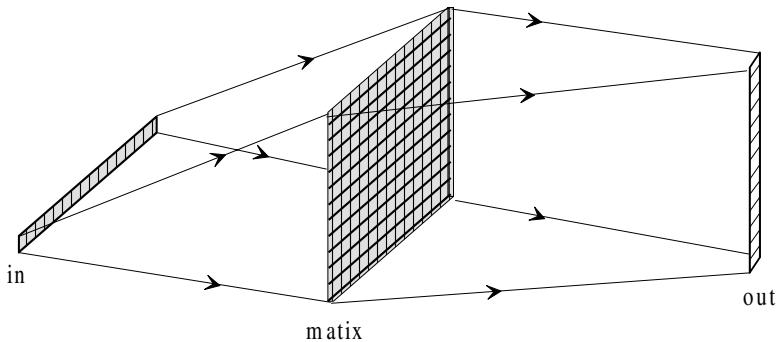
lens imaging. Unlike the systems discussed above, the resulting time skew is not an intrinsic character of the system and it can be easily compensated by an additional lens or observation over a spherical surface. Moreover, the Fermat degeneracy indicates that all rays from object point to image point have the same optical length and, if illuminated by a pulsed source, there will be no pulse broadening over a point detector but the detection at different points may be delayed with respect to each other.

## 6 Mathematical Optical Processors

While in classical optical processes the discussed time skew can be usually neglected this is not always true in optical mathematical processors. One such example is the typical vector-matrix multiplier presented in Fig. 5. While the schematic sketch of the figure indicates implementation by free space propagation, destructive diffraction effects must be mitigated by much more complicated architectures. In any case, in its free space form it suffers from the free space skew while a more practical implementation, which contains astigmatic optics performing FT in one dimension and imaging in the other one, the time-skew effects of the FT comes into play, limiting the ultimate operation speed.

Another example is the matrix-matrix multiplier (Fig. 6) proposed in Ref. [10] and analyzed in Ref. [5], which also suffers from similar limitations.

The time skew as well as diffraction and other limitations, as discussed for example in Ref. [5], are quite similar in all bulk optical systems. The time skew increases with NA and system size and so does the information content that can be handled in parallel. Thus, the larger the information content, the slower will be the speed. There is no “free lunch” but optimization of specific systems should be possible and is a subject to further study.



**Fig. 5.** A vector-matrix multiplier

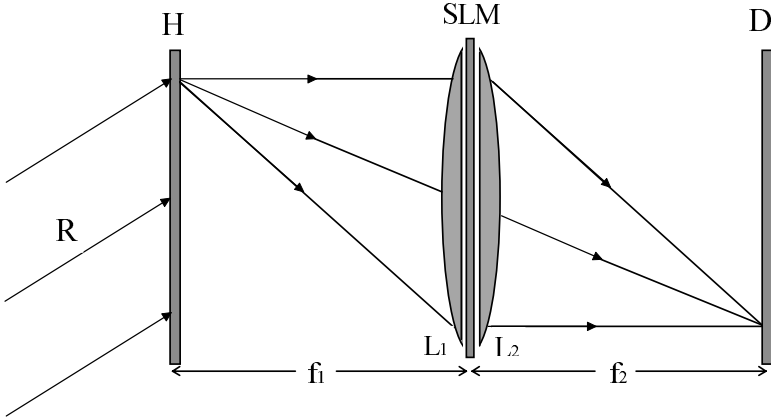


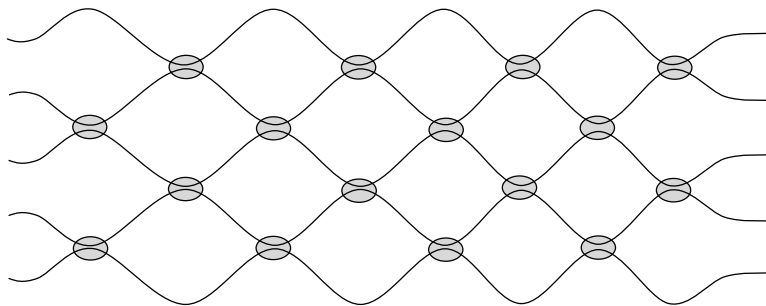
Fig. 6. A matrix-matrix multiplier or an  $N^4$  interconnection network

## 7 Guided Optics

As indicated by the above examples, time skew and diffraction will always limit the performance of bulk optical systems. The same is true for architectures implemented in a slab waveguide, which is the physical implementation of 1D optical systems as discussed above. One way to bypass these limitations is to constrain the light into wave guides, optical fibers, channel guides, etc. While at present such wave guides are relatively thick their size already approaches the extent of diffraction limitations in bulk optical systems and there are good prospects for additional miniaturization employing optical crystals and plasmonics. In guided optics time skew problems can always be mitigated by adjusting the lengths of the guides and it remains to design architectures that can perform a desired operation. The best proven attribute of guided optics is its ability to convey information rather than to process it. As indicated above, the reason for this is the main property of non-interaction of light with light. Nevertheless, the flow of light in guides can be controlled electronically or even opto-electronically using an external control channel.

We represent here a large class of processors based on guided optics by the interconnection network [11] based on the optical Fredkin gate [12]. The network of Fig. 7 is a section of a larger interconnection network. Each line represents a wave guide channel and the ovals are control sections that determine if the light in the corresponding channels continues to propagate in the same channel or the information is interchanged between the two adjacent channels — this is an optical Fredkin gate. Considering the left hand side of the array as the input and the right hand side as the output this array can be programmed by the Fredkin gates to perform any permutation among the input signals.

In an alternative application, the implementation of directed logic [13] is achieved by considering the control signals as the input information and the



**Fig. 7.** Interconnection network. Lines represent wave guides and the ovals are the controls of wave guide couplers.

light traveling in the guides transmit the information. Properly arranged, this network can implement all logic functions.

## 8 Conclusions

The emphasis of this paper was on the temporal limitations on optical processes. It was shown that there are intrinsic limitations caused by time skew — a fundamental property of several optical architectures. One possibility to mitigate this limitation is to let the light propagate in wave guides as illustrated by a representative example.

## References

1. Gabor, D.: Light and information. In: Wolf, E. (ed.) *Progress in Optics*, vol. 1, pp. 109–153 (1964)
2. Shamir, J.: Fundamental speed limitations on parallel processing. *Appl. Opt.* 26, 1567–1593 (1987)
3. Bor, Z.: Distortion of femtosecond laser pulses in lenses and lens systems. *J. Mod. Opt.* 35, 1907–1918 (1988)
4. Weigelt, J.: Space-bandwidth product and crosstalk of spatial filtering methods for performing binary logic optically. *Opt. Eng.* 27, 883–892 (1988)
5. Shamir, J., Caulfield, H.J., Johnson, R.B.: Massive holographic interconnection networks and their limitations. *Appl. Opt.* 28, 311–324 (1989)
6. Lohmann, A.W., Marathay, A.S.: Globality and speed of optical parallel processors. *Appl. Opt.* 28, 3838–3842 (1989)
7. Feldman, M.R., Guest, C.C., Drabik, T.J., Esner, S.C.: Comparison between electrical and free space optical interconnects for fine grain processor arrays based on interconnect density capabilities. *Appl. Opt.* 28, 3820–3829 (1989)
8. Guha, A., et al.: Optical interconnections of massively parallel architectures. *Appl. Opt.* 29, 1077–1093 (1990)
9. Shamir, J., Caulfield, H.J.: Parallel optical processors — some basic considerations. *Int. J. of Opt. Comp.* 2, 73–78 (1991)

10. Caulfield, H.J.: Parallel  $N^4$  weighted optical interconnections. *Appl. Opt.* 26, 4039 (1987)
11. Shamir, J., Caulfield, H.J.: High-efficiency rapidly programmable optical interconnections. *Appl. Opt.* 26, 1032–1037 (1987)
12. Shamir, J., Caulfield, H.J., Miceli, W., Seymour, R.J.: Optical Computing and the Fredkin Gate. *Appl. Opt.* 25, 1604–1607 (1986)
13. Hardy, J., Shamir, J.: Optics inspired logic architecture. *Optics Express* 15(1), 150–165 (2007)

# Optical Designs for Non-deterministic Turing Machines<sup>\*</sup>

## (Extended Abstract)

Shlomi Dolev and Yuval Nir

Department of Computer Science, Ben-Gurion University of the Negev, Beer-Sheva,  
84105, Israel  
dolev@cs.bgu.ac.il,  
nyoval@gmail.com

**Abstract.** The construction of an optical computer that can explore the computation tree of a non-deterministic Turing machine in the time it takes to explore one path of the computation has been described in Dolev and Nir 2003. In this paper, we elaborate on the design considerations of Dolev and Nir 2003. The construction of such an optical computer will allow solving NP problems in polynomial time. The limitation is space, where every beam location (hitting a prism) represents a different Turing machine configuration.

By the use of writable (holographic) memory, we are able to reduce the space only by a constant factor. Tradeoffs between the use of *semantics* for each location in space, and the use of digital storage is discussed. In the writable model, configurations can be represented in binary (or higher base digital) representation, rather than mapping each location in space to a single configuration. We show that, the benefit of such a digital representation in the scope of concurrent exhaustive search is limited.

## 1 Introduction

Optical computing is viewed as a promising computational model. Most research projects focus on replacing current computer components with optical equivalents, resulting in an optical digital computer system processing binary data. This approach appears to offer short-term prospects for commercial optical computing, since optical components could be integrated into traditional computers to produce an optical/electronic hybrid device. Our research is in the non-traditional direction, similar to e.g., [3,27,26,23,31,9,34,33,6,2], attempting to develop entirely new methods of computing that are not physically possible with electronics, and truly exploit the full parallel capabilities of light beams.

---

<sup>\*</sup> Partially supported by Rita Altura Trust Chair in Computer Sciences, Lynne and William Frankel Center for Computer Sciences.

The technology today seeks multi-core solutions in order to cope with the clock frequency limitations of VLSI technology. Namely, to implement a parallel/distributed system on a single chip, where a bus is used for communication among the processing units. Therefore, the communication overhead associated with distributed/parallel processing is reduced dramatically. One may take the multi-core technology to the extreme — having a very large number of cores that are incorporated into the processing by sending signals over high-speed buses, maybe using optical/laser communication instead of traditional buses [28,18,17].

Optical communication may be chosen due to the free space transmission capabilities of laser beams or the need to transmit signals from/to the processing unit through fiber optic channels. In such cases one may try to avoid the optical to digital conversion (and the digital to optical conversion) and use optical switches for computing. The straightforward solution is to implement optical logical gates, such as logical *and* gate and logical *or* gate, a design that directly maps the current VLSI design to an all-optical processor [11,22].

On the other hand, electronic computers are not structured as mechanical computers, such as the Babbage machine [16], and it is possible that optical computers should be designed differently as well. In fact, some success in using many beams in free space for computing has been recently reported [21]. The design of [21,32] is based on parallel optical multiplication. The use of similar multiplication devices to solve NP-Complete problems is suggested in [29,30], where a bounded device which is designed to solve NP-Complete problems bounded by  $n$ , is able to solve instances of size smaller than or equal to  $n$ . Still, use of the fact that beams propagate in three dimensions is limited in the architectures of [21,29] as the propagation of beams is in approximately the same direction. The beam traversal time is not used in the architectures that use Multiplication; we propose to use the space in a multi directional fashion and use the time dimension as well e.g., [9,24,15].

The seminal work of [27] presents mapping between beam propagation and the computation of the deterministic Turing machine. In [27] it is proven that the problem of ray tracing in three dimensional optical systems which consist of a finite set of mirrors, with endpoints that are rational coordinates, is PSPACE-hard. In [9] the use of a mapping similar to the non-deterministic Turing machine by (amplifying and) splitting beams is suggested. The mapping can be viewed as a theoretical existence proof for a solution, rather than an efficient solution.

The classic deterministic Turing Machine model is the base for the computation complexity classes, since any (electronic) computer can be viewed as a version of a Turing machine. Interesting enough, the definition of the classical Turing machine has been extended to the case of non-deterministic Turing machine [27], where the choice of the next state is chosen arbitrarily, in fact all possible choices should be examined in order to reject the input. The new definition fits many very important classic problems such as the traveling salesman problem. Is there a computation device (a computer) that can execute non-deterministic Turing machine programs in the same time it takes for the non-deterministic Turing machine?



In this paper we intend to give some formal model of computation based on non-deterministic Turing machine implementation. In this model non-determinism will be achieved in a realizable way by the inherent parallel properties of optical computation. This model will be based on optical ray tracing presented in [27]. By enhancing the model of [27] we simulate non-determinism as a parallel computation of all non-deterministic choices, simultaneously. The simultaneous computation will be achieved by power enhancement and splitting of the optical ray of computation into two separate optical beams, each representing a possible non-deterministic choice of the computation.

In [27] it is shown that using only refractive components (prisms) and using only rational representation coordinates, one can build an optical machine that simulates any Reversible Turing Machine. By adding additional optical components that are partially refractive, we will show that an optical machine can be made to simulate non-deterministic Turing Machines as well. These partially refractive components are also capable of splitting an incoming ray into two separate outgoing rays (each, with the same energy as the incoming ray). The basic reversibility principle in the optical machine of [27] is that for any state configuration there exists a single possible prior configuration. This restriction is due to the lack of complex partially refractive optical components in the optical machine. By adding this more complex component we are able to achieve (a) non-reversibility simulation and (b) parallel computation of any number of possible (originally non-deterministic) computations.

In addition to presenting this optical model, we will present some notions of complexity that are well known in computability theory, into our new model. These computability classes include time and space, both deterministic and non-deterministic and will be translated to appropriate time, space, and energy classes.

Modern computers use digital representation to exponentially enlarge the domain that can be handled by a single analog signal. The position of each signal defines the significance of the signal, rather than the strength of the signal. Moreover, the digital binary (or higher based digital systems) is exponentially smaller than an unary representation. One may conclude that a binary digital representation will dramatically save space and allow a solution for larger instances compared with the architecture presented in [9]. We examine such possibilities assuming the existence of writable (holographic) digital memory. We show that in the case of concurrent exhaustive computations, where the number of computation paths that should developed at time unit grows, and at time  $t$  is  $n_t$ , the writable memory capabilities will not avoid the need to store  $n_t$  bits of information. In the particular implementation of the non-deterministic Turing Machine only a saving of a factor of two is possible.

The rest of the paper is organized as follows, in the next section we present the main ideas for the construction of the optical computers. Then in Section 2 we elaborate concerning the properties of the non-deterministic Turing machine and in Section 3 we elaborate concerning complexity issues. In Section 4 we suggest the use of Binary, or other digital representation with a base greater than one,

to reduce the required space. Holographic read/write memory is suggested for supporting such a representation.

## 2 Optical Implementation of Non-deterministic Turing Machines

In [27] it is shown that the states of an optical Turing machine are a finite set of refractive objects that have an entrance (input window) and two exit windows, the beam of light enters perpendicular to the entrance window and its location in relation to the window represents the state of the tape. Inside a state, the beam of light is transformed in accordance to a deterministic transition function to the appropriate exit window and the beam location will represent the new configuration of the machine tape. The beam is then redirected to the appropriate next state to continue computation. To simulate non-reversibility we need to allow incoming beams from any possible prior state to enter the current state at any possible beam location relative to the input window, this is achieved using the partially reflective surface much like a one-sided mirror, any beam hitting this surface on the external side will continue towards the current state, and any beam hitting this surface on the internal side will be reflected to the current state, thus non-reversibility is achieved.

Achieving non-determinism is possible by splitting any outgoing beam from some state to all possible state transitions as defined by the non-deterministic transition function [9].

We assume that all non-deterministic machines' state transitions are defined as two possible state transitions, at each step of the computation execution. To deal with machines that can change states (non-deterministically) to a larger number of possible states we may transform the states of the given machine into the former form (of at most two beams fan-out) with only  $\log(|Q|)$  multiplication factor over the execution time, where  $Q$  is the set of machine states.

We assume a universal non-deterministic machine  $U$  that receives an encoding of any two-fanout non-deterministic machine and can simulate that machine on any input, this simulating of the given machine over the universal non-deterministic Turing machine will result in an additional multiplication factor over the execution time that is proportional to the length of the original machine description.

**The optical hardware:** We are now ready to describe the actual components of the non-deterministic optical computer. In addition to the components described in [27], we need a device that:

- (a) splits the outgoing beam from some exit window into two outgoing beams while maintaining the relative location of these beams to two possible exit locations,
- (b) enhances the energy of the split beams back to the original minimal energy of the original beam before splitting.

In fact the device can be a one shot energy device where each location has to split a beam into two beams with the same energy of the original only once.

The reason is that the computations that started in this configuration have been already explored following the arrival of the first beam to this location.

In this manner we can proceed simultaneous computation of all possible non-deterministic computations. Note that the polynomial time achieved by the optical non-deterministic computer cost (exponential) space (and energy), since we have to ensure that every possible configuration of the Turing machine can be represented and that from every configuration the beam can be split amplifying both output beams to the original energy of the arriving beam. It turned out that the space restriction is not a new restriction since the optical deterministic computer presented in [27] has the same limitation (it has to represent every possible configuration), and still is of practical interest for large (enough) inputs.

As for energy one can propose to use the laser amplifier technology that is currently integrated in fiber optics. In our case the amplifying method will be applied to (prisms) surfaces instead of the fiber optic cable e.g., [19,20]. The delay that is associated with the amplifying process is in the order of  $10^{-9}$  seconds, so it will not influence the time required for the computation (in a polynomial path of the computation). As for space, a 1 meter by 1 meter square can represent  $10^6 \times 10^6$  configurations. We note that one would prefer to replace the general description of the non deterministic Turing machine, with a specific NP-complete solver, such as 3-sat or TSP solver [27]. In this way the  $10^{12}$  configurations may be used in a more efficient way.

The machine will accept an input if a beam arrives to the accepting state and will reject an input iff following a predefined time bound (polynomial in the input) elapses without reaching the accepting state (or no beam exists, due to loops in the same set of configurations).

Next we elaborate on a few specific issues concerning the construction.

**Universal Non-deterministic Turing Machine.** We assume that a given non-deterministic Turing machine have a single working tape and a limited non-deterministic choice fanout of 2. Any state transition will contain two possible non-deterministic choices, and the non-deterministic machine will choose the correct state transition to reach an accepting configuration if such a choice exists. A universal non-deterministic Turing machine  $U$  will simulate a non-deterministic machine  $N$  in much the same manner as a deterministic universal machine simulates a deterministic Turing machine. The difference being; Upon reaching a state transition with two possible non-deterministic choices,  $U$  will make a non-deterministic choice to simulate the choice made by  $N$ , it will then proceed with the simulation as if  $N$  had made that choice.

Universal non-deterministic simulation incurs the same time factor as deterministic simulation, assuming  $U$  uses two tapes it will incur a runtime factor linear in the size of the encoding of the simulated machine i.e., simulating a universal non-deterministic machine is greater by a factor of the length of the machine encoding.

### 3 Complexities

**Time Complexity.** An optical Turing machine computes some computation  $C$  in  $f(n)$  time where  $n$  is the size of the encoded problem (input)  $x$ , if  $C(x)$  is computed by the passage of the ray through no more than  $f(n)$  obstacles. Since a Turing machine time is computed as the number of steps the machine makes, each step corresponding to a transition through some state, and each state transition in the optical machine corresponds to passage through a constant bounded number of obstacles, Turing time complexity is bounded by a constant factor of optical time complexity.

**Space Complexity.** As noted in [27] the configuration of the optical ‘tape’ is defined by the relative location of the beam of light to the I/O windows in each state.

Let  $W$  be the size of the I/O windows in the optical machine, and let  $V$  be the size of the minimal distance between two locations of the beam of light in a single computation. Then we can define an optical Turing machine to compute some function  $C$  in  $f(n)$  space where  $n$  is the size of the encoding of the problem input, if  $W/V$  is bounded by  $f(n)$ .

In general, the precision ratio is exponentially smaller than the number of bits capable of representing. It seems possible to improve this restriction to a much tighter bound for representing computational memory space.

**Energy Complexity.** We define an energy unit as the minimal energy of the beam needed to pass in the expected manner through an obstacle, or to be sensed by an optical sensor. We assume that any splitting of the beam into separate beams or any passage through some obstacle incurs a constant fraction reduction of the energy of the incoming beam for splitting beams and passing through obstacles. We also assume negligible energy loss due to heat, friction, and other physical aspects.

We define the energy complexity of an optical Turing machine to be the minimal energy required for the input beam to be sensed by the output sensors. It is evident that  $N_{\text{energy}}(C)$  is exponential in time for non-deterministic machines. This is due to the fact that every non-deterministic choice is likely to reduce the energy of the incoming beam into two outgoing beams of approximately half the original beam’s energy.

The above considerations for complexity result  $N_{\text{time}}(C) = \text{Opticaltime}(C)$  for any computation  $C$ , in exchange we pay exponential price in energy and space.

### 4 Writable Holographic Memory

The fact that each beam represents a computation path, and the fact that all computation paths should propagate simultaneously, imply the need to simultaneously represent all the leaves of the computation. The number of computation paths can be doubled in every step, thus, the computation tree obey the binary

tree structure with a total number of nodes that is almost twice the number of leaves. Thus, the use of a writable (possibly holographic [1]) memory may save space (dedicated to representing previous time steps in [9]) that is proportional to half of the computation tree, hence saving a factor of two.

Another aspect in using writable memory is the possibility to use digital representation of information which is proven to exponentially reduce the required memory. In the scope of our concurrent exhaustive search there is a need to represent each possible path of computation at the same time without comparing intermediate Turing Machine configurations. Therefore a use of a single bit (location in memory) to represent a configuration is minimal.

## 5 Conclusion

Our results show that it is possible to compute any non-deterministic computation using optical computing in time proportional to that of a non-deterministic Turing machine. In the scope of exhaustive search as suggested in [9], the use of digital representation turned to be less significant than it is in the scope of current computer architectures.

**Acknowledgments.** We thank John H. Reif for his helpful remarks.

## References

1. Curtis, K.: Holographic Storage Tutorial. In: Phase Technologies (2009)
2. Anter, A., Dolev, S.: Optical Solution for Hard in Average #P-Complete Instances (Using Exponential Space for Solving Instances of the Permanent). In: Proc. of the 12th IEEE Meeting on Optical Engineering and Science in Israel, 2nd OASIS (March 2009)
3. Caulfield, H.J.: Space-time complexity in optical computing. In: SPIE Optical information-processing systems and architectures II, vol. 1347, pp. 566–572 (1990)
4. Dolev, S., Fitoussi, H.: Primitive Operations for Graph-Optical Processor. In: 6th Haifa Workshop on Interdisciplinary Applications of Graph Theory, Combinatorics, and Algorithms (May 2006)
5. Dolev, S., Fitoussi, H.: The Traveling Beams: Optical Solutions for Bounded NP-Complete Problems. Technical report #07-04, Ben Gurion University of the Negev. A journal version will appear in Theoretical Computer Science (January 2007)
6. Dolev, S., Fitoussi, H.: The Traveling Beams: Optical Solutions for Bounded NP-Complete Problems. In: Crescenzi, P., Prencipe, G., Pucci, G. (eds.) FUN 2007. LNCS, vol. 4475, pp. 120–134. Springer, Heidelberg (2007)
7. Dolev, S., Fitoussi, H.: Black Boxes and Rays, Optical Solutions for Bounded Instances of the Hamiltonian Path Problem. In: 7th Haifa Workshop on Interdisciplinary Applications of Graph Theory, Combinatorics, and Algorithms (May 2007)
8. Dolev, S., Leshem, I., Shapira, S., Fitoussi, H., Shaked, N.T.: Optical implementation of a microprocessor for solving the Hamiltonian-path problem. In: The 11th Meeting on Optical Engineering and Science in Israel (OASIS) (March 2007)
9. Dolev, S., Nir, Y.: Optical implementation of bounded non-deterministic Turing machines. US Patent 7,130,093 B2, January 2005, Field May 2004, Field in Israel May 2003

10. Dubash, M.: Moore's Law is dead, says Gordon Moore, Techworld (April 13, 2005), <http://www.techworld.com/opsys/news/index.cfm?NewsID=3477>
11. Feitelson, G.: Optical Computing: A Survey for Computer Scientists. MIT Press, Cambridge (1988)
12. Fitoussi, H.: The Traveling Beams: Optical Solutions for Bounded NP-Complete Problems. In: Summer School on Algorithmic Data Analysis (SADA 2007), Helsinki, Finland (2007); Poster Presentation
13. Garey, M.R., Johnson, D.S.: Computers and Intractability, a guide to the theory of NP-completeness. W. H. Freeman and Company, San Francisco (1979)
14. Goswami, D.: Optical Componenets and Storage Systems. Resonance 8(6), 56–71 (2003)
15. Haist, T., Osten, W.: An Optical Solution For The Traveling Salesman Problem. Opt. Express 15, 10473–10482 (2007)
16. Hyman, A.: Charles Babbage: Pioneer of the Computer. Princeton University Press, Princeton (1982)
17. Optochip green optical network technology, <http://www-03.ibm.com/industries/media/us/detail/news/H255927V64727A97.html>
18. Kash, J.A.: Internal optical interconnects in next generation high performance servers. In: IEEE Conference on Avionics Fiber-Optics and Photonics, pp. 29–30 (2005)
19. <http://www.photonics.com/Spectra/NewProds/jun02/fAmp.ps>
20. [http://www.globalspec.com/ProductFinder/Optics\\_Optical\\_Components/Fiber\\_Optics](http://www.globalspec.com/ProductFinder/Optics_Optical_Components/Fiber_Optics), the Fiber Optic Amplifiers link
21. Lenslet LTD, <http://www.hpcwire.com/hpcwire/hpcwireWWW/03/1017/106185.html>, use <http://www.archive.org>
22. McAulay, A.D.: Optical computer architectures. John Wiley, Chichester (1991)
23. Naughton, T.J.: A model of computation for Fourier optical processors. In: Proc. of SPIE, Optics in Computing, vol. 4089, pp. 24–34 (2000)
24. Oltean, M.: A light-based device for solving the Hamiltonian path problem. In: Calude, C.S., Dinneen, M.J., Păun, G., Rozenberg, G., Stepney, S. (eds.) UC 2006. LNCS, vol. 4135, pp. 217–227. Springer, Heidelberg (2006)
25. Oltean, M., Muntean, O.: Solving the subset-sum problem with a light-based device. Natural Computing (2007) (to appear)
26. Reif, J.H., Tyagi, A.: Efficient parallel algorithms for optical computing with discrete Fourier transform (DFT) primitive. Applied optics 36(29), 7327–7340 (1997)
27. Reif, J.H., Tygar, D., Yoshida, A.: The Computability and Complexity of Optical Beam Tracing. In: 31st Annual IEEE Symposium on Foundations of Computer Science, pp. 106–114 (1990); The Computability and Complexity of Ray Tracing. Discrete and Computational Geometry 11, 265–287 (1994)
28. Rong, H., Liu, A., Jones, R., Cohen, O., Hak, D., Nicolaescu, R., Fang, A., Paniccia, M.: An all-silicon Raman laser. Nature 433, 292–294 (2005)
29. Shaked, N.T., Messika, S., Dolev, S., Rosen, J.: Optical Solution for Bounded NP-Complete Problems. In: A poster in the *Bi-National (Israeli-Italian) Workshop on Optronics, Il-It-Opt* (2005); Proc. of SPIE Symposium on Optics & Photonics the Optical Information Systems IV Conference. San Diego, August 2006, vol. 63110G-1 (2006); Journal version, Journal of Applied Optics. 46(5), 711–724 (February 2007)

30. Shaked, N.T., Simon, G., Tabib, T., Messika, S., Dolev, S., Rosen, J.: Optical Binary Matrix Synthesis for Solving Bounded NP-complete Combinatorial Problems. *Journal of Optical Engineering* 46(10), 108201 (2007)
31. Shamir, A., Tromer, E.: Factoring Large Numbers with the TWIRL Device. In: Boneh, D. (ed.) *CRYPTO 2003*. LNCS, vol. 2729, pp. 1–26. Springer, Heidelberg (2003)
32. Tamir, D., Shaked, N., Wilson, P., Dolev, S.: Electro-Optical DSP of Tera Operations per Second and Beyond. *Journal of the Optical Society of America A, JOSA* (2009); special feature on Optical High-Performance Computing
33. Woods, D.: Optical Computing and Computational Complexity. In: Calude, C.S., Dinneen, M.J., Păun, G., Rozenberg, G., Stepney, S. (eds.) *UC 2006*. LNCS, vol. 4135, pp. 27–40. Springer, Heidelberg (2006)
34. Woods, D., Gibson, J.P.: Lower Bounds on the Computational Power of an Optical Model of Computation. In: Calude, C.S., Dinneen, M.J., Păun, G., Jesús Pérez-Jimenez, M., Rozenberg, G. (eds.) *UC 2005*. LNCS, vol. 3699, pp. 237–250. Springer, Heidelberg (2005); Journal version. *Natural Computing* 7(1), 95–108 (2008)

# Evolutionary Design of Graph-Based Structures for Optical Computing

Mihai Oltean and Oana Muntean

Department of Computer Science,  
Faculty of Mathematics and Computer Science,  
Babeş-Bolyai University, Kogălniceanu 1,  
Cluj-Napoca, 400084, Romania  
{moltean,oanamuntean}@cs.ubbcluj.ro  
<http://www.cs.ubbcluj.ro/~moltean/optical>

**Abstract.** Designing optical devices for solving NP-complete problems is a difficult task. The difficulty consists in constructing a graph which - when traversed by light - generates all possible solutions of the problem to be solved. So far only few devices of this type have been proposed. Here we suggest the use of evolutionary algorithms for solving this problem: the graphs are generated using a special Genetic Programming approach. We have tested our idea on the subset sum problem. Numerical experiments shows the effectiveness of the proposed approach.

**Keywords:** evolutionary algorithms, genetic programming, optical computing, unconventional computing, NP-complete.

## 1 Introduction

The purpose of this research is to assess the usefulness of Evolutionary Algorithms (EAs) [8,12,20] for designing graph-based devices for delay-based optical computing systems.

A common feature of all these devices is the fact that the signals are delayed by a certain amount of time. The existence of a solution is determined by checking whether there is at least one signal which was delayed by a precise amount of time. If we don't find a signal at that moment it means that the problem has no solution.

The difficulty of this approach resides in the design of a delaying system such that the solution can simply be read at an exact moment of time [25]. Up to now these graphs have been manually designed for only few problems: Hamiltonian path [5,6,9,10,21,22], Travelling Salesman problem [5,6,9,10], subset sum [6,23], Diophantine equations [16,18], Exact Cover [24], Clique [5,6], Vertex Cover [5,6], 3-Sat [5,6], 3D-matching [5,6], the unbounded subset sum [17] and Ricochet Robot [11].

Here we use a Genetic Programming [12] variant called Multi Expression Programming (MEP) [20,26] for automatic generation of graphs fitting the requirements imposed by the optical computing. Each MEP chromosome encodes



a possible solution for the problem. Each gene of the chromosome represents a node of the graph together with its neighbors and associated delays. When the evaluation of individuals takes place, all possible paths for the signal are generated.

Offspring obtained by crossover and mutation are always syntactically correct MEP individuals. Thus, no extra processing for repairing newly obtained individuals is needed.

We exemplify our approach by evolutionary designing the graph for the subset sum problem [7,23]. For this purpose we have performed several numerical experiments with various settings for our evolutionary algorithm. Instances up to 4 numbers in the set have been successfully tackled with reasonable populations and number of generations.

The paper is organized as follows: Section 2 describes some basic principles of delayed based optical devices. Section 3 contains a short description of the subset sum problem. The graph where the light is running to form a solution is described in section 4. Section 5 contains a brief description of Evolutionary Algorithms and Genetic Programming. Next section (6) gives a short description of standard Multi Expression Programming. Section 7 deeply describes the proposed evolutionary system. It contains details about the representation, initialization, genetic operators and fitness function. Several numerical experiments are performed in section 8. Section 9 concludes our paper.

## 2 The Manually Designed Optical Devices

This section describes some elements behind the delay-based optical devices used for solving NP-complete problems. For more information the reader is asked to read the following papers: [23,25].

The idea is based on two properties of light (signal):

- The speed of light has a limit. We can delay the ray by forcing it to pass through an optical fiber cable of a certain length.
- The ray can be easily divided into multiple rays of smaller intensity/power. Beam-splitters are used for this operation.

The optical devices have a graph like structure. Generally speaking one operation is performed when a ray passes through a node and one operation is performed when a ray passes through an edge.

- When passing through an arc the light ray is delayed by the amount of time assigned to that arc.
- When the ray is passing through a node it is divided into a number of rays equal to the external degree of that node. Each obtained ray is directed toward one of the nodes connected to the current node.

### 3 The Subset Sum Problem

We exemplify our idea with a classic NP-complete problem: the subset sum [7] which can be simply stated as:

Given a set of positive numbers  $A = \{a_1, a_2, \dots, a_n\}$  and another positive number  $B$ . Is there a subset of  $A$  whose sum equals  $B$ ?

We focus our attention on the YES / NO decision problem. We are not interested in finding the subset generating the solution. Actually we are interested to find only if such subset does exist.

### 4 The Graph for the Subset Sum

The most important part of the device is the graph which - when traversed by light - generates all possible solutions for the problem.

In the current case that we analyze (the subset sum problem) numbers from the given set  $A$  represent the delays induced to the signals (light) that passes through the device. For instance, if numbers  $a_1$ ,  $a_3$  and  $a_7$  generate the expected subset, then the total delay of the signal should be  $a_1 + a_3 + a_7$ .

Thus our graph is composed of a set of nodes and a set of arcs whose length are taken from the given set  $A$ . We also need arcs of 0 lengths whose purpose is to avoid the use of a given number from the initial set.

Such device [23] is depicted in Figure 1. A light ray sent to start node will have the possibility to either traverse a given arc (from the upper part of figure) or to skip it (by traversing the arc of length 0 from the bottom of figure).

In each node (but the last one) a beam-splitter is placed which will split a ray into 2 subrays of smaller intensity.

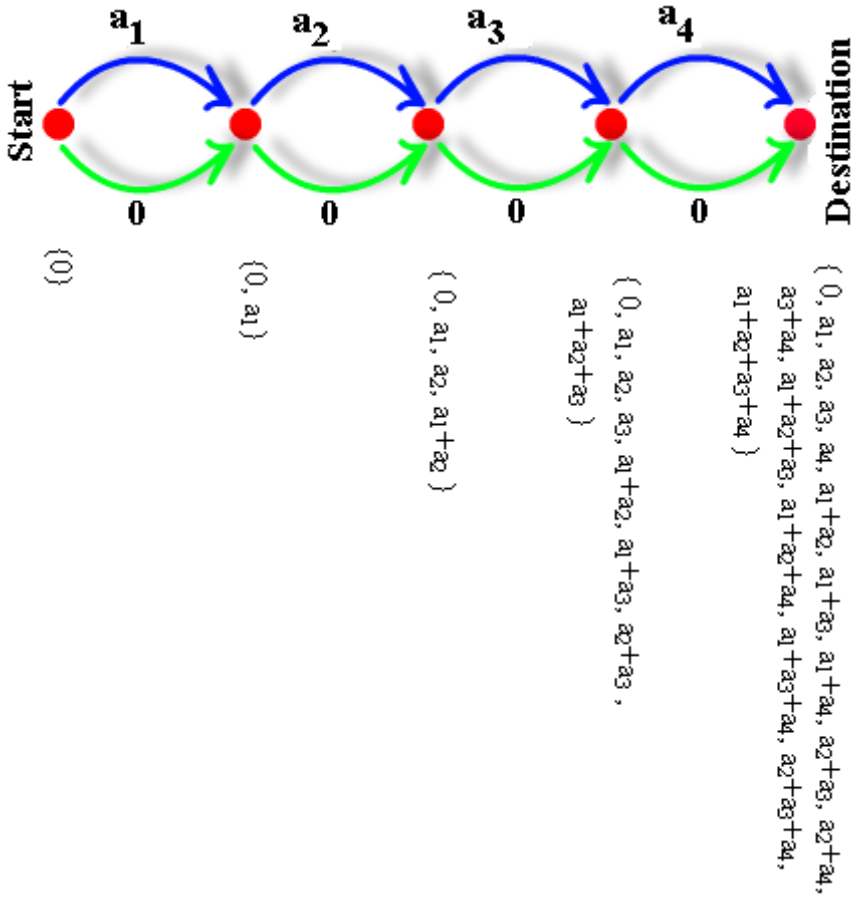
The device will generate all possible subsets of  $A$ . Each subset will delay one of the rays by an amount of time equal to the sum of the lengths of the arcs in that path.

In the graph depicted in Figure 1 the light will enter in *Start* node. It will be divided into 2 subrays of smaller intensity. These 2 rays will arrive into the second node at moments  $a_1$  and 0. Each of them will be divided into 2 subrays which will arrive in the  $3^{rd}$  node at moments 0,  $a_1$ ,  $a_2$ ,  $a_1 + a_2$ . These rays will arrive at no more than 4 different moments.

In the destination node the rays arrive at no more than  $2^n$  different moments. The ray arriving at moment 0 means the empty set. The ray arriving at moment  $a_1 + a_2 + \dots + a_n$  represents the full set. If there is a ray arriving at moment  $B$  means that there is a subset of  $A$  of sum  $B$ .

### 5 Evolutionary Algorithms and Genetic Programming

Evolutionary Algorithms (EAs) [8] are approximation tools for solving difficult real-world problems. They were developed under the pressure generated by the inability of classical (mathematical) methods to solve some real-world problems.



**Fig. 1.** The device for the subset sum problem. Each subset of  $A$  is generated. Skipping arcs have 0 lengths. We have also depicted the moments when different rays arrive in nodes. The moments are represented as sets because they might not be distinct.

Many of these unsolved problems are (or could be turned into) optimization problems. Solving an optimization problem means finding of solutions that maximize or minimize a criteria function [20].

One of the most important algorithms belonging to this class is Genetic Programming (GP) [12,13,14]. Genetic Programming is widely known as the technique which writes computer programs. Instead of evolving solutions for a particular problem instance, GP is mainly intended for discovering computer programs able to solve classes of problems.

Many variants of GP have been proposed in the recent years. Their aims were various: simpler implementation, higher speed, smaller memory requirements, the capability of working with particular hardware architectures etc. Another motivation is given by the problems where some representations work better than the others [26].

One of the GP variants is Multi Expression Programming (MEP) [20,26]. This technique will be used in this paper for performing several numerical experiments. In the next section we briefly describe standard Multi Expression Programming and then we modify it for adapting it to our current purpose.

## 6 Multi Expression Programming

Multi Expression Programming (MEP) [20] is a Genetic Programming variant that uses a linear representation of chromosomes. MEP individuals are strings of genes encoding complex computer programs.

When MEP individuals encode expressions, their representation is similar to the way in which compilers translate *C* or *Pascal* expressions into machine code.

An example of chromosome  $C$  using the function set  $F = \{+, *\}$  and the set of terminals  $T = \{a, b, c, d\}$  is given below:

```

1: a
2: b
3: + 1, 2
4: c
5: d
6: + 4, 5
7: * 3, 5
8: + 2, 6

```

A unique MEP feature is the ability of storing multiple solutions of a problem in a single chromosome. What we have encoded in chromosome  $C$  are the following expressions:

$$\begin{aligned}
 E_1 &= a \\
 E_2 &= b \\
 E_4 &= c \\
 E_5 &= d \\
 E_3 &= a + b \\
 E_6 &= c + d \\
 E_7 &= (a + b) * d \\
 E_8 &= b * (c + d)
 \end{aligned}$$

Usually, the best solution is chosen for fitness assignment. When solving symbolic regression or classification problems (or any other problems for which the training set is known before the problem is solved) MEP has the same complexity as other techniques storing a single solution in a chromosome.

Evaluation of the expressions encoded into a MEP individual can be performed by a single parsing of the chromosome.

Offspring obtained by crossover and mutation are always syntactically correct MEP individuals (computer programs). Thus, no extra processing for repairing newly obtained individuals is needed.

There are 2 main differences between GP and MEP. First of all MEP encodes multiple solutions instead of one and secondly, MEP uses a linear representation while GP has a tree based representation of solutions. Linear encoding of computer programs means that we usually work with arrays of fixed or variable lengths. Specifically:

1. we generate arrays of instructions, having a particular meaning,
2. we recombine them by using string-based crossover operators such as those from binary encoding (such as one-cutting point, two cutting points, uniform recombination etc.) [8],
3. we mutate them using operators inspired from the binary encoding or from other representations [8].

## 7 The Proposed MEP-Based Approach

Here we deeply describe the proposed evolutionary approach. We have made several modifications to standard MEP in order to make it suitable for our purpose.

### 7.1 Representation

MEP genes are strings of a variable length. The number of genes per chromosome is fixed. This number defines the length of the chromosome. Even if this number is fixed we still can have solutions of variable length because usually not all genes are utilized.

Each gene represent a node and stores the arcs leaving that node (the adjacency list) and the length for those arcs.

Cycles can appear in this structure because there is no restriction on why what kind of nodes appear in the adjacency list. This makes the fitness function computationally expensive and difficult to compute.

There is still one natural restriction: a node cannot appear multiple times in the adjacency list of another node. A node may appear in its own adjacency list.

#### Example

Consider a representation where the numbers on the left positions stand for gene labels. Labels do not belong to the chromosome. They represent the node index.

Since all nodes are identical (contain a beam splitter) we don't need a function set as in the standard MEP.

The set of terminals is made of a set of nodes and the possible lengths for the arcs connecting the current node with node from its adjacency list.

Suppose that we deal with a problem with a set of 4 numbers:  $A = \{a_1, a_2, a_3, a_4\}$ . In this case the terminal set could be:

$T = \{1, 2, 3, \dots, a_1, a_2, a_3, a_4, 0\}$ , where  $1, 2, 3, \dots$  are the nodes and  $a_1, a_2, a_3, a_4, 0$  are the arcs' length. The number of nodes employed by our solution is not known the beginning. The maximal number of nodes is equal the chromosome length. We do provide a large initial chromosome length.

The length of each arc is given right after a node.

Choosing the length for each arc is a difficult task. For some problems (such as the subset sum) the lengths are taken directly from the problem's input, but for some other cases (take for instance the Hamiltonian path [21]) the lengths have complicated formulas:  $2^n - 2^i$ , where  $0 \leq i \leq n$ . In this case we also need to use Genetic Programming for generating complex mathematical formulas. However, for the case currently analyzed we will simplify this aspect by using only some values taken from the problem input.

An example of chromosome  $C$  is given below:

1: 3,  $a_2$ , 5, 0  
 2: 4,  $a_1$ , 2, 0, 6,  $a_4$   
 3: 6, 0  
 4: 1,  $a_2$ , 2,  $a_1$ , 5,  $a_3$   
 5: 2,  $a_4$   
 6: 4,  $a_4$ , 3, 0

This chromosome must be interpreted as follows:

- The maximal number of nodes in a solution is 6. However, any number between 1 and 6 can be the actual solution since not all nodes must be used.
- Node 1 has 2 out nodes: 3 and 5. The arc (1,3) has length  $a_2$  and arc (1,5) has length 0.
- Node 2 has 3 out nodes: 4, 2 and 6. The arc (2,4) has length  $a_1$ , arc (2,2) has length 0 and arc (2,6) has length  $a_4$ . Note here that 2 has an arc to itself.
- Node 3 has 1 out node: 6. The arc (3,6) has length 0.
- Node 4 has 3 out nodes: 1, 2 and 5. The arc (4,1) has length  $a_2$ , arc (4,2) has length  $a_1$  and arc (4,5) has length  $a_3$ .
- Node 5 has 1 out node: 2. The arc (5,2) has length  $a_4$ .
- Node 6 has 2 out nodes: 4 and 3. The arc (6,4) has length  $a_4$  and arc (6,3) has length 0.

As explained in section 2 each device has a *start* node and a *destination* node. In our case the *start* node is node 1 and the *destination* node will be computed during the fitness evaluation.

## 7.2 Initialization

Generation of chromosomes is done randomly. For each node we randomly choose the number of nodes in its adjacency list and then we randomly generate each node in the list. After each node we randomly choose the length of the arc connecting that node with its predecessor.

## 7.3 Fitness Assignment

During fitness evaluation we compute how good the current chromosome is.

For the subset sum problem which is investigated here we want to generate all possible subsets of the given set.

A perfect solution is that one which contains a destination node in which arrive delayed rays encoding all subsets of the given set. A less perfect solution is the one for which not all subsets are generated. This is why a natural way to define the fitness is to count how many subsets have been generated.  $2^n$  is the best fitness possible while 0 is the worst fitness possible.

For computing the fitness we have no choice but to simulate the signal passing through the device. Of course, this operation requires an exponential amount of memory because the number of signals grows exponentially. Partial results are stored similarly with Dynamic Programming [3].

Also, for each signal we have to store its entire path. When the signal is divided by the beam-splitters each subsignal will inherit the information carried by its parent signal.

Because we want to limit the amount of computer resources involved in this operation we have imposed the following constraints:

- When the total delay of a given signal exceeds a certain threshold we stop propagating that signal. In the case of the subset sum problem we stop when the delay of a signal is larger than  $B$ . It makes no sense to continue since we are interested only in finding a subset of sum  $B$ .
- Because we allow arcs of length 0, we can have a huge number of divisions of the signal without increasing the total delay of that signal. In this case we have imposed a limit on the total number of divisions that a signal can have.

The problem now is which node will be the destination node. There is neither practical nor theoretical evidence that one of the nodes is better than the others. Moreover, Wolpert and McReady [30] with their well known theorems for No Free Lunch for Search and Optimization proved that we cannot use the search algorithm's behavior so far for a particular test function to predict its future behavior on that function.

Preserving the MEP basic-idea with multiple solutions in the same chromosome we say again that the fitness of the entire chromosome is set as the fitness of the best solution encoded by that chromosome. In our case the fitness is given by the best *destination* node (in which arrive the highest number of signals encoding subsets of A) in that device. There is no extra cost of doing that because when the signal was propagated through the graph it is propagated through all reachable nodes.

Note that if some other signals not encoding subsets arrive in a node, the quality of that node is decreased correspondingly. Thus, we can have negative fitnesses too.

It is obvious that some parts of a MEP chromosome are not used. Some GP techniques, like Linear GP, remove non-coding sequences of chromosome during the search process. As already noted [4] this strategy does not give the best results. The reason is that sometimes, a part of the useless genetic material has to be kept in the chromosome in order to maintain population diversity.

Other techniques such as Cartesian GP (CGP) [15] employ a different strategy for selecting the nodes which provide the output: they simply evolve these nodes as part of the chromosome. This is also good, but during numerical experiments we have noticed that selecting the best solution found works better than evolving it.

### 7.4 Search Operators

The search operators used within MEP algorithm are crossover and mutation. These search operators preserve the chromosome structure.

**Crossover.** By crossover two parents are selected and are recombined.

Two variants of recombination have been considered and tested within our MEP implementation: one-point recombination and uniform recombination.

#### One-point recombination

One-point recombination operator in MEP representation is similar to the corresponding binary representation operator. One crossover point is randomly chosen and the parent chromosomes exchange the sequences at the right side of the crossover point.

#### Example

Consider the parents  $C_1$  and  $C_2$  given below. Choosing the crossover point after position 3 two offspring,  $O_1$  and  $O_2$  are obtained as given in Table 1.

Table 1. MEP one-point recombination

Parents		Offspring	
$C_1$	$C_2$	$O_1$	$O_2$
<b>1: 3, a<sub>2</sub>, 5, 0</b>	1: 2, 0	<b>1: 3, a<sub>2</sub>, 5, 0</b>	1: 2, 0
<b>2: 4, a<sub>1</sub>, 2, 0, 6, a<sub>4</sub></b>	2: 3, a <sub>2</sub> , 1, 0	<b>2: 4, a<sub>1</sub>, 2, 0, 6, a<sub>4</sub></b>	2: 3, a <sub>2</sub> , 1, 0
<b>3: 6, 0</b>	3: 6, a <sub>1</sub>	<b>3: 6, 0</b>	3: 6, a <sub>1</sub>
<b>4: 1, a<sub>2</sub>, 2, a<sub>1</sub>, 5, a<sub>3</sub></b>	4: 4, a <sub>2</sub> , 2, a <sub>1</sub> , 1, a <sub>2</sub>	4: 4, a <sub>2</sub> , 2, a <sub>1</sub> , 1, a <sub>2</sub>	<b>4: 1, a<sub>2</sub>, 2, a<sub>1</sub>, 5, a<sub>3</sub></b>
<b>5: 2, a<sub>4</sub></b>	5: 5, a <sub>4</sub>	5: 5, a <sub>4</sub>	<b>5: 2, a<sub>4</sub></b>
<b>6: 4, a<sub>4</sub>, 3, 0</b>	6: 1, a <sub>3</sub>	6: 1, a <sub>3</sub>	<b>6: 4, a<sub>4</sub>, 3, 0</b>

#### Uniform recombination

During the process of uniform recombination, offspring genes are taken randomly from one parent or another.

#### Example

Let us consider the two parents  $C_1$  and  $C_2$  given below. The two offspring  $O_1$  and  $O_2$  are obtained by uniform recombination as given in Table 2.

**Mutation.** Each symbol in the chromosome may be the target of the mutation operator. Some symbols in the chromosome are changed by mutation.



**Table 2.** MEP uniform recombination

Parents		Offspring	
$C_1$	$C_2$	$O_1$	$O_2$
<b>1: 3, a<sub>2</sub>, 5, 0</b>	1: 2, 0	<b>1: 3, a<sub>2</sub>, 5, 0</b>	1: 2, 0
<b>2: 4, a<sub>1</sub>, 2, 0, 6, a<sub>4</sub></b>	2: 3, a <sub>2</sub> , 1, 0	2: 3, a <sub>2</sub> , 1, 0	<b>2: 4, a<sub>1</sub>, 2, 0, 6, a<sub>4</sub></b>
<b>3: 6, 0</b>	3: 6, a <sub>1</sub>	3: 6, a <sub>1</sub>	<b>3: 6, 0</b>
<b>4: 1, a<sub>2</sub>, 2, a<sub>1</sub>, 5, a<sub>3</sub></b>	4: 4, a <sub>2</sub> , 2, a <sub>1</sub> , 1, a <sub>2</sub>	4: 4, a <sub>2</sub> , 2, a <sub>1</sub> , 1, a <sub>2</sub>	<b>4: 1, a<sub>2</sub>, 2, a<sub>1</sub>, 5, a<sub>3</sub></b>
<b>5: 2, a<sub>4</sub></b>	5: 5, a <sub>4</sub>	<b>5: 2, a<sub>4</sub></b>	5: 5, a <sub>4</sub>
<b>6: 4, a<sub>4</sub>, 3, 0</b>	6: 1, a <sub>3</sub>	6: 1, a <sub>3</sub>	<b>6: 4, a<sub>4</sub>, 3, 0</b>

The number of nodes in the adjacency list of each node can be changed. Also the length associated to each arc can be changed.

### Example

Consider the chromosome  $C$  given below. If the boldfaced symbols are selected for mutation an offspring  $O$  is obtained as given in Table 3.

**Table 3.** MEP mutation

$C$	$O$
1: 3, a <sub>2</sub> , 5, 0	1: 3, a <sub>2</sub> , 5, 0, <b>4, a<sub>1</sub></b>
2: 4, a <sub>1</sub> , 2, 0, 6, a <sub>4</sub>	2: 4, a <sub>1</sub> , 2, <b>a<sub>5</sub></b>
3: 6, 0	3: 6, 0
4: 1, a <sub>2</sub> , 2, a <sub>1</sub> , 5, a <sub>3</sub>	4: 1, a <sub>2</sub> , 2, <b>a<sub>3</sub></b> , 5, a <sub>3</sub>
5: 2, a <sub>4</sub>	5: 2, a <sub>4</sub> , <b>1, a<sub>2</sub></b>
6: 4, a <sub>4</sub> , 3, 0	6: 4, a <sub>4</sub> , 3, 0

## 7.5 MEP Algorithm

Standard MEP algorithm uses steady-state evolutionary model [29] as its underlying mechanism.

The MEP algorithm starts by creating a random population of individuals. The following steps are repeated until a given number of generations is reached: Two parents are selected using a standard selection procedure. The parents are recombined in order to obtain two offspring. The offspring are considered for mutation. The best offspring  $O$  replaces the worst individual  $W$  in the current population if  $O$  is better than  $W$ .

The variation operators ensure that the chromosome length is a constant of the search process. The algorithm returns as its answer the best solution evolved along a fixed number of generations.

The standard MEP algorithm is outlined below:

**Standard MEP Algorithm**

```

S1. Randomly create the initial population  $P(0)$ 
S2. for  $t = 1$  to  $Max\_Generations$  do
S3.   for  $k = 1$  to  $|P(t)| / 2$  do
S4.      $p_1 = Select(P(t));$  // select one individual from the current population
S5.      $p_2 = Select(P(t));$  // select the second individual
S6.      $Crossover(p_1, p_2, o_1, o_2);$  // crossover the parents  $p_1$  and  $p_2$ 
           // the offspring  $o_1$  and  $o_2$  are obtained
S7.      $Mutation(o_1);$  // mutate the offspring  $o_1$ 
S8.      $Mutation(o_2);$  // mutate the offspring  $o_2$ 
S9.     if  $Fitness(o_1) > Fitness(o_2)$ 
S10.    then if  $Fitness(o_1) >$  the fitness of the worst individual
           in the current population
S11.    then Replace the worst individual with  $o_1$ ;
S12.    else if  $Fitness(o_2) >$  the fitness of the worst individual
           in the current population
S13.    then Replace the worst individual with  $o_2$ ;
S14.    endifor
S15. endifor

```

## 8 Numerical Experiments

In this section we perform several numerical experiments for evolving graph structures for optical computing devices. Subset sum problem with sets of 3 and 4 numbers are used. For larger sets we can design a solution by generalizing from the smaller sets.

The parameters of the MEP algorithm are given in Table 4.

We have performed 30 independent runs with different seeds because evolutionary algorithms use random numbers and a single run is not conclusive.

**Table 4.** The parameters for the MEP algorithm used for discovering solutions for the subset sum problem with 3 and 4 numbers

Parameter	Value
Population size	500
Number of generations	50
Chromosome length	8
Maximal divisions allowed per signal	10
Mutation probability	0.2
Crossover type	Uniform
Crossover probability	0.9
Selection	Binary tournament
Number of runs	30

For the subset sum problem with 3 nodes the success rate was 90%. That is in 27 out of 30 runs we have obtained a perfect solution (all  $2^3$  subsets have been generated in the *destination* node).

For the subset sum problem with 4 nodes the success rate was 36%. That is in 11 out of 30 runs we have obtained a perfect solution (all  $2^4$  subsets have been generated in the *destination* node). It is obvious that the difficulty of the problem will increase as the size of the set increases.

In almost all cases the standard design (see Figure 1) was obtained. However, in some particular runs, some other strange designs were obtained (which are not presented here due to the space limitation). We expected to obtain such designs because usually the evolution can follow a path which is not always the logical one. However, the strange designs were not as efficient (in the number of nodes and arcs) as the standard design. This is why we have not focused too much on analyzing them.

## 9 Conclusions and Future Work

Here we have used evolutionary algorithms as an automatic tool for designing graphs for optical delay-based systems. Numerical experiments have shown good results for several small instances of the subset sum problem. Large instances can be easily solved by generalizing the design obtained in the experiments.

Further work directions are focused on:

- Improving the speed of MEP by using Sub Machine Code GP [27,28]. Experiments performed in [27] have shown that speed of GP was increased more than 1 order of magnitude. This will help us to solve larger instances of the problem.
- Improving the search by using Automatically Defined Functions (ADFs) [13]. This will help us to solve larger instances due to the generalization ability of ADFs.
- Using Genetic Programming for generating the length of arcs required by the device. Some other problems, such as the Hamiltonian path, use complex formulas for expressing the length based on the values given as input.
- Analyzing the relationship between the success rate and different parameters of the algorithm (such as the population size, number of generations, search operators probability etc). This could help us to solve larger instances of the problem.

## Acknowledgment

This work was supported by grant CNCSIS-IDEI-543/2007.

The source code for Multi Expression Programming can be downloaded from [www.mep.cs.ubbcluj.ro](http://www.mep.cs.ubbcluj.ro).

## References

1. Aaronson, S.: NP-complete problems and physical reality. ACM SIGACT News Complexity Theory Column, March. ECCC TR05-026, quant-ph/0502072 (2005)
2. Banzhaf, W., Nordin, P., Keller, E.R., Francone, F.D.: Genetic Programming - An Introduction. Morgan Kaufmann, San Francisco (1998)
3. Bellman, R.: Dynamic Programming. Princeton University Press, Princeton (1957)
4. Brameier, M., Banzhaf, W.: A Comparison of Linear Genetic Programming and Neural Networks in Medical Data Mining. IEEE Transactions on Evolutionary Computation 5, 17–26 (2001)
5. Dolev, S., Nir, Y.: Optical Implementation of Bounded non Deterministic Turing Machine, Patent Filed May 2003 in Israel, May 2004 USA (2004)
6. Dolev, S., Fitoussi, H.: The Traveling Beams, Optical Solutions for Bounded NP-Complete Problems. In: Crescenzi, P., Prencipe, G., Pucci, G. (eds.) FUN 2007. LNCS, vol. 4475, pp. 120–134. Springer, Heidelberg (2007)
7. Garey, M.R., Johnson, D.S.: Computers and intractability: A guide to NP-Completeness. Freeman & Co., San Francisco (1979)
8. Goldberg, D.E.: Genetic Algorithms in Search, Optimization, and Machine Learning. Addison-Wesley, Reading (1989)
9. Haist, T., Osten, W.: An Optical Solution For The Traveling Salesman Problem. Opt. Express 15, 10473–10482 (2007)
10. Haist, T., Osten, W.: An Optical Solution For The Traveling Salesman Problem:erratum. Opt. Express 15, 12627–12627 (2007)
11. Haist, T., Osten, W.: Ultra-fast digital optical arithmetic using waveoptical computing. In: Dolev, S., Haist, T., Oltean, M. (eds.) OSC 2008. LNCS, vol. 5172, pp. 33–45. Springer, Heidelberg (2008)
12. Koza, J.R.: Genetic Programming: on the Programming of Computers by Means of Natural Selection. MIT Press, Cambridge (1992)
13. Koza, J.R.: Genetic Programming II: Automatic Discovery of Reusable Subprograms. MIT Press, Cambridge (1994)
14. Koza, J.R., et al.: Genetic Programming III: Darwinian Invention and Problem Solving. Morgan Kaufmann, San Francisco (1999)
15. Miller, J.F., Thomson, P.: Cartesian Genetic Programming. In: Poli, R., Banzhaf, W., Langdon, W.B., Miller, J., Nordin, P., Fogarty, T.C. (eds.) EuroGP 2000. LNCS, vol. 1802, pp. 121–132. Springer, Heidelberg (2000)
16. Muntean, O.: Optical Solutions for NP-complete problems, graduation thesis, Faculty of Mathematics and Computer Science, Babes-Bolyai University, Cluj-Napoca, Romania, defended July 3 (2007)
17. Muntean, O., Oltean, M.: Using light for solving the unbounded subset-sum problem. International Journal of Innovative Computing, Information and Control 5(8), 2159–2167 (2009)
18. Muntean, O., Oltean, M.: Deciding whether a linear Diophantine equation has solutions by using a light-based device (submitted) (2008)
19. Nordin, P.: A Compiling Genetic Programming System that Directly Manipulates the Machine Code. In: Kinnear Jr., K.E. (ed.) Advances in Genetic Programming, pp. 311–331. MIT Press, Cambridge (1994)
20. Oltean, M., Groşan, C.: Evolving evolutionary algorithms using multi expression programming. In: Banzhaf, W., Ziegler, J., Christaller, T., Dittrich, P., Kim, J.T. (eds.) ECAL 2003. LNCS (LNAI), vol. 2801, pp. 651–658. Springer, Heidelberg (2003)

21. Oltean, M.: A light-based device for solving the Hamiltonian path problem. In: Calude, C.S., Dinneen, M.J., Păun, G., Rozenberg, G., Stepney, S. (eds.) UC 2006. LNCS, vol. 4135, pp. 217–227. Springer, Heidelberg (2006)
22. Oltean, M.: Solving the Hamiltonian path problem with a light-based computer. *Natural Computing* 7(1), 57–70 (2008)
23. Oltean, M., Muntean, O.: Solving the subset-sum problem with a light-based device. *Natural Computing* 8(2), 321–331 (2009)
24. Oltean, M., Muntean, O.: Exact Cover with light. *New Generation Computing* 26(4), 329–346 (2008)
25. Oltean, M., Muntean, O.: Solving NP-Complete Problems with Delayed Signals: An Overview of Current Research Directions. In: Dolev, S., Haist, T., Oltean, M. (eds.) OSC 2008. LNCS, vol. 5172, pp. 115–127. Springer, Heidelberg (2008)
26. Oltean, M., Grosan, C., Diosan, L., Mihaila, C.: Genetic Programming with linear representation: a survey. *International Journal on Artificial Intelligence Tools* 19(2), 197–238 (2009)
27. Poli, R., Langdon, W.B.: Sub-machine Code Genetic Programming. In: Spector, L., Langdon, W.B., O'Reilly, U.-M., Angeline, P.J. (eds.) *Advances in Genetic Programming* 3, ch. 13. MIT Press, Cambridge (1999)
28. Poli, R., Page, J.: Solving High-Order Boolean Parity Problems with Smooth Uniform Crossover, Sub-Machine Code GP and Demes. *Journal of Genetic Programming and Evolvable Machines*, 1–21 (2000)
29. Syswerda, G.: Uniform Crossover in Genetic Algorithms. In: Schaffer, J.D. (ed.) *Proceedings of the 3rd International Conference on Genetic Algorithms*, MKP, CA, pp. 2–9 (1989)
30. Wolpert, D.H., McReady, W.G.: No Free Lunch Theorems for Optimisation. *IEEE Transaction on Evolutionary Computation* 1, 67–82 (1997)

# Computing a Solution for the Subset Sum Problem with a Light Based Device

Md. Raqibul Hasan<sup>1</sup> and M. Sohel Rahman<sup>1,2</sup>

<sup>1</sup> Department of CSE, BUET, Dhaka-1000, Bangladesh

[raqib\\_cse@yahoo.com](mailto:raqib_cse@yahoo.com)

<http://www.buet.ac.bd/cse>

<sup>2</sup> Algorithm Design Group

Department of Computer Science

King's College London, Strand, London WC2R 2LS, England

[msrahman@cse.buet.ac.bd](mailto:msrahman@cse.buet.ac.bd)

<http://www.dcs.kcl.ac.uk/adg>

**Abstract.** We propose a new way for computing a solution to the subset sum problem. Here, we use a special computational device which uses light ray. The device has a graph-like representation and the light traverses it by following the routes given by the connections between nodes. Our device can solve the subset sum decision problem as well as can compute a solution instance for it.

## 1 Introduction

One of the interesting areas in computer science research is to explore unconventional methods to solve various problems. Different problems that are hard to solve efficiently in conventional methods, have received significant attention in the literature from this point of view and hence a number of unconventional approaches have been explored. Example of these unconventional methods include DNA computing [1], Quantum computing [2], Soap bubbles [3,4], Gear-based computers [5], Adiabatic algorithms [6] etc. Optical computing is another interesting and exciting avenue for research in this regard. Various properties of light enables us to solve some real world problems more easily than conventional electric based counterparts. To the best of our knowledge, the idea of using light instead of electric power to perform computations dates back to 1929 when G. Tauschek obtained a patent on Optical Character Recognition (OCR) in Germany [7]. Later various researchers have used the properties of light to achieve faster solutions to problems than is possible in conventional computers. An example is the  $n$ -point discrete Fourier Transform Computation which can be performed in only unit time [8,9]. Quite recently, an important practical step was taken by the Intel researchers who developed the first continuous wave all-silicon laser using a physical property called the Raman Effect [10,11,12,13].

Very recently, a number of researchers have suggested light-based devices to solve combinatorially interesting problems. Most of the problems handled in this way are hard to solve in the conventional computing paradigm and are

categorized as NP-Complete or NP-Hard problems. For example, a system which solves the Hamiltonian Path problem (an NP-Complete problem [14]) using light and its properties has been proposed in [15]. Similar system was devised in [16] and [17] to solve the Exact Cover Problem and the subset sum problem as a decision problem respectively, both of which are NP-Complete problems [14].

The quest for optical solutions by no means is confined only on NP-Complete and/or NP-Hard problems. A number of interesting polynomial-time solvable (in conventional computing) problems have been investigated from this point of view as well. For example, in [18], the physical concept of refraction and dispersion of light have been cleverly explored to solve the sorting problem. An stable version of this sort, known as the Rainbow Sort, has been proposed in [19]. Very recently, solutions to the string matching problem has also been proposed [20] using light and optical filters for performing computations.

In this paper, we revisit the Subset Sum problem. The Subset Sum Problem is NP-Complete and has been explored before from optical computing point of view [17]. In [17] the authors have given the solution for the corresponding decision problem of the subset sum problem. In [17] it was posed as an open problem to efficiently compute the solutions to the optimization version of the subset sum problem. In this paper, we solve that open problem and present a way to compute a solution of the problem efficiently. The paper is organized as follows. Section 2 formally defines and discuss about the subset sum problem. In Sections 3 proposed device is presented. Finally we briefly conclude in in Section 7.

## 2 Subset Sum Problem

We start this section with a formal definition of the subset sum problem.

*Problem 1.* Subset Sum Problem

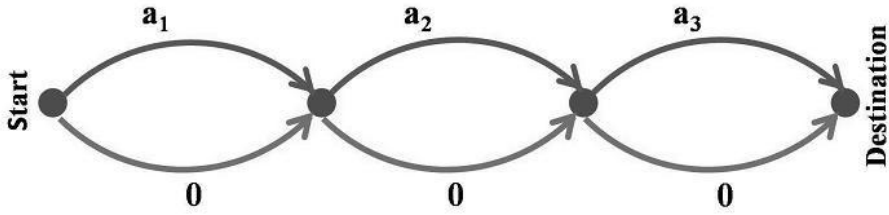
**Instance:** We are given a set of positive numbers  $A = \{a_1, a_2, \dots, a_n\}$  and another positive number  $B$ .

**Question:** Is there a subset  $S$  of  $A$  such that the summation of the values of  $S$  equals  $B$

The problem belongs to the class of NP-complete problems [11]. No polynomial time algorithm is known for it. In the paper [17], the authors presented a light based device to solve the Subset Sum problem efficiently. Notably, the device presented in [17] only can solve the problem as a decision problem; it doesn't have the capability to provide a solution. Indeed, the author pointed out in the conclusion that designing a device with such capability should be explored as a future research.

## 3 The Device

We design our device in a step by step manner. We start from the device proposed in [17] (Figure 1).



**Fig. 1.** Each subset of  $A$  is generated, but this device cannot be implemented in practice because we cannot have cables of length  $0$

The main two properties of light that are used in the device are listed below:

1. The speed of light has a limit and we can delay the ray by forcing it to pass through an optical fibre cable of a certain length.
2. The ray can be easily divided into multiple rays of smaller intensity/power. Beam splitters are used for this operation [21,22].

As can be seen from the Figure 1, the device has a graph-like structure. The following two simple operations are performed by the device.

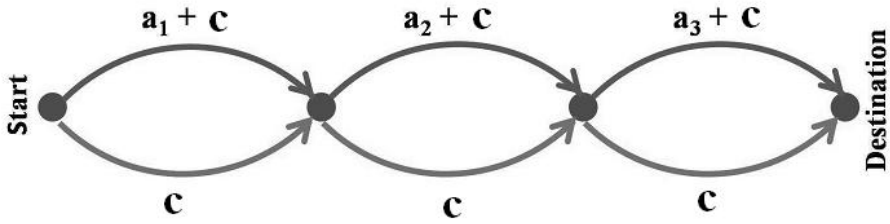
1. When passing through an arc the light ray is delayed by the amount of time assigned to the arc.
2. When passing through a node the light ray is divided into a number of rays equal to the external degree of that node.

The basic idea of the system is as follows. The system is constructed in such a way that if  $B = a_1 + a_4 + a_5$ , then we must be able to sense a light ray at the destination node at time  $a_1 + a_4 + a_5$ . One problem is that, in reality, it is not possible to have arcs (cables) of length  $0$ . To overcome this problem, a constant  $c$  is added to the length of each cable. The schematic view of this device is depicted in Figure 2. It is easy to realize that, now, at the destination will have to sense a light array at moment  $B + n * c$  instead of  $B$ .

## 4 The Modified Device

Recall that our goal is to provide a solution for the problem in addition to the answer of the decision problem. In this section we will modify the device accordingly. The main idea of the system is as follows. First we will find answer for the corresponding decision version of the subset sum problem according to the strategy of [17] described in the previous section (Figure 2). If the answer to the question asked in the decision problem turns out to be positive, only then we will compute the solution. Essentially, the new device would be a modification of the device of Figure 2. In what follows, we will say that a problem instance is positive if there exists a solution for that problem instance and negative otherwise.

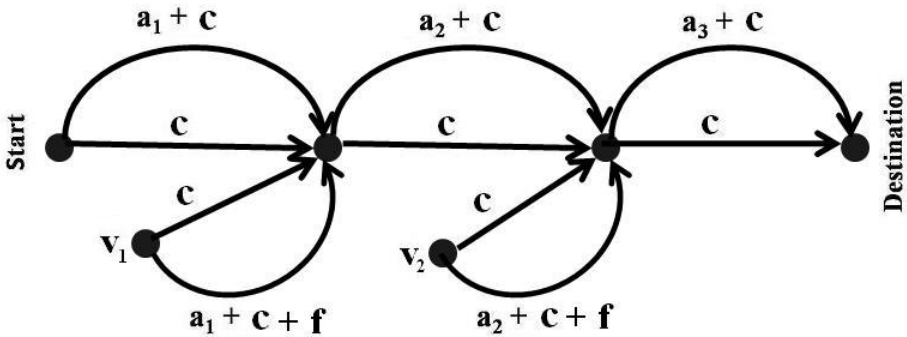




**Fig. 2.** A schematic representation of the device used for solving an instance with 3 numbers. On each arc we have depicted its length. There are  $n$  cables of length  $c$  and  $n$  cables of length  $a_i + c$  ( $1 \leq i \leq n$ ). This device does generate all possible subsets of  $A$  and it can be implemented in practice.

Assume that for a particular positive problem instance, there is only one subset  $S$  of  $A$  whose sum equals  $B$ . As there is a solution, in the device of Figure 2, a ray will arrive at moment  $B + n * c$  at the destination node. Now we want to find out the subset  $S$  of  $A$  whose sum equals  $B$ . For this purpose, we need to extend our device as illustrated in Figure 3. The value of  $f$  will be such that  $f \neq a_i$  for  $i = 1, 2, \dots, n$  and  $a_i + f \neq a_j$  for  $i = 1, 2, 3, \dots, n$  and  $j = 1, 2, 3, \dots, n$ . For instance we can take  $f = 0.5$ . Note that, in the modified device we have added  $n - 1$  new nodes  $v_i, 1 \leq i \leq n - 1$ . Now, to find out the solution set  $S$  we have to execute the following algorithm. sequence of steps. Assume that,  $B_1 = B$  and  $S = \emptyset$ .

1. For each node  $v_i$  where  $i = 1, 2, \dots, n - 1$ , do the following in sequence:
2. Send light ray from node  $v_i$
3. If there is a ray arriving at moment  $B_i + (n - i + 1) * c + f$  at the destination node then  $a_i \in S$ . So, set  $S = S \cup a_i$ ; otherwise  $a_i \notin S$ .
4.  $B_{i+1} = B_i - a_i$  if  $a_i \in S$ ; otherwise  $B_{i+1} = B_i$ .



**Fig. 3.** Final version of the device

After executing the above steps, if  $B_n \neq 0$ , then  $a_n \in S$  and we set  $S = S \cup a_n$ ; otherwise  $a_n \notin S$ . Now we will give an proof that according to the strategy stated above we can find out the subset whose sum equals  $B$  if only one such subset exist.

**Lemma 1.** *The device can find out the subset  $S$  of  $A$  whose sum equals  $B$  if only one such subset exist.*

*Proof.* First we prove that it is decided correctly whether  $a_1 \in S$  or not. Assume that  $a_1 \in S$ . If  $a_1 \in S$ , then, the ray which reach the destination of the device of Figure 2 at moment  $B + n * c$  use the arc with delay  $a_1 + c$ . In the modified device (Figure 3), the arc of delay  $a_1 + c$  is basically replaced by an arc with delay  $a_1 + c + f$ . Thus, when light is sent from node  $v_1$ , the ray will arrive at the destination at moment  $B + n * c + f$ . On the other hand, it is easy to realize that if  $a_1 \notin S$ , the light ray sent from node  $v_1$  will arrive at the destination at moment  $B + n * c$ ; not at  $B + n * c + f$ . This is ensured by the definition of  $f$  and hence we can correctly decide whether  $a_1 \in S$  or not.

Now, in general, once we are decided about  $a_i$ , we adjust  $B_{i+1}$  accordingly and hence we can apply the same strategy to decide about  $a_{i+1}$  and hence the result follows.  $\square$

#### 4.1 Existence of More Than One Solution

In set  $A$  we have  $n$  numbers. There are  $2^n$  subsets of  $A$ , among them  $2^n - 1$  are nonempty. Let, we have two subset  $S_i$  and  $S_j$ . We will arrange the elements of  $S_i$  and  $S_j$  such that if  $p < q$ ,  $a_p$  will appear before  $a_q$ . Let, after sorting  $S_i = \{a_{i_1}, a_{i_2}, \dots, a_{i_k}\}$  and  $S_j = \{a_{j_1}, a_{j_2}, \dots, a_{j_m}\}$ .  $S_i$  will appear before  $S_j$  in the list if there is at least one  $i_\ell$  such that  $i_p = j_p$  for  $p = 1, 2, \dots, \ell - 1$  and  $i_\ell < j_\ell$ . If there is more than one subset of  $A$  whose sum equals  $B$ , our device will give the subset which appear earlier in the list of the solution subsets listed according to the stated strategy.

## 5 Physical Implementation

For implementing the proposed device the following components are required:

- a light source for the start node and each of node  $v_i$  for  $i = 1, 2, \dots, n - 1$ .
- Beam-splitters for splitting a light beam into two light rays. Half silvered mirror is a good example for beam-splitter.
- Optical fibers of various length.
- Light sensor at the destination node, which converts optical pulses to electric signals. Photo diode is a good example for light sensor.
- Oscilloscope, a tool for detecting a fluctuation of power generated by photo diode.

## 6 Complexity

Number of node is of  $O(n)$  and number of subpath is of  $O(n)$ . The ray encoding the solution takes  $O(B + n * c)$  time to reach the destination node. So the overall running time of the device is  $O(B * n + n^2)$ .

The intensity of the signal decreases exponentially with the number of nodes. This is why the required power is proportional to  $2^n$ .

## 7 Conclusion and Future Work

In this paper we have designed a light based device to solve the subset sum problem and find out the solution set. Our device can find out one solution set if more than one solution exist. Techniques to enumerate all the solution sets (if more than one solution exist) may be investigated as future work.

## References

1. Adleman, L.: Molecular computation of solutions to combinatorial problems. *Science* 266 (1994)
2. Shor, P.W.: Polynomial-time algorithms for prime factorization and discrete logarithms on a quantum computer. *SIAM J. Comput.* 26(5), 1484–1509 (1997)
3. Bringsjord, S., Taylor, J.: P=np. *cs.CC/0406056* (2004)
4. Aaronson, S.: Np-complete problems and physical reality. *ACM SIGACT News Complexity Theory Column ECCC TR05-026* (2005)
5. Vergis, A., Steiglitz, K., Dickinson, B.: The complexity grave of analog computation. *Mathematics and Computers in Simulation* 28, 91–113 (1986)
6. Kieu, T.D.: Quantum algorithm for hilbert's tenth problem. *Intl. Journal of Theoretical Physics* 42, 1461–1478 (2003)
7. [http://en.wikipedia.org/wiki/optical\\_character\\_recognition](http://en.wikipedia.org/wiki/optical_character_recognition)
8. Goodman, J.W.: Architectural development of optical data processing systems. *Aust. J. Electr. Electron. Eng.* 2, 139–149 (1982)
9. Reif, J., Tyagi, A.: Efficient parallel algorithms for optical computing with the discrete fourier transform primitive. *Applied optics* 36(29), 7327–7340 (1997)
10. Rong, H., Liu, A., Jones, R., Cohen, O., Hak, D., Nicolaescu, R., Fang, A., Paniccia, M.: An all-silicon raman laser. *Nature* 433, 292–294 (2005)
11. Rong, H., Jones, R., Liu, A., Cohen, O., Hak, D., Fang, A., Paniccia, M.: A continuous wave raman silicon laser. *Nature* 433, 725–728 (2005)
12. Paniccia, M., Koehl, S.: The silicon solution. *IEEE Spectrum*, IEEE Press
13. Faist, J.: Optoelectronics: silicon shines on. *Nature* 433, 691–692 (2005)
14. Garey, M.R., Johnson, D.S.: *Computers and Intractability: A Guide to the Theory of NP-Completeness*. W. H. Freeman, New York (1979)
15. Oltean, M.: Solving the hamiltonian path problem with a light-based computer. *Natural Computing* 7(1), 57–70 (2008)
16. Oltean, M., Muntean, O.: Exact cover with light. *New Generation Comput.* 26(4), 329–346 (2008)
17. Oltean, M., Muntean, O.: Solving the subset-sum problem with a light-based device. *Natural Computing* (to appear)

18. Schultes, D.: Rainbow sort: Sorting at the speed of light. *Natural Computing* 5(1), 67–82 (2006)
19. Murphy, N., Naughton, T.J., Woods, D., Henley, B., McDermott, K., Duffy, E., van der Burgt, P.J.M., Woods, N.: Implementations of a model of physical sorting, pp. 79–100. Luniver Press (2006)
20. Oltean, M.: Light-based string matching. *Natural Computing* 8(1), 121–132 (2009)
21. Agrawal, G.: *Fibre-optic communication systems*, 3rd edn. Wiley-Interscience, Hoboken (2002)
22. Feitelson, D.: *Optical computing: A survey for computer scientists*. MIT Press, Cambridge (1988)

# An Optical Wavelength-Based Solution to the 3-SAT Problem

Sama Goliaei and Saeed Jalili

SML Lab, Electrical and Computer Engineering Department, Tarbiat Modares University, Tehran, Iran  
{goliaei,jalili}@modares.ac.ir

**Abstract.** The NP-complete is a class of complexity including many real-world problems. Although many efforts made to find efficient solutions to NP-complete problems, no such a solution having polynomial complexity of used resources is found yet.

Optical computing, as a branch of unconventional computing, provides new capabilities to solve NP-complete problems, using physical properties of light such as high parallelism nature of it. Some optical approaches to solve NP-complete problems in efficient manner are already provided, such as delaying the light motion, using optical masks, and using continuous space machines. In this paper, a new optical approach, using wide range of wavelengths exist in a light ray, is provided to solve the 3-SAT problem, a well-known NP-complete problem, in polynomial time. Each instance of the 3-SAT problem is a CNF-formula consisting  $m$  clauses be composed of  $n$  boolean variables. The question is if there is a value-assignment to the boolean variables which satisfies the formula or not. In the method provided in this paper, wavelengths presented in a light ray are considered as possible value-assignments to  $n$  variables. Basic optical devices such as prisms and mirrors are used to discriminate proper wavelengths which satisfy the CNF-formal. The method uses exponential size blocks to drop improper wavelengths, which may be constructed in a preprocessing phase and be used in many 3-SAT problem instances. After the preprocessing phase, the method takes  $O(m)$  time and exponential number of different wavelengths in light rays to find the answer of each 3-SAT problem instance.

**Keywords:** Optical Computing, Wavelength-Based Approach, NP-Complete, 3-SAT Problem, Unconventional Computing.

## 1 Introduction

The 3-Satisfiability or 3-SAT problem is a classic NP-complete problem in the complexity theory [1] having many real-world applications such as planning [2] and model checking [3]. The important property of NP-complete problems is that if one of them was solvable in polynomial time with a computational machine, then all NP problems will be also solvable in polynomial time. As many important real-world problems belong to the NP class of complexity, the problem of solving NP-complete problems using efficient time (and other resources)

has been investigated from many years ago, but no solution is found yet. In the other words, no solution is found yet to solve any problem belonging to the NP-complete class of complexity using polynomial amount of resources such as time, space, and energy.

Optical computing or light based computing is a branch of unconventional computing which uses the physical property of light to bring more computational capacity and performance. Many efforts have been performed to solve NP-complete problems using light properties such as high velocity of light, high parallel nature of light, and the ability to split a light ray into several rays.

The optical solutions to NP-complete problems can be classified according to their approaches. In the first approach, some devices are arranged as a graph and the light rays pass through vertices. The delays originated from passage of the light through optical fibers are taken into consideration to calculate the answer of problems. This approach is used to solve maximum clique problem which belongs to the NP-complete complexity class [4] and is also used to solve another NP-complete problem, named Hamiltonian path problem [5]. The subset sum problem is another NP-complete problem which an optical device is designed to solve [6] with similar approach. The NP-complete version of the traveling salesman problem is also solved using a similar approach to the previous works [7].

Another optical approach to solve NP-complete problems is to construct optical masks in preprocessing phase, and using the masks to solve the problems in efficient time [8,9,10].

The third optical approach to solve NP-complete problems is to use continuous space machine. Continuous space machine (CSM) is an abstract computational machine designed relying on physical properties of the light. The machine implements a continuous space memory, instead of conventional computers digital memory [11]. Basic machine operations are defined according to Fourier optics [11] and some efforts are done to implement the machine [12]. It has been shown that CSM simulates Turing machine and it is able to solve NP-complete problems in efficient time [13].

Although these efforts provide good results to get closer to efficient solutions to NP-complete problems, but more efforts are needed yet to achieve efficient optical solutions to NP-complete problems. In this paper, a new optical approach to solve the 3-SAT problem in efficient time is provided. The approach uses different wavelengths presented in a light ray to calculate the answer of the problem. In section 2, a clear mathematical definition of the 3-SAT problem is presented. In section 3, the proposed approach to solve the problem is explained. The conclusion chapter, compares presented work to related works. Possible future works are finally described in the section 4.

## 2 Problem Definition

The 3-SAT problem is a combinatorial problem dealing with  $n$  boolean variables  $x_1, \dots, x_n$ . To define the problem precisely, first we define literals, clauses, CNF-formula, and then we define the 3-SAT problem itself.

A **value-assignment** for  $n$  variables  $x_1, \dots, x_n$  is a function  $v : \{x_1, \dots, x_n\} \rightarrow \{0, 1\}$  which assigns a value “1” or “0” to each  $x_i$  for  $1 \leq i \leq n$ . For example  $v(x_1) = 0, v(x_2) = 1, v(x_3) = 0$  is a value-assignment for three variables.

A **literal** is a boolean expression which is a variable or negation of a variable denoted by  $x_i$  or  $\overline{x_i}$  respectively. Each literal in the form of  $x_i$  ( $\overline{x_i}$ ) for  $1 \leq i \leq n$  is satisfied via a value-assignment  $v$  if and only if  $v(x_i) = 1$  ( $v(x_i) = 0$ ).

A **clause** is a boolean expression in the form of disjunction of three literals denoted by  $l_u \vee l_v \vee l_w$  for some literals  $l_u, l_v$ , and  $l_w$ . For example,  $x_1 \vee \overline{x_3} \vee x_4$  is a clause. Each clause  $C = l_u \vee l_v \vee l_w$  is satisfied by a value-assignment  $v$  if and only if at least one of its literals  $l_u, l_v$ , and  $l_w$  satisfied by  $v$ .

A **CNF-formula** is a boolean expression in the form of conjunction of some clauses. An example of CNF formula is  $F = (x_1 \vee \overline{x_2} \vee x_7) \wedge (x_2 \vee x_6 \vee \overline{x_5}) \wedge (\overline{x_4} \vee \overline{x_6} \vee \overline{x_7})$ . Each CNF-formula is satisfied by a value-assignment  $v$  if and only if  $v$  satisfies all clauses of the CNF-formula.

Now we are ready to define the 3-SAT problem: An instance of the **3-SAT Problem** is a CNF-formula called  $F$ . The question is that “is there any value-assignment satisfying  $F$ , given a CNF-formula?” If there is such a value-assignment, the answer is “Yes”, otherwise “No”.

For example, consider a 3-SAT problem instance, having the example formula mentioned above as the CNF-formula. It can be easily seen that the answer to this problem is “Yes” and one of such value-assignment named  $v$  to satisfy the formula is  $v(x_1) = v(x_2) = v(x_3) = v(x_6) = v(x_7) = 1$ , and  $v(x_4) = v(x_5) = 0$ .

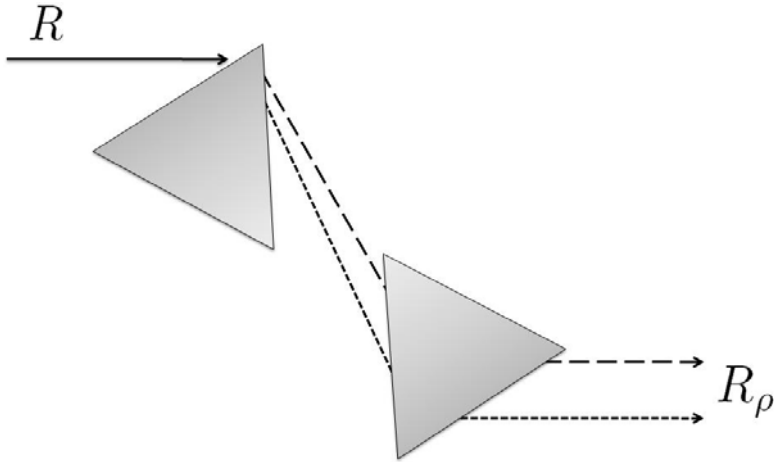
### 3 Wavelength-Based Method

To solve a given instance of the 3-SAT problem with  $n$  variables, a straight forward way is to create all  $2^n$  possible value-assignments for the variables, and check them to find a proper value-assignment satisfying the 3-SAT formula. This is a time consuming job in conventional computers, taking exponential time to create and check all possible value-assignments. In this paper, we show how to use light to create and check the proper value-assignment in an efficient time. The main idea in the light based provided solution is that there may be several wavelengths in a single light ray, which can be used as the possible value-assignments. The operations on a single ray are applied on the all wavelengths simultaneously, providing the ability to check all  $2^n$  value-assignments in an efficient time.

The provided solution will be explained in three steps: 1) The mapping of wavelengths presented in a single light ray to the value-assignments. 2) Optical filter modules to obtain satisfying wavelengths for a boolean expression from a light ray, and 3) Applying the optical filter modules to solve the 3-SAT problem.

#### 3.1 Mapping the Wavelengths to the Value-Assignments

Consider a continuous spectrum light ray named  $R$ , such as the sun light or halogen lamp light ray. The ray consists of different wavelengths, covering a

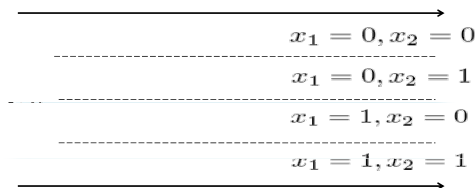


**Fig. 1.** Obtaining light ribbon  $R_\rho$  from light ray  $R$  using two prisms

continuous interval of wavelengths. When such a ray is passed through two prisms as shown in Fig. 1, a continuous spectrum is obtained. We call such a wide ray of light a “light ribbon” denoted by  $R_\rho$ .

The wavelengths presented in the light ribbon can be mapped to the possible value-assignments for the 3-SAT variables (In this paper, we consider a wavelength interval for computation, which can be just a section of whole sun light spectrum. The wavelengths out of this interval are not considered). Consider each value-assignment for  $n$  variables as an  $n$ -digit binary number, which the  $k$ -most significant digit is equal to the value assigned to  $k$ th variable. If the light ribbon  $R_\rho$  consisting of a continuous spectrum be divided into  $2^n$  section, the wavelengths presented in the  $i$ th section are mapped to the value-assignment associated to  $i$ th binary number. The mapping for  $n = 2$  is shown in Fig. 2. Hence, each light ray including the wavelengths in a continuous spectrum in the wavelength interval selected for the computation, contains all  $2^n$  possible value-assignments, as the resulted light ribbon from passing a continuous spectrum ray from the prisms will be continuous.

As the position of each wavelength after passing through the prisms is independent from existence of other wavelengths in the ray, each wavelength is



**Fig. 2.** Mapping the presented wavelengths in a light-ray  $R_\rho$  to the possible value-assignments to the 3-SAT variables for  $n = 2$



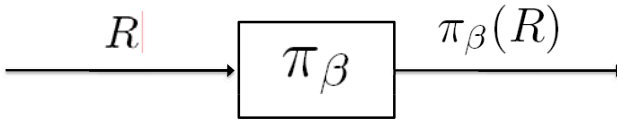
mapped to a value-assignment independently from the existence of other wavelengths in the ray.

**Definition.** Each wavelength  $w$  satisfies a literal  $l$  if and only if the value-assignment  $v$  mapped to  $w$  satisfies  $l$ .

### 3.2 Optical Filter Modules

In this section, we define optical filter modules (or OFMs) and see how to design OFMs for different boolean expressions.

**Optical Filter Module (OFM).** Consider a boolean expression (such as a literal, a clause, or a 3-SAT formula)  $\beta$ . An optical filter module for  $\beta$  is a module of optical devices, which for each light ray  $R$  consisting of some wavelengths, if  $R$  be passed through the module, the wavelengths not satisfying  $\beta$  are dropped from  $R$ . Hence, the output ray of the module contains exactly those wavelengths of  $R$  satisfying  $\beta$ . The filter module is denoted by  $\pi_\beta$  and the output ray is denoted by  $\pi_\beta(R)$ . The general schema of an OFM is shown in Fig. 3.

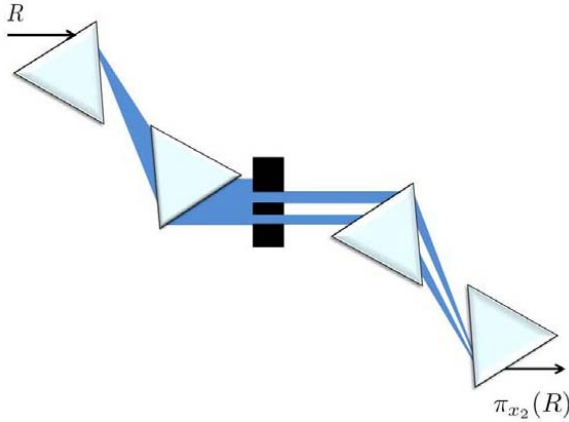


**Fig. 3.** The general schema of an optical filter module for boolean expression  $\beta$

**Literal OFMs.** To design an OFM for a literal  $x_i$  ( $\overline{x_i}$ ), note that each wavelength  $w$  in the light ray  $R$  satisfies  $x_i$  ( $\overline{x_i}$ ) if and only if it belongs to the section number  $2k+1$  (for some  $k$ ,  $0 \leq k < 2^{i-1}$ ) if  $R\rho$  be divided to  $2^i$  sections. Hence, to obtain the wavelengths satisfying  $x_i$  ( $\overline{x_i}$ ) it is sufficient to place a light blocker on the light ribbon  $R\rho$ . The light blocker is partitioned into  $2^i$  sections, where the odd (even) sections are holes which allows the light to pass, and the even (odd) sections does not allow the light to pass. In Fig. 4 a literal OFM for  $x_2$  is shown.

Using the provided design for literal OFMs, the light takes  $O(1)$  time (not dependent on  $n$  or  $m$ ) to pass the OFM. The time required to construct the light blockers is considered in the preprocessing, as the literal OFMs (and light blockers) are the same in any instance of the 3-SAT problems. To construct a light blocker for OFM of literal  $x_i$  ( $\overline{x_i}$ ), it is required to create  $2^i$  sections on a black plane and punch the even (odd) sections such as 2th and 4th (1th and 3th) sections to pass the light. So the area of the light blocker is exponential according to  $i$ .

**Clause OFMs.** Having OFMs for any literal, how can we design an OFM for a clause?

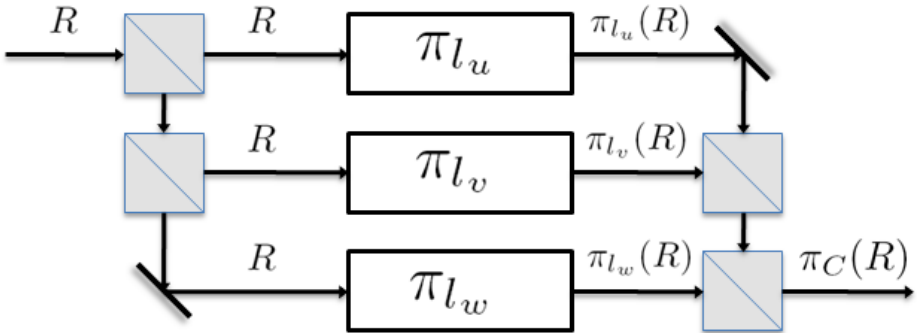


**Fig. 4.**  $\pi_{x_2}$ , a literal OFM for  $x_2$ . A light blocker including two holes is placed on the light ribbon to block the wavelengths which does not satisfy  $x_2$ .

Consider each clause  $C$  as  $C = l_u \vee l_v \vee l_w$  for some literals  $l_u$ ,  $l_v$ , and  $l_w$ . A value-assignment satisfy  $C$  if and only if it satisfies at least one of the literals. The main idea to design the optical filter for a clause is: first repeating the input ray into three rays having the same wavelengths as the input ray, then passing each of the three rays through the corresponding OFM of the literals simultaneously. Finally, integrate the three output rays of the literal OFMs to obtain a single ray, as the output for clause OFM.

We call the first step, repeating the input ray called  $R$  into three equal rays, as the repeating phase. The repeating phase can be done using cubic beam-splitters and plain mirrors as shown in Fig.5.

In the second step, called filtering phase, the three equal rays are passed through the literal OFMs  $\pi_{l_u}, \pi_{l_v}, \pi_{l_w}$  simultaneously. Each of the three output rays, denoted by  $\pi_{l_u}(R), \pi_{l_v}(R)$ , and  $\pi_{l_w}(R)$ , contains exactly those wavelengths of  $R$  which satisfy literals  $l_u, l_v$ , and  $l_w$ .



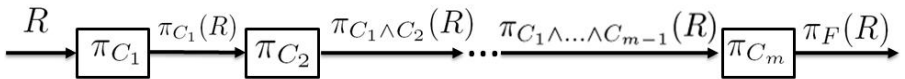
**Fig. 5.** The general schema of an OFM for clause  $C = l_u \vee l_v \vee l_w$

In the last step, called union phase, to collect the satisfying wavelengths of the clause, it is sufficient to obtain a ray containing exactly those wavelengths presented in at least one of  $\pi_{l_u}(R)$ ,  $\pi_{l_v}(R)$ , and  $\pi_{l_w}(R)$ . Such a ray can be easily obtained using again cubic beam-splitters and plain mirrors as shown in Fig. 5. Each beam-splitter splits the input rays into two rays having the same wavelength of the input rays. These output rays come from two other sides of the beam splitters. Hence, each light ray outgoing from these sides of beam-splitter contains all wavelengths presented in the input rays.

The general schema of a clause OFM is shown in Fig. 5, using optical devices and literal OFMs. As each literal OFM requires at most  $O(1)$  time to pass the light, the time required for the light ray to pass a clause OFM is at most  $O(1)$ .

**CNF-Formula OFMs.** Now we are ready to design an optical filter for 3-SAT formula. Each 3-SAT formula  $F$  is the conjunction of  $m$  clauses, denoted as  $F = C_1 \wedge C_2 \wedge \dots \wedge C_m$  for some  $m$ . An idea to design the OFM for  $F$  is to start from an input ray  $R$  and pass the ray through the clause OFMs of  $F$  one by one, and finally, collect the from the last clause OFM which contains exactly the wavelengths satisfying  $F$ .

More precisely, to obtain an OFM for  $F$ , at the first step,  $R$  is passed through the clause OFM of  $C_1$  denoted by  $\pi_{C_1}$ . The outgoing ray denoted by  $\pi_{C_1}(R)$  contains those wavelengths of  $R$  which satisfy  $C_1$ . In the second step, the outgoing ray from  $\pi_{C_1}$  is passed through the clause OFM of  $C_2$ . In this case, the outgoing ray contains exactly those wavelengths of  $R$  which satisfy both  $C_1$  and  $C_2$  (or  $C_1 \wedge C_2$ ). By repeating this procedure for other clauses of  $F$  after  $m$  steps,  $R_m$  contains exactly wavelengths of  $R$  which satisfy  $C_1 \wedge C_2 \wedge \dots \wedge C_m$ , i.e., satisfy 3-SAT formula  $F$ . The general schema of the optical filter for 3-SAT formula is shown in Fig. 6. As each clause OFM requires  $O(1)$  time to pass the light, the time required for the light ray to pass each CNF-Formula OFM is  $O(m)$ .



**Fig. 6.** The general schema of an OFM for CNF-formula  $F = C_1 \wedge C_2 \wedge \dots \wedge C_m$

### 3.3 Using OFMs to Solve the 3-SAT Problem

Now we can easily solve the 3-SAT problem using OFMs. Starting from a continuous spectrum light ray  $R$  (in a selected wavelength interval) and pass it through the OFM for 3-SAT formula  $F$ . The output ray, denoted as  $\pi_F(R)$  contains exactly those wavelengths of  $R$  which satisfy  $F$ . As  $R$  is a continuous spectrum light ray (in a selected wavelength interval) and hence contains all possible value-assignments for the variables, the out going ray, denoted by  $\pi_F(R)$  contains exactly those wavelengths which mapped to the value-assignments satisfying the corresponding 3-SAT formula. So, a given 3-SAT problem has a satisfying value-assignment if and only if the outgoing ray  $\pi_F(R)$  contains some wavelengths, and

the answer is “Yes”, otherwise “No”. This can be easily be tested using a light sensor. Hence, if the light sensor detects any light ray consisting of wavelengths from the selected wavelength interval, the answer is declared as “Yes”, otherwise “No”.

Now consider an instance of the 3-SAT problem having  $n$  variables and  $m$  clauses. As the required time for a light ray to pass a CNF-formula OFM is  $O(m)$ , the provided method takes  $O(m)$  time to solve each instance of the 3-SAT problem (excluding the preprocessing time). Also the number of optical divides such as prisms and beam-splitters is  $O(m)$ .

## 4 Conclusion and Future Works

3-SAT problem is an NP-complete problem which no polynomial time solution for it on the conventional computers is found yet. In this paper, a new optical approach to solve the 3-SAT problem is provided using polynomial time, based on different wavelengths presented in a light ray. The wavelengths are considered as the possible value-assignment to the variables in the 3-SAT problem and optical filters are designed using optical devices such as beam-splitters and prisms to drop those wavelengths which do not satisfy the 3-SAT formula. At the end, outgoing wavelengths from the filter are those which are mapped to the satisfying value-assignments for the 3-SAT formula.

Some other optical approaches are already provided to solve NP-complete problems. In the first approach, some optical devices using optical fibers to make delays in the light motion is used. This approach is used to solve NP-complete problems such as exact cover problem [4], Hamiltonian path problem [5], sub-set sum problem [6], and traveling sales man problem [7]. The methods provided in these works take takes exponential time and space to solve each problem instance.

Another optical approach to solve NP-complete problems uses optical masks. The masks are created in a preprocessing phase, and they are used to solve the instances of NP-complete problems in polynomial time, but required space (the size of designed optical masks) has exponential complexity according to the input size [8,9,10].

Continuous space machine (or CSM) is an optical machine which uses Fourier property of light to do some operations on optical images. Using CSM is another optical approach to solve NP-complete problem. NP-complete problems (also class of P-space problems) can be solved in CSM using polynomial time but exponential space [13].

The provided wavelength-based method in this paper takes exponential time according to  $n$  (the number of Boolean variables) for preprocessing to construct light blockers. After preprocessing time, the method takes  $O(m)$  time to solve each 3-SAT problem instance, where  $m$  is the number of clauses. The complexity of number of optical devices is also  $O(m)$  but the space complexity is exponential according to the size of input. The number of different wavelengths in a light ray is also exponential according to  $n$ , where  $n$  is the number of Boolean variables in each 3-SAT problem instance.

In the future works, we will focus on the light blockers used in literal OFMs. As the exponential space and pre-processing time is dependent on these blockers, some methods are required to replace these blockers with other optical devices to achieve polynomial time and space to solve the 3-SAT problem. If such a methods be found, it does not still yield that the famous problem  $P \stackrel{?}{=} NP$  is solved, because the number of wavelengths required in light rays is still exponential according to the size of input. The used energy to solve each instance of the 3-SAT problem is the other subject to be investigated. We will focus on some methods to reduce the required energy for each light ray and also overall energy required in the provided solution.

*Acknowledgment.* This work is partially supported by (Iranian) National Institute of Elites.

## References

1. Cook, S.A.: The complexity of theorem-proving procedures. In: Proceedings of the third annual ACM symposium on Theory of computing, Shaker Heights, Ohio, United States, pp. 151–158. ACM, New York (1971)
2. Rintanen, J., Heljanko, K., Niemel, I.: Planning as satisfiability: parallel plans and algorithms for plan search. *Artificial Intelligence* 170(12-13), 1031–1080 (2006)
3. Amla, N., Du, X., Kuehlmann, A., Kurshan, R.P., McMillan, K.L.: An analysis of SAT-Based model checking techniques in an industrial environment. In: Borriane, D., Paul, W. (eds.) CHARME 2005. LNCS, vol. 3725, pp. 254–268. Springer, Heidelberg (2005)
4. Oltean, M., Muntean, O.: Exact cover with light. 0708.1962 (August 2007). In: *New Generation Computing*, vol. 26(4), pp. 327–344. Springer, Heidelberg (2008)
5. Oltean, M.: Solving the hamiltonian path problem with a light-based computer. *Natural Computing: an international journal* 7(1), 57–70 (2008)
6. Oltean, M., Muntean, O.: Solving the subset-sum problem with a light-based device. *Natural Computing: an international journal* 8(2), 321–331 (2009)
7. Haist, T., Osten, W.: An optical solution for the traveling salesman problem. *Optics Express* 15(16), 10473–10482 (2007) PMID: 19547400.
8. Dolev, S., Fitoussi, H.: The traveling beams optical solutions for bounded NP-Complete problems. In: Crescenzi, P., Prencipe, G., Pucci, G. (eds.) FUN 2007. LNCS, vol. 4475, pp. 120–134. Springer, Heidelberg (2007)
9. Shaked, N.T., Tabib, T., Simon, G., Messika, S., Dolev, S., Rosen, J.: Optical binary-matrix synthesis for solving bounded NP-complete combinatorial problems. *Optical Engineering* 46(10), 108–201 (2007)
10. Shaked, N.T., Messika, S., Dolev, S., Rosen, J.: Optical solution for bounded NP-complete problems. *Applied Optics* 46(5), 711–724 (2007) PMID: 17279159.
11. Woods, D., Gibson, J.: Lower bounds on the computational power of an optical model of computation. *Natural Computing* 7(1), 95–108 (2008)
12. Woods, D., Naughton, T.J.: An optical model of computation. *Theor. Comput. Sci.* 334(1-3), 227–258 (2005)
13. Woods, D., Naughton, T.: Parallel and sequential optical computing. In: Dolev, S., Haist, T., Oltean, M. (eds.) OSC 2008. LNCS, vol. 5172, pp. 70–86. Springer, Heidelberg (2008)

# Incoherent Optical Spatial Image Processing

Melania Paturzo<sup>1</sup>, Pietro Ferraro<sup>1</sup>, Alexander Zlotnik<sup>2</sup>, and Zeev Zalevsky<sup>2</sup>

<sup>1</sup> CNR - Istituto Nazionale di Ottica Applicata – Sez. Napoli, Via Campi Flegrei  
34 – 80078, Pozzuoli, Italy

<sup>2</sup> School of engineering, Bar-Ilan Univ., Ramat-Gan 52900, Israel  
zalevsz@eng.biu.ac.il

**Abstract.** In this paper we present a new configuration for real-time spatial image processor that is based upon an *imaging* setup in which a grating with Fourier coefficients with tunable phase is attached to the object plane. The illumination that is used for the proposed concept is spatially incoherent. By proper adjusting of the magnification of the imaging system to the spatial period of the grating and the sampling grid of the camera, the aliasing effect due to the digital sampling realizes a non uniform and tunable spectral distribution (a filter) that is applied over the spectrum of the object.

**Keywords:** Optical signal processing subsystems.

## 1 Introduction and Motivation

Optical realization of real time spatial processor or a filter is a very important task since the advantage of optics in which the processing even of large images is done in parallel and not in serial manner. Various configurations tried to realize such a processor based upon spatial light modulators (SLM) usually positioned in an optical Fourier transforming setup [1-4]. In other approaches the all-optical realization used some non linear effect such as the photo refractive effect in order to mix two spatial distributions (the input data and the filter) together [5-10].

The aim of this paper is to build an ultra fast spatial image processor that may for instance be based on the  $\text{LiNbO}_3$  periodically poled gratings that allow fast and controlled tuning of their optical parameters. The optical system as to be described includes a tunable grating (where only the phase of its Fourier coefficients can be varied while its period remains unchanged) that is attached to the object plane and an imaging system which is defocused or it has a special spatial mask that is attached to the aperture of the imaging lens. Except of that the proposed system does not require any time integration or movement of two gratings (encoding and decoding) as appears in conventional filtering configurations that are imaging based [11]. The setup is very simple and allows realization of tunable spatial filters to be applied over the image of the object.

The idea is to attach a tunable grating to the object in an imaging setup and to use the aliasing effect generated due to the sampling in the detection array such that the differently replicated spectral information will realize different spectral filtering applied over the spectrum of the input object. Especially this concept may be appealing in case where very fast tunable grating is used. As an example, assume that one has a

grating made of  $\text{LiNbO}_3$  in which one may control the phase of its Fourier coefficients (its diffraction orders). The temporal response time of such gratings can easily be few GHz. Note that we do not require to have a modulator where every pixel can be tuned individually but rather a grating where the control is applied over the entire structure.

Note that the purpose of the proposed configuration is to achieve spatial filtering as done in regular configuration. However, our intension is to obtain this filtering with-out applying tunable filter in the Fourier domain. In some applications and especially those that deal with practical cases of incoherent illumination, the Fourier plane is not accessible. This is true for instance in the cases when the aperture plane of the imaging lens is inside the lens. The main advantage of the proposed technique is that it does not depend on the lens configuration and it allows the realization of any spatial filter without the need to access various planes in the lens or to insert anything into the imaging module. Our filtering is obtained by combining partially tunable spatial mask positioned in the object plane together with the sampling effect done anyhow by the detection array. In addition, the tunability that is required from our spatial mask (that is positioned near the object) in order to realize basic image processing operations as low, band and high passing is reduced in comparison to the tunability needed from a mask when it is positioned in the Fourier plane in order to obtain similar result.

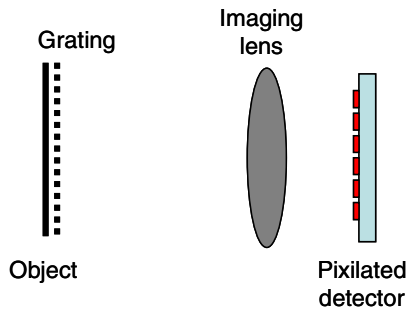
Note also that in previous works, the aliasing effect was treated as undesired distortion or noise that needs to eliminate [12,13]. Other optical computing processing schemes were suggested as well [14]. The difference in the approach presented in this paper is that in our case we use the aliasing effect for our benefit in order to realize the tunable filtering functionality.

The mathematical derivation is presented in section 2. In Section 3 we experimentally validate the proposed approach. Section 4 concludes the paper.

## 2 Mathematical Derivation

We will perform the mathematical derivation for spatially incoherent illumination and therefore all the functions in the mathematical description designate intensity distributions.

The schematic sketch of the setup that we will analyze appears in Fig. 1. We will denote by  $H$  the OTF of an imaging system that images an object while the modulation grating is attached to the object (multiplies its transmission).



**Fig. 1.** Schematic illustration of the optical setup

The Fourier transform of the image of the object  $s(x)$  that is generated due to the grating that is attached to the object equals to:

$$\bar{H}(\mu) = H(\mu) \cdot \int [s(x) \cdot g(x)] \exp(2\pi i \mu x) dx \quad (1)$$

where  $s(x)$  is the imaged object and  $g(x)$  is the grating attached to it. All spatial distributions are intensities.

In case that a defocused imaging is used and the aperture of the lens has a dimension of  $2b$ , the one-dimensional OTF function  $H$  has the form of a *sinc* function:

$$H(\mu) \approx \text{sinc} \left( \frac{4W_m Z_i \mu}{b} \right) \quad (2)$$

The coefficient  $W_m$  determines the severity of the error. The coefficient  $W_m$  is also denoted as:

$$W_m = \frac{b^2}{2} \left( \frac{1}{Z_i} + \frac{1}{Z_o} - \frac{1}{F} \right) \quad (3)$$

$Z_o$  and  $Z_i$  are the distances between the imaging lens and the object and the imaging lens and the image respectively.  $F$  is the focal length. When the imaging condition is fulfilled, then:

$$\frac{1}{Z_i} + \frac{1}{Z_o} = \frac{1}{F} \quad (4)$$

Since  $g(x)$  is a grating, we will express it as a Fourier series:

$$g(x) = \sum_n a_n \exp(2\pi i n \mu_0 x) \quad (5)$$

Therefore substitution of the last equation into Eq. 1 yields:

$$\bar{H}(\mu) = \sum_n a_n H(\mu) S(\mu - n\mu_0) \quad (6)$$

while  $S(\mu)$  is the Fourier transform of  $s(x)$ . We assume that  $\mu_0$  is larger than the bandwidth of  $S(\mu)$ . We will denote the various spectral slots of the OTF  $H(\mu)$  having width of  $\mu_0$  by specific names, i.e.:

$$H_m(\mu) = H(\mu) \cdot \text{rect} \left( \frac{\mu - m\mu_0}{\mu_0} \right) \quad (7)$$

Therefore Eq. 6 will become:

$$\bar{H}(\mu) = \sum_n a_n H_n(\mu) S(\mu - n\mu_0) \quad (8)$$

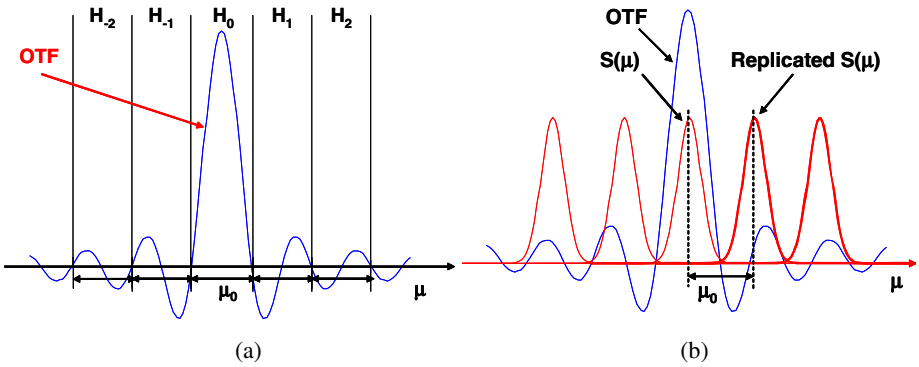
In Fig. 2(a) one may see schematic illustration of the notations and of the assumptions presented in the mathematical derivation. In Fig. 2(b) we added the schematic illustration of the spectral distribution  $\bar{H}(\mu)$  due to the replication of  $S(\mu)$ .

The image captured at the detector is sampled. Sampling in the space domain is equivalent to convolving the spectral domain (spatial spectrum) with a train of delta functions. Therefore, the spectrum of the sampled image, which we denote by  $\bar{H}_d(\mu)$ , is periodic.

We assume that the sampling is at frequency of  $\mu_0$  which is enough for full information reconstruction since the bandwidth of  $S(\mu)$  is smaller than  $\mu_0$ :

$$\bar{H}_d(\mu) = \bar{H}(\mu) \otimes \sum_n \delta(\mu - n\mu_0) \quad (9)$$

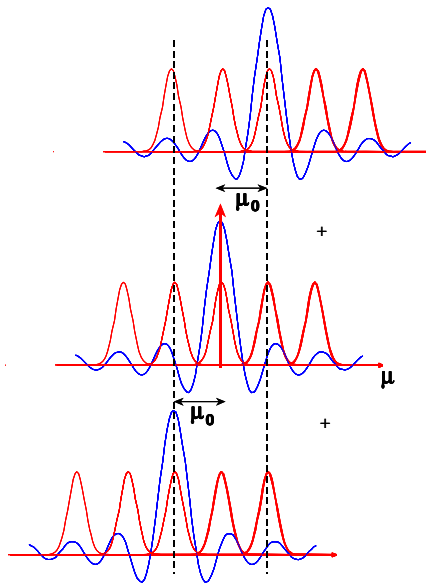




**Fig. 2.** (a). Schematic illustration of the OTF and the notations we use. (b). Schematic illustration of the spectral distribution  $\bar{H}(\mu)$  due to replication of  $S(\mu)$ .

We denote by the symbol of  $\otimes$  the convolution operation. As previously mentioned, sampling means replicating in the spectrum domain. All identical replications interact through overlapping (aliasing) and create a periodic spectral distribution. The spectral information that is eventually seen by the detector is the information contained in one period of the replication. The spectral information of every period equals to:

$$\bar{H}_d^{(\text{inf})}(\mu) = \sum_n a_n H_n(\mu) S(\mu) = S(\mu) \left[ \sum_n a_n H(\mu - n\mu_0) \right] \quad (10)$$



**Fig. 3.** Schematic illustration of the spectral replication due to the sampling at the detector plane

In Fig. 3 one may see schematic illustration of the spectral distribution due to sampling. Therefore the expression appearing in the brackets could be described as a special filter applied over the spectral content of the image  $s(x)$ . The assumption that the imaging system is defocused (OTF has *sinc* like shape) was important in order to have non uniform filter (the filter appears in the brackets of Eq. 10). Instead of defocusing one may also attach a non uniform spatial mask to the aperture lens as well.

Note that the defocusing was proposed as one example of aberration allowing to have negative parts for the OTF and to assist in realizing various types of spatial filters without doing pixel wise modification of the modulation grating. This is especially important if one wishes to be able to realize basic filters without applying a pixel wise modulation of the grating. Other types of aberrations can be used as well, and even aperture coding masks where one may attach a non uniform spatial mask to the aperture or to other principle planes of the lens.

Let us see what the realized filter really is. We denote the Fourier transform of this filter by  $f(x)$ . In this case we have:

$$f(x) = h(x) \cdot \sum_n a_n \exp(2\pi i n \mu_0 x) \quad (11)$$

which means that if we know the desired filter and therefore its Fourier transform (i.e. the point spread function distribution in the space domain), the required Fourier coefficients  $a_n$  can be found as:

$$a_n = \int_{1/\mu_0} \left[ \frac{f(x)}{h(x)} \right] \exp(-2\pi i n \mu_0 x) dx \quad (12)$$

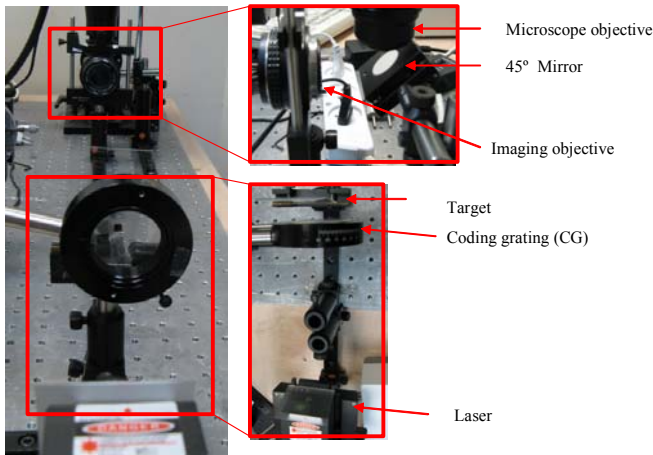
Those coefficients  $a_n$  can be time varied and by that the filter can be tuned with time as well.

Note that as seen from Eq. 12 if one wishes to do general processing or to realize a general filter he needs to perform a pixel-wise modulation of the grating and then the shape of the OTF is also less important except of allowing the existence of solution for Eq. 12 (i.e. the ratio of  $f(x)/h(x)$  is mathematically defined). However, as we are about to present, for basic image processing operations such as low, band and high pass filtering one does not need to do a pixel wise tuning of the grating. The constraints we have regarding the shape of the OTF (e.g. performing aberration to its shape by defocusing or by usage of spatial mask) are mainly relevant to this case of non pixel wise modulation.

Note also that the sensitivity of the synthesized filter to noise mainly depends on the strength of the Fourier components of the grating given that the OTF has spectral width which is wider than  $1/\mu_0$  (this is also seen in Eq. 10). If one observes again Eq. 12 indeed zeros in  $h(x)$  may be problematic for the computing. However, when a narrow OTF is generated (e.g. due to defocusing) it results by wider  $h(x)$  distribution and thus the dividing operation may be preferred since then  $h(x)$  is wider than  $f(x)$  and thus there is smaller probability to have zeros in the denominator or sensitivity to existing noises.

### 3 Experimental Validation

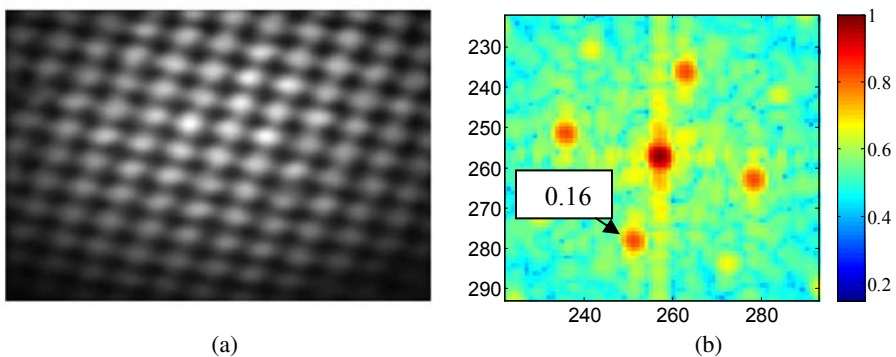
The proposed concept was experimentally validated. In the experimental configuration, the coding grating (CG) was a transmittance rectangular grating with period of



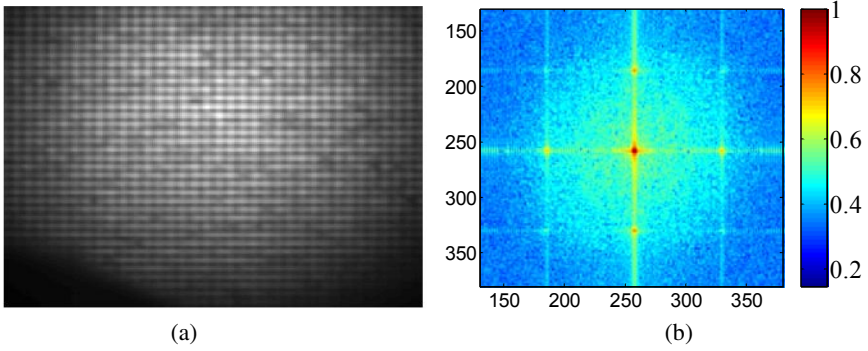
**Fig. 4.** The experimental setup

100 $\mu\text{m}$  (Fig. 4). The CG plane was imaged by lens objective of  $F = 50\text{mm}$ ,  $F/\# = 8$  to an intermediate image plane located at working distance of a capturing device (magnifying objective + sensor). The distance of the CG from imaging objective was 60cm. The target object was positioned in the vicinity of the CG. The imaging MTF is degraded by defocus of the target. The chosen target was a rectangular grating with period of 330 $\mu\text{m}$ . The illumination is monochromatic, using 532nm green laser. The illumination beam is opened by a holographic diffuser. The illumination is made spatially incoherent by means of a rotating diffuser.

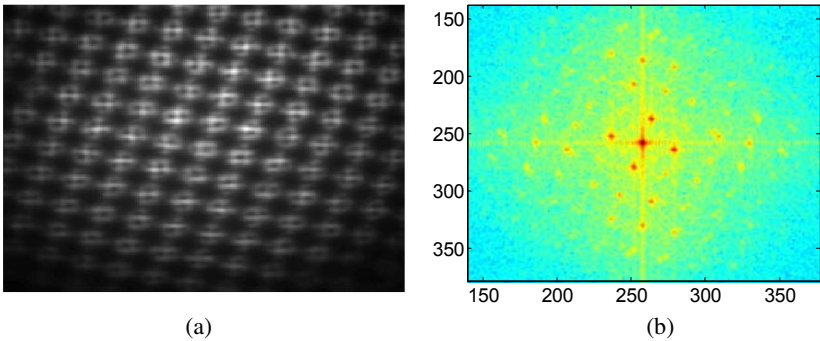
The obtained results are presented in Figs. 5-8. The target image without CG is shown in Fig. 5(a). Figure 5(b) shows the absolute value of Fourier Transform (FFT) of the target, while the plot is normalized to have a DC component equal to unity. The modulation value (contrast) of the 1<sup>st</sup> order is 0.16.



**Fig. 5.** (a). The original object. (b). Its spectrum.



**Fig. 6.** (a). The coding grating (CG). (b). Its spectrum.

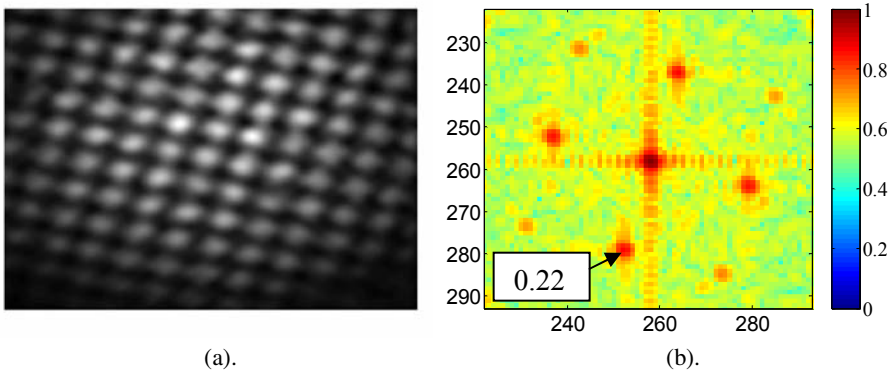


**Fig. 7.** (a). Captured image of the CG with target, prior to aliasing effect. (b). The obtained spectrum.

Since the camera had pixels of  $12\mu\text{m}$  and in the computation we had 512 pixels, the units (i.e. the units of every pixel in the charts) for the results presented in Figs. 5-8 are  $2/(512 \times 12\mu\text{m}) = 0.326$  (1/mm). In Fig. 6 the coding grating CG plots are shown.

Figure 7 describes the captured results, **prior** to aliasing effect. It is possible to see that as expected the object spectrum is replicated by a CG. The aliasing effect was simulated by a proper re-sampling, without applying anti-aliasing filter. The results are demonstrated in Fig. 8. The modulation value (contrast) of 1<sup>st</sup> order is now 0.22. Thus, due to the aliasing the contrast of the first order was improved from 0.16 to 0.22 which is an improvement of approximately 40%.

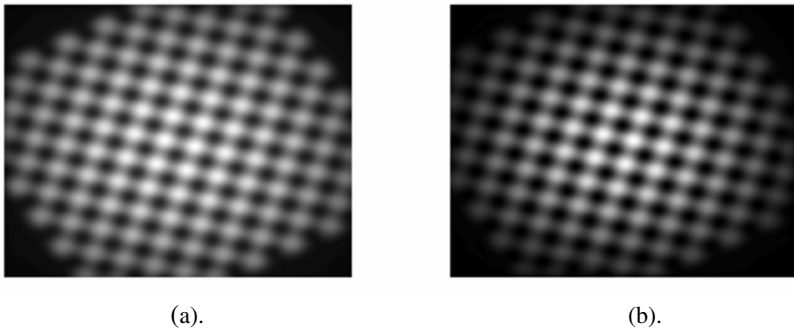
A comment regarding the processing we performed. If one marks the CG replicating frequency by  $v_s$ , then the maximum allowed target frequency component will be  $0.5v_s$ . Due to the CG this component is replicated to  $v_s + 0.5v_s$  as shown in Fig 7(b). Therefore, for proper simulation we will zero all frequency data beyond the  $1.5v_s$  in the Fourier domain, and crop the central  $3v_s$  bandwidth out of the captured spectrum and then inverse Fourier transform the distribution to go back to the image plane. We decimate the resulted distribution by a factor of three (we took every third pixel). This way the resulted image has its maximal frequency component located at  $0.5v_s$  (bandwidth of  $v_s$ ).



**Fig. 8.** Final results. (a). Applying aliasing on the re-sampled captured image results in a contrast enhanced target image. (b). The spectrum.

That way we obtained the required matching between the CG replicating frequency and the effective aliasing frequency due to the sampling by the pixels of the sensor.

In order to validate the experimental results we have performed a numerical simulation following the experimental conditions providing the result of Fig. 8. The results are presented in Fig. 9. The first harmonic of an original object was enhanced from 0.167 to 0.235 which is an enhancement factor of about 40% similar to the one obtained in our experimental results of Fig. 8.



**Fig. 9.** Numerical simulations. (a). Original object with contrast of first harmonic of 0.167. (b). Enhanced object with contrast of first harmonic of 0.235.

## 4 Conclusions

In this paper we have presented a new approach for realization of a real-time all-optical spatial image filtering or even processing in the next step. The concept consists of attaching, to the object, a grating capable of tuning in real-time the phase of its Fourier coefficients and an imaging lens having proper spatial mask attached to it, or a lens with proper defocus, as well as a magnification factor that adjusts the aliasing

due to the sampling of the pixelized detector to the period of the tunable grating. Tuning the grating varied the aliasing and thus realizes a different spectral filter.

## References

1. Gaeta, C.J., Mitchell, P.V., Pepper, D.M.: Optical real-time defect-enhancement diagnostic system. *Opt. Lett.* 17, 1797–1799 (1992)
2. Poon, T.-C., Schilling, B.W., Wu, M.H., Shinoda, K., Suzuki, Y.: Real-time two-dimensional holographic imaging by using an electron-beam-addressed spatial light modulator. *Opt. Lett.* 18, 63–65 (1993)
3. Wang, Z.Q., Cartwright, C.M., Gillespie, W.A.: Real-time intensity correlation with a synthetic discriminant function filter. *J. Opt. Soc. Am.B* 11, 1842–1847 (1994)
4. Huang, G., Jin, G., Wu, M., Yan, Y.: Developed, binary, image processing in a dual-channel, optical, real-time morphological processor. *Appl. Opt.* 36, 5675–5681 (1997)
5. Joseph, J., Kamra, K., Singh, K., Pillai, P.K.C.: Real-time image processing using selective erasure in photorefractive two-wave mixing. *Appl. Opt.* 31, 4769–4772 (1992)
6. Sreedhar, P.R., Sirohi, R.S.: Real-time image processing with a cat conjugator. *Appl. Opt.* 34, 333–337 (1995)
7. Chang, T.Y., Hong, J.H., Yeh, P.: Spatial amplification: an image-processing technique using the selective amplification of spatial frequencies. *Opt. Lett.* 15, 743–745 (1990)
8. Shen, X.A., Kachru, R.: Time-domain optical memory for image storage and high-speed image processing. *Appl. Opt.* 32, 5810–5815 (1993)
9. Marom, D.M., Panasencko, D., Sun, P., Fainman, Y.: Real Time Spatial-Temporal Signal Processing by Wave-Mixing with Cascaded Second-Order Nonlinearities. In: *Optics in Computing, OSA Technical Digest (Optical Society of America, 1999)*, paper OThC2. (1999)
10. Babbitt, W.R., Mossberg, T.W.: Spatial routing of optical beams through time-domain spatial-spectral filtering. *Opt. Lett.* 20, 910–912 (1995)
11. Mendlovic, D., Farkas, D., Zalevsky, Z., Lohmann, A.W.: High frequency enhancement via super resolution optical system for temporally restricted objects. *Opt. Lett.* 23, 801–803 (1998)
12. Leger, J.R., Schuler, J., Morphis, N., Knowlden, R.: Optical antialiasing filters based on complementary Golay codes. *Appl. Opt.* 36, 4692–4701 (1997)
13. Braunecker, B., Hauck, R., Rhodes, W.T.: Pupil function replication in OTF synthesis. *Appl. Opt.* 18, 44–51 (1979)
14. Woods, D., Naughton, T.J.: Parallel and sequential optical computing. In: Dolev, S., Haist, T., Oltean, M. (eds.) *OSC 2008. LNCS*, vol. 5172, pp. 70–86. Springer, Heidelberg (2008)

# A Scheme for SIMD Processing in Two Dimensional Binary Images and Its Applications

Kouichi Nitta and Osamu Matoba

Department of Computer Science and Systems Engineering,  
Graduate School of Engineering, Kobe University,  
Rokkodai-cho 1-1, Nada-ku, Kobe, Hyogo, 657-8501, Japan  
{nitta,matoba}@kobe-u.ac.jp

**Abstract.** A scheme for SIMD (Single Instruction stream Multi Data stream) pattern processing for two dimensional (2D) binary images is introduced as a brief announcement. This scheme consists of image compression of target images and some elemental operations for compressed data in order to achieve large scale information processing with less processing costs. We have applied the scheme to prime factorization and the travelling salesman problem (TSP). Advantaged features of the scheme are discussed.

**Keywords:** SIMD pattern processing, 2D binary image, image compression, huge scale information processing.

## 1 Introduction

SIMD (Single Instruction stream) processing in two dimensional (2D) images have been studied in the research field called digital optical computing because this processing is suitable for optical implementation [1, 2]. Also, this processing form seems to be useful for electronic processing since parallel processing is generally utilized with consumer use workstations.

In such a situation, we have proposed a specific scheme based on the form. Image compression is a key technology in the scheme. First of the procedure in the scheme, a set of input images are compressed in accordance with a specific encoding. A sequence of operations is applied to compressed datum. As a result, desired output images can be extracted by decoding which is inverse process of encoding.

We have developed one of the solutions based on the scheme [3]. This solution is to reduce processing costs of an algorithm for prime factorization. Usefulness of the solution is shown by verification. Also, the scheme has been applied to the traveling salesman problem (TSP) and effectiveness of it has been investigated.

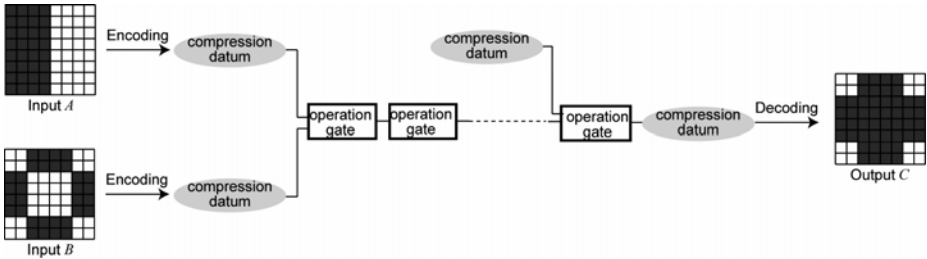
In this announcement, we describe the proposed scheme. The processing procedure in the scheme is briefly explained. Two kinds of solutions are shown. We discuss on features of them.

## 2 SIMD Pattern Processing with Image Compression

An elemental operation in SIMD pattern processing for 2D images is represented as a logical operation between neighborhood pixels on the target images. This processing format has been defined in optical array logic (OAL) [1]. Several applications with OAL such as image processing, numerical one, and so on have been researched. In these applications, input information is expressed as binary patterns on 2D discrete images. Output images are obtained by a sequence of elemental gates.

Our solutions for prime factorization and the TSP is examples of trial for the problems requiring hard computation tasks based on the processing. In the solutions, operational steps increase polynomial whereas image size grows exponentially. Note that only growth of the vertical direction of the image size is serious problem in the solutions.

Therefore, we study on a scheme to solve the problem. Fig.1 shows a schematic diagram of the scheme. In the scheme, input images are converted into a set of datum by a specific coding for compression. Sets of the datum are operated by a sequence of elemental gates. These gates correspond to logical operations in image domain. Output datum is obtained by a sequence of the gates. Finally, output images are given by the decoding. An encoding rule for the scheme should be a lossless compression so that output images are reconstructed as final results.



**Fig. 1.** Diagram of a scheme for SIMD pattern processing of 2D binary images with image compression

Fig. 2 shows a scheme for an encoding method presented in Ref. [3]. As described in the figure, a target image is divided into a set of column patterns. Then, two kinds of datum  $W_j$  and  $B_j$  are generated from one column data.  $W_j$  and  $B_j$  are sets of  $i$ 's satisfied with Eqs. (1) and (2), respectively.

$$a_{i-1,j} = 0 \cap a_{i,j} = 1 \tag{1}$$

$$a_{i-1,j} = 1 \cap a_{i,j} = 0 \tag{2}$$

In these two equations,  $a_{i,j}$  shows the pixel value at  $(i, j)$  on the image.



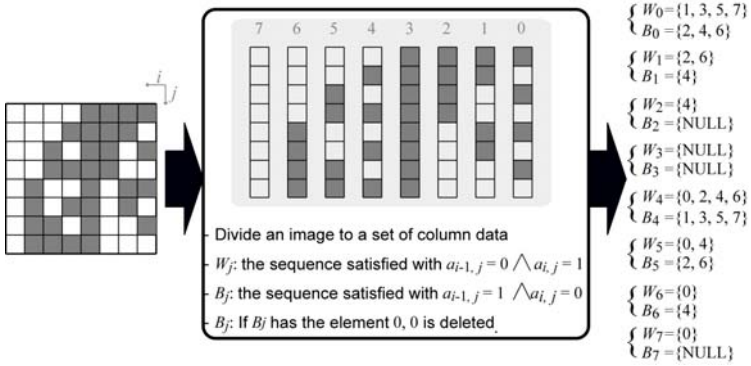


Fig. 2. Scheme for procedure of encoding from 2D patterns to a set of compressed datum

We have constructed three elemental operations. These operations execute SIMD process equivalent to NOT, AND, and XOR gates in image domain. Fig. 3 summarizes an operation corresponding XOR as an example of the elements. Fig. 3 (a) indicates the relations between the input and the output patterns. From the figure, output patterns are inverted where either  $a_{i,j}$  or  $b_{i,j}$  is inverted. Considering the relations, we design a procedure for the datum of compression domain. This procedure is described in Fig. 3(b). Details of this operation and other two elemental ones are explained in Ref. [3].

In our solution for prime factorization, so called modulo exponentiation is implemented in accordance with the scheme. We have proposed an improvement of the solution in Ref. [4]. In the improvement, the encoding is modified to reduce computational tasks. It is confirmed that the processing costs in the improved solution is less than 1/100 than that with simple pattern processing.

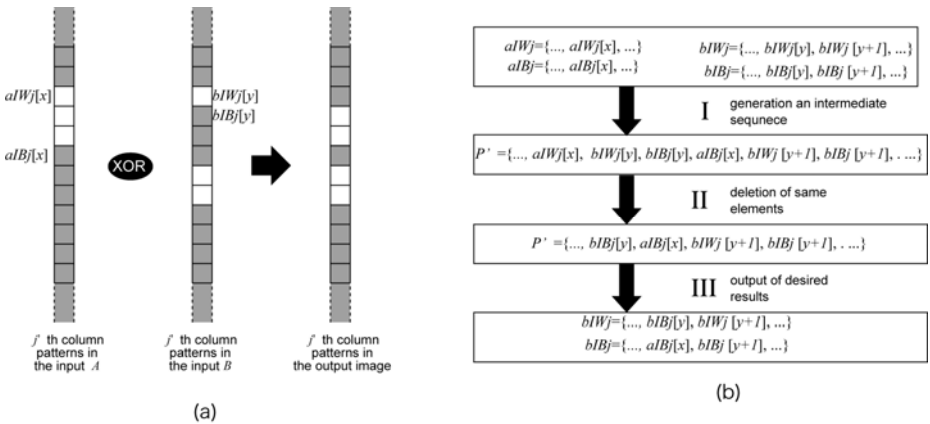


Fig. 3. (a) Relations between input and output patterns in XOR operation and (b) Data flow of the XOR operation in compression domain

In a solution for the TSP based on the scheme, on the other hand, matrix-vector multiplication is executed with the scheme [5, 6]. Additionally, a procedure to extract the tour with minimum path length has been designed. Note that encoding and elemental operations in the solution are quite same as that for prime factorization. As results of verification, usefulness of the scheme by use of data compression has been clarified.

The proposed scheme is considered to be useful for the both solutions. However, processing costs of these solutions seems to grow exponentially. We should modify encoding and elemental operations to reduce computational costs. Also, methodology to estimate the solutions should be constructed to progress our studies. These are considered to be important as future issues.

### 3 Summary

A scheme for SIMD processing for 2D binary images has been reported. One of the features of the scheme is to use image compression. It has been shown that some methods developed in digital optical computing are effectively implemented using the presented scheme.

### References

1. Tanida, J., Ichioka, Y.: A paradigm for digital optical computing based on coded pattern processing. *Intl. J. Opt. Comput.* 1, 113–128 (1990)
2. Yu, F.T.S., Jutamulia, S.: *Optical Signal Processing, Computing, and Neural Networks*. Wiley-Interscience, Hoboken (1992)
3. Nitta, K., Tado, Y., Matoba, O., Yoshimura, T.: A method for factorization by means of digital optical computing and image compression. In: *Proc. SPIE*, 6695, 66950B (2007)
4. Nitta, K., Minami, T., Matoba, O.: Two dimensional pattern processing by means of image compression. In: *Proc. SPIE*, 7072, 70720W (2008)
5. Nitta, K., Ohta, S., Matoba, O.: Implementation of the TSP based on pattern processing with a graphic processing unit. In: *Proc. SPIE*, 7442 (in print)
6. Nitta, K., Ohta, S., Matoba, O.: A method for traveling sales man problem by use of pattern processing with image compression. In: *Proc. SPIE* (in print)

# Proposal for Secure Key Distribution Using Classical Optics

Tobias Haist and Wolfgang Osten

Institut für Technische Optik, Universität Stuttgart, Germany  
haist@ito.uni-stuttgart.de

**Abstract.** We propose a new method for secure key distribution using white-light interferometry. In contrast to quantum key distribution, only classical waves are used and, therefore, single photons (and the practical problems associated with them) are avoided. The core idea is the employment of random but discrete delays on both sides of the communication channel. The security of the method currently cannot be proven and further investigations are necessary towards this goal.

## 1 Introduction

In 1949 Shannon proved that secure communication between two parties, in the following denoted by “Alice” and “Bob”, is possible once they share a common secret key with a length larger or equal to the message to be transmitted [1]. There are three ways to ensure the necessary key distribution between Alice and Bob. 1) Public key cryptography is using public known keys and mathematical methods (unfortunately with unproven security) to achieve communication [2]. 2) Personal exchange of keys (e.g. identical hard-disks filled with random numbers) gives very high security but, of course, is often not practical or even impossible. 3) Quantum key distribution currently seems to be the only secure method to generate a secret shared key between two parties that are separated by a certain distance. Different quantum methods have been proposed [3] but the corner stones of these techniques are the no-cloning theorem of quantum physics, the non-commutativity of certain pairs of observables (e.g. different polarizations) and the use of single photons. Practical systems using quantum key distribution have been realized but the use of single photons over large distances is still technically challenging and expensive.

## 2 Key Distribution Using White-Light Interferometry

Fig. 1 shows the core idea of using white-light interferometry for the secure key generation. A short coherent signal pulse is send by Alice to Bob. Bob delays the signal with delay  $D_2+D_3$  before returning it to Alice. Alice detects the interference between the signal delayed by Bob and her reference signal delayed by  $D_1$ . Therefore, interference will be detected if  $D_1$  equals  $D_2+D_3$  (a constant path length due to the communication channel omitted because one can always eliminate that).

The basic method for generating one key bit is as follows:

1. Alice chooses D1 randomly out of N discrete values (e.g.  $N=100$ ).
2. Bob chooses D2 randomly out of the same N discrete values.
3. Bob chooses D3 randomly to be 0 or  $\lambda/2$ . 0 corresponds to the bit zero and  $\lambda/2$  corresponds to bit one.
4. Alice sends a wave packet with (on average) M photons with  $M < N$ .
5. Alice detects if interference is present. If this is the case she also detects whether Bob has set D3 to 0 or  $\lambda/2$ .
6. Alice informs Bob (via a classical channel) if the bit is usable or not.

Each successful interference detection (probability for that is  $1/N$ ) leads to one shared random key bit. Of course, for practical implementation one would make a lot of changes to this core idea.

Now, why is it not possible for an eavesdropper, whom we will denote “Eve”, to share the key of Alice and Bob? Wouldn’t it be possible for Eve to intercept part of the wavepacket and thereby to detect the setting of D3 of Bob? At most, Eve could intercept L photons, with  $L < M < N$ . For every intercepted photon she can check a different delay  $D_e$ . For the simplest case of  $L=1$ , that is Eve intercepts one photon and therefore tests one delay the probability that she uses the same delay as Alice and Bob is  $1/N^3$ . On the other hand, the probability that Alice and Bob use the same delay is  $1/N^2$ . Therefore, everytime Alice and Bob use the same delay and exchange one secret bit, the probability for Eve for successfully measuring that bit is only  $1/N$ .

Of course, Eve can parallelize by intercepting L photons but still she will not be able to obtain *all* key bits and, therefore, classical techniques for privacy amplification [4] can be used by Alice and Bob to avoid such attacks.

Other attack approaches are possible for Eve. Most important, she might clone the wavepackets by using coherent amplification because for classical light, of course, the no-cloning theorem will not apply.

We think (a detailed analysis will be presented in a future publication) that Alice and Bob can defend against such an attack by using additional incoherent noise on the communication channel. The signal photons then are hidden in the noise signal. During interference detection the noise will only lead to an incoherent background. Coherent amplification amplifies both sorts of photons

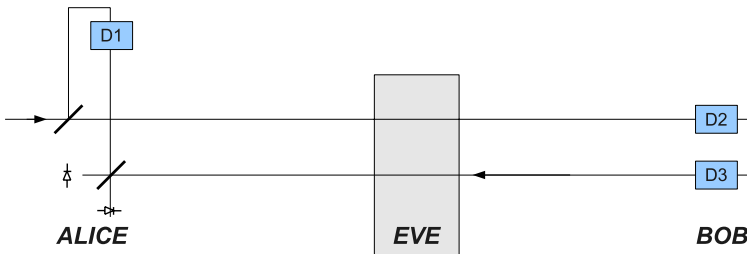


Fig. 1. Principle of white-light interferometry based key distribution

(noise and signal). If the noise is large enough than a lot of noise photons will be amplified and the photon statistics lead to large noise levels because with the total number of photons also the overall photon noise will increase (e.g. by the square root of the total number for the Poissonian statistics).

This also helps together with some wavelength multiplexing and filtering (at least we think so) against possible attacks by Eve where Eve actively sends light to Bob's delay.

### 3 Conclusions

We presented the basic idea of our proposal of using white-light interferometry (and therefore classical light) to realize secure key distribution. Details about some obvious attacks and their countermeasures will be presented in a future publication. At the moment, although we did not succeed in finding a working method for eavesdropping the key, a proof for the security of the method is not available.

### References

1. Shannon, C.E.: Communication theory of secrecy systems. Bell System Technical journal 28(4), 656 (1949)
2. Delfs, H., Knebl, H.: Introduction to cryptography: principles and applications. Springer, Heidelberg (2007)
3. Mermin, N.D.: Quantum Computer Science. Cambridge University Press, Cambridge (2007)
4. Watanabe, Y.: Privacy amplification for quantum key distribution. Journal of Physics A 40, F99–104 (2007)

# Analyze the Discrete Photo-Induced Current Pulses of the Photorefractive Spatial Light Modulator

Xiujian Li, Xiaoguang Hou, Yongming Nie, Wenhua Hu,  
Jiankun Yang, and Junbo Yang

Institute of Techno-physics, Science College, National University of Defense Technology,  
Changsha 410073, China  
optics\_nudt@188.com

**Abstract.** With excellent photo-electric and electro-optical effects, the photorefractive spatial light modulators can work as optically addressed modulators in optical information processing systems and parallel optical computing systems. The photo-induced current pulses of the photorefractive spatial light modulator observed in the experiments are analyzed to conclude the characteristics, and to find the relationship between the properties of the current pulse and the structural parameters. Furthermore, the origin of the photo-induced current pulse is analyzed, and the methods to improve the operation speed of the spatial light modulators are proposed. The research results will be significant for extending the applications of the photorefractive spatial light modulators, and pushing ahead the research of all-optical modulation materials and devices for optical supercomputing.

**Keywords:** optical computing, optically addressed spatial light modulator, photorefractive, photo-induced current pulse, discrete.

## 1 Introduction

Spatial light modulators (SLMs) are the infrastructure for most parallel optical information processing systems, parallel optical interconnection and parallel optical computing systems<sup>[1-4]</sup>. Based on the excellent photorefractive crystals<sup>[5-7]</sup>, such as BaTiO<sub>3</sub>, BSO (Bi<sub>12</sub>SiO<sub>20</sub>) and GaAs, the photorefractive SLMs can work as optically addressed modulators in these parallel optical systems, which focus on modulating speed and parallel capability. In order to improve the contrast ratio, usually the photorefractive crystals work in longitudinal modulation mode in which applied voltage is necessary.

However, the operation speed of the photorefractive SLMs can not still match the requirements of the high-speed optical supercomputing nowadays, and the high-speed 2-D full-optical modulators are still in seeking for.

With excellent optical and physical properties<sup>[8-15]</sup>, the BSO photorefractive SLMs attract many investigations in optical information processing and optical computing, and the research results are representative and referencable for other photorefractive crystals. The photo-induced current pulses of the BSO-film SLM have been observed in the experiments<sup>[16]</sup>, which may be one of the factors to induce irreversible

damage<sup>[17]</sup>. Combined with the irreversible damage, the current pulses are analyzed to sum up the characteristics so as to find out the relationship between the properties of the photo-induced current pulses and the structure parameters of the SLM. Furthermore, the origin of the current pulse is analyzed so as to propose the methods to improve the operation speed of the SLMs under various operation modes.

The research results will be significant for the designing, the optimizing and the extending applications of the photorefractive SLMs, and will push the research of high-speed full-optical modulation materials and devices for optical supercomputing.

## 2 Experiment Setup

The experiment setup for measuring the photo-induced current pulses flowing through the external circuit is shown in Fig.1, in which the SLM works in longitudinal modulation mode.

The SLM is asymmetric and conical, in which the transparent electrodes (marked [1] and [5]) are made of ITO, and the insulator (marked [2]) is made by Parylene C, which thickness is 20 and 10  $\mu\text{m}$  respectively to endure at least DC voltage of 4 and 2 kV respectively. The center wavelength of the high reflective film (HR film, marked [3]) is 633 nm, which is actually the wavelength of the He-Ne laser. And the BSO film (marked [4]) is about 15mm $\times$ 15mm (length $\times$ width) and 500  $\mu\text{m}$  or 1000  $\mu\text{m}$  thickness, which are wedge cut<sup>[13]</sup> with an angle of 1° to eliminate the interference between the input light beam and the output light beam. The incident surface

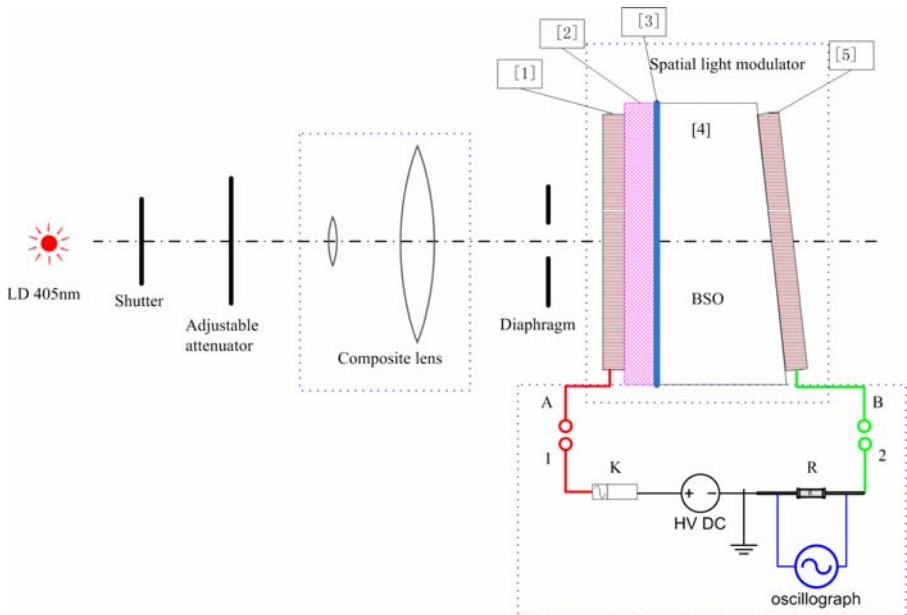


Fig. 1. Experiment setup

of write-light beam which coated with HR film is perpendicular to the axis [001] of the BSO crystal.

In the experiment setup, the write-light source is a LD with wavelength of 405nm and output power of 60mW.

A series-wound resistor are connected to the external circuit which provides the applied voltage of the SLM, and the Tektronix TDS 2022 oscilloscope will measure the voltage of the two ends of the series-wound resistor to observe the variation of the photo-induced current properly.

### 3 Experiment Results

#### 3.1 Experiment Conditions

The experiment conditions for the measurements are shown in table 1, in which the thickness of the BSO film is 500  $\mu m$  or 1000  $\mu m$ , the connections of the electrodes A, B to 1 and 2 are optional, and the resistance of the resistor R is 50  $\Omega$  or 50  $k\Omega$ . For all the experiment conditions, the wavelength of the write-light is 405nm, and the applied voltage is set to 1500 V when in operation.

**Table 1.** Experiment conditions

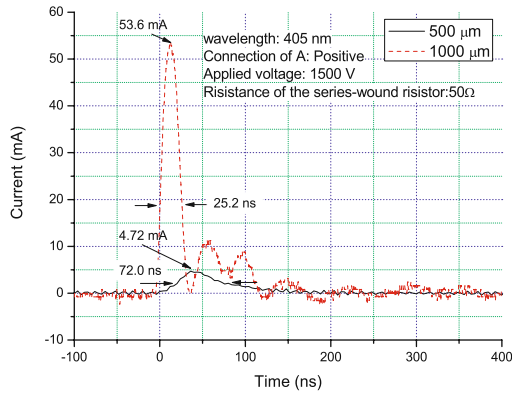
Experiment condition NO.	Thickness of BSO film ( $\mu m$ )	Connection of electrode A	resistance of R
1-500	500	1	50 $\Omega$
2-500			50 $k\Omega$
3-500		2	50 $\Omega$
4-500			50 $k\Omega$
1-1000	1000	1	50 $\Omega$
2-1000			50 $k\Omega$
3-1000		2	50 $\Omega$
4-1000			50 $k\Omega$

In the measurements, the diameter of the write-light beam is 1mm and distributed uniformly.

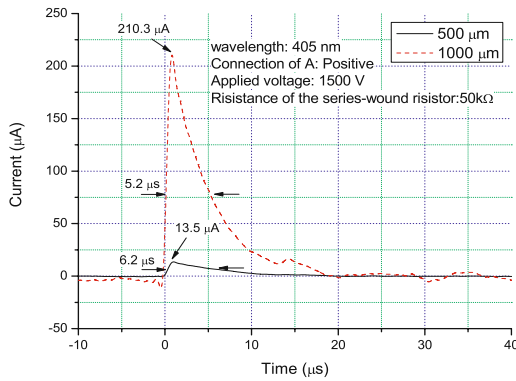
#### 3.2 Photo-Induced Current Pulses Measurement

Under all the experiment conditions, the photo-induced current pulses can be observed by the oscilloscope remarkably during the exposure. The observed current pulses for different experiment conditions shown in table 1 are shown in Fig.2~5. When all the measurements are performed, and the expose time of the write-light beam is about 2 seconds during which the applied voltage is being held on.

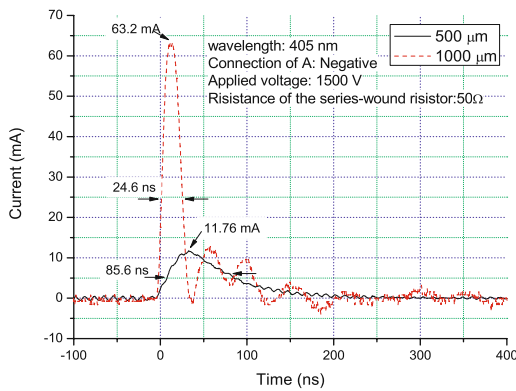




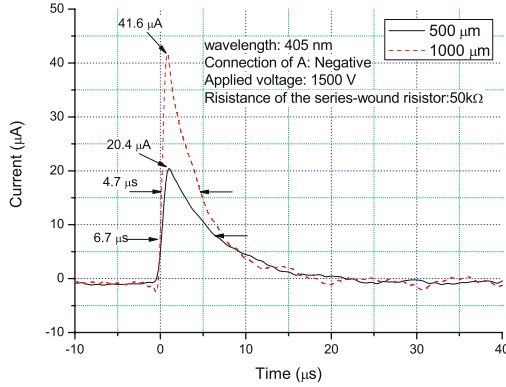
**Fig. 2.** Photo-induced current pulses of 1-500 and 1-1000



**Fig. 3.** Photo-induced current pulses of 2-500 and 2-1000



**Fig. 4.** Photo-induced current pulses of 3-500 and 3-1000



**Fig. 5.** Photo-induced current pulses of 4-500 and 4-1000

**Table 2.** Basic properties of the pulses

Experiment condition NO.	1/e time width	Full time width
1-500	72.0 ns	~200 ns
2-500	6.2 $\mu$ s	~20 $\mu$ s
3-500	85.6 ns	~200 ns
4-500	6.7 $\mu$ s	~20 $\mu$ s
1-1000	25.2 ns	~200 ns
2-1000	5.2 $\mu$ s	~20 $\mu$ s
3-1000	24.6 ns	~200 ns
4-1000	4.7 $\mu$ s	~20 $\mu$ s

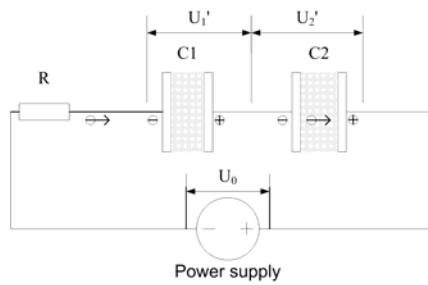
Furthermore, all the measurements are achieved in the middle of exposure rather than at the beginning or the end.

In Table 2, the 1/e time width denotes the time width of the pulses range rising from 1/e full range and dropping to 1/e full range, and the full time width denotes the full life-time of the continuous pulse.

## 4 Discussion

As the measurements are achieved in the middle of the exposure, and the expose time of the write-light beam is long enough, the shape and the pulse width of the current pulses will primarily be determined by the properties of the external circuit, the materials and the structure parameters of the SLM rather than by the properties of the write-light pulses.

As the SLM and the power supply can be considered as a RC circuit as shown in Fig.6, in which the composite capacitor is made up of the equivalent capacitor of the equivalent capacitor of the BSO film (marked C1) and the insulator(marked C2),

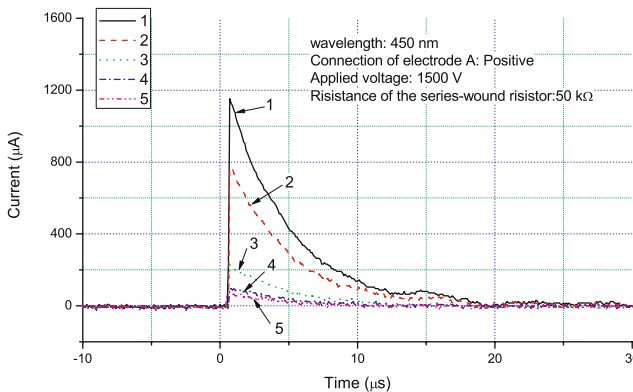


**Fig. 6.** Equivalent RC circuit of the SLM

which capacitance can be calculated with the properties of the materials and the structure parameters i.e. the thickness and the width of various films.

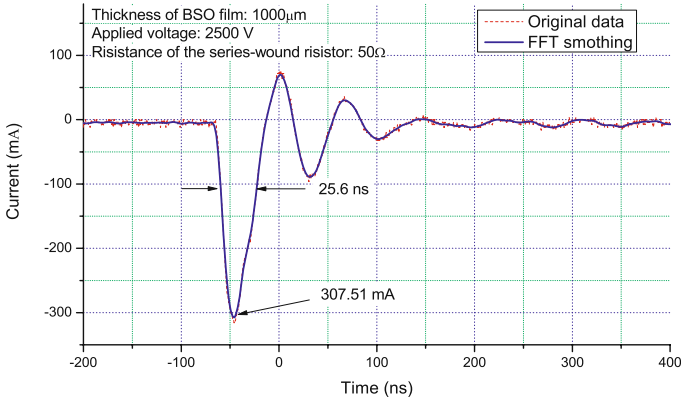
According to Table 2, though the  $1/e$  time width is different for various experiment conditions, the full time width may be uniform so far as the experiment conditions have the same series-wound resistor and the thickness of the BSO films.

When the resistance of the series-wound resistor is  $50\text{ k}\Omega$  and the thickness of the BSO film is  $500\text{ }\mu\text{m}$ , the RC time constant of the equivalent RC circuit is about  $6.5\text{ }\mu\text{s}$ , which is close to the  $1/e$  time width of experiment condition NO. 2-500 and NO. 4-500. When the thickness of the BSO film is  $1000\text{ }\mu\text{m}$ , the RC time constant of the equivalent RC circuit is about  $5\text{ }\mu\text{s}$ , which is close to the  $1/e$  time width of experiment condition NO. 2-1000 and NO. 4-1000. And the Photo-induced current pulses after various exposure time are measured, as shown in Fig.7. The pulse NO.1 is measure first, and 2~5 are measured in sequence with distance of 5 seconds. The pulses indicate that, even through the range is various, the full time width and the  $1/e$  time width of the pulses are almost uniform. These may indicate that, the operation speed of the SLM is determined rather by the external circuit properties, i.e. the RC time constant of the equivalent RC circuit, than by the photo- response speed of the photorefractive crystals.



**Fig. 7.** Photo-induced current pulses after various exposure time

In order to confirm the rule, the current pulses are measured when the write-light is moved away and at the time of turning of the applied voltage, as shown in Fig.8.



**Fig. 8.** Photo-induced current pulses after various exposure time

The pulses in Fig.8 show that, the  $1/e$  time width and the full time width are close to that of experiment condition NO. 1-1000.

In fact, the photo-induced current pulses represent the transfer of the photo-induced electrons along the circuit and the variation of the voltage across the SLM. Therefore, the operation speed of the SLM is mostly determined by the external equivalent circuit, i.e. the material properties of the photorefractive crystals and the insulator, and the structure parameters of the SLM.

## 5 Conclusion and Outlook

The photo-induced current pulses observed in the asymmetric BSO photorefractive SLM are determined by the electric properties of the external equivalent circuit, i.e. the material properties of the photorefractive crystals and the insulator, and the structure parameters of the SLM. The pulse characteristic of the photo-induced current will affect the writing process and limit the operation speed of the SLM. In order to optimize the operation speed of the photorefractive SLM, the material and the structure parameters should be designed to decrease the RC time constant of the external equivalent circuit. For instance, the continuous area of the photorefractive film should be cut to little areas, so as to decrease the equivalent capacitance. And, the photorefractive crystal and the insulator should be chosen with little dielectric constant.

Furthermore, in order to build up efficient all-optical architecture for the future parallel optical high performance computers, other materials such as organic compound should be tried. In which the limit of RC time constant won't exist, and the operation speed will mostly determined by the response time of the materials.

**Acknowledgments.** This work was partially supported by NSFC/China (project No. 60673147). The authors are grateful to Ning Chen of Science College of NUDT (China) for supporting for the work, and Jiayao Xu of Shanghai Institute of Ceramics and Yangzhu Yu of Cstech Crystal Co., Ltd. (China) for providing the BSO film.

## References

1. Yu, W., Takumi, M.: Performances of an all-optical subtracted joint transform correlator that uses a photorefractive crystal. *Optical and Quantum Electronics* 32, 367–382 (2000)
2. Tavassoli, A., Becker, M.F.: Optical correlation of spatial- frequency-shifted images in a photorefractive BSO correlator. *Applied Optics* 43(8), 1695–1702 (2004)
3. Das, A.K., Mukhopadhyay, S.: An all-optical matrix multi- plication scheme with non-linear material based switching system. *Chinese Optics Letters* 3(3), 172–175 (2005)
4. Engstrom, D., Hard, S., Rudquist, P., et al.: Beam steering experiment with two cascaded ferroelectric liquid-crystal spatial light modulators. *Applied Optics* 43(7), 1559–1569 (2004)
5. Golubovi, A., Nikoli, S.: The Growth and Optical Properties of  $\text{Bi}_{12}\text{SiO}_{20}$  Single Crystals. *J.Serb.Chem.Soc* 67(4), 279–289 (2002)
6. Bloom, D., McKeever, S.W.S.: Temperature dependence of electron mobility in  $\text{Bi}_{12}\text{GeO}_{20}$  and  $\text{Bi}_{12}\text{SiO}_{20}$  using the time-of-flight technique. *J. Appl. Phys.* 82(1), 249–258 (1997)
7. Buse, K.: Light-induced charge transport processes in photorefractive crystals II: Materials. *Appl. Phys. B* 64, 391–407 (1997)
8. Arizmendi, L., Cabrera, J.M., Agullo-Lopez, F.: Material properties and photorefractive behaviour of BSO family crystals. *International Journal of Optoelectronics* 7, 149–180 (1992)
9. Aldrich, R.E., Hou, S.L., Harvill, M.L.: Electrical and Optical Properties of  $\text{Bi}_{12}\text{SiO}_{20}$ . *J. Appl. Phys.* 42, 493–494 (1971)
10. Attard, A.E.: Photoconductive and photorefractive effects in BSO. *Applied Optics* 28(23), 5169–5174 (1989)
11. Ganeev, R.A., Rysanyansky, A.I., Tugushev, R.I., et al.: Nonlinear optical characteristics of BSO and BGO photorefractive crystals in visible and infrared ranges. *Optical and Quantum Electronics* 36, 807–818 (2004)
12. Hou, S.L., Lauer, R.B., Aldrich, R.E., et al.: Transport Process of Photoinduced Carries in  $\text{Bi}_{12}\text{SiO}_{20}$ . *Journal of Applied Physics* 44(6), 2652–2658 (1973)
13. Wintermantel, M., Biaggio, I.: Temperature-dependent electron mobility and large polaron interpretation in  $\text{Bi}_{12}\text{SiO}_{20}$ . *Physical Review B* 67(16), 165108 (2003)
14. McCullough, J.S., Georgalas, A.M., Hunt, C.A., et al.: Kinetics of the photorefractive response of bismuth silicon oxide. *Journal Of Applied Physics* 89(10), 5276–5281 (2001)
15. Golubovic, A., Nikolic, S., Gajic, R., et al.: The Growth and Optical Properties Of  $\text{Bi}_{12}\text{SiO}_{20}$  Single Crystals. *J.Serb.Chem.Soc.* 67(4), 279–289 (2002)
16. Li, X., Hu, W., Zhang, J., et al.: Discrete photoinduced current pulses of an asymmetric bismuth silicate photorefractive spatial light modulator. In: *Proc. of SPIE* 6624: 66241Q (2007)
17. Li, X., Yang, J., Yang, J., et al.: Unexpected irreversible damage of an asymmetric bismuth silicate photorefractive spatial light modulator. *Appl. Opt.* 46(18), 3774–3779 (2007)

# Optical Multiplexing Techniques for Photonic Clos Networks in High Performance Computing Architectures

Dietmar Fey<sup>1</sup>, Max Schneider<sup>1</sup>, Jürgen Jahns<sup>2</sup>, and Hans Knuppertz<sup>2</sup>

<sup>1</sup> Departement Computer Science, University Erlangen-Nuremberg, Germany

<sup>2</sup> FernUniversität in Hagen, Optical Information Technology, Germany

**Abstract.** Future high-performance computing (HPC) architectures will consist of whole parallel computing systems integrated on chip-level and boards mounted with lots of computing chips and chip-external main memory. Photonic networks on board and photonic network on chips (NoCs) offer the potential to fulfill the high bandwidth requirements in such systems. In addition they need less power, offer better EMC capabilities and can reduce cabling effort compared to electronic networks. Due to their non-blocking property Clos networks are frequently used in HPC architectures. Therefore we investigated how a photonic on-board Clos network can be realized using Coarse Wavelength-Division-Multiplexing (CWDM) techniques with state-of-the art components based on fibre technology. In addition we present a new photonic Clos NoC architecture based on Wavelength Interchanging (WI) elements, optical waveguide structures, mode-locked laser sources, nanophotonic microrings and passive optical deflection elements to reduce the number of switches. We discuss the benefits and drawbacks for using different optical technologies for such an architecture.

## 1 Introduction

Current microprocessors contain multiple compute cores and a hierarchy of cache-level memory. This trend of integrating more and more whole parallel computing systems on chip-level, which have been implemented on boards before, will continue. In addition, we will still find boards mounted with lots of computing chips and chip-external main memory in future, e.g. for signal processing applications. For such high computing performance systems high speed communication networks are necessary in order to fulfill the high bandwidth requirements. Photonic networks on board and also photonic network on chips (NoCs) offer a lot of benefits in this context. They can deliver a significant contribution to power reduction compared to electronic networks in which data buffering and signal restoration are required in order to sustain high cycle times.

Space craft applications, which first have been the driving force of this presented research study, put some additional strict requirements on the hardware realization. It is not only the performance in the processing and networking modules, e.g. in a satellite, which plays an important role. Also other factors

like EMC and the weight of the components have to be considered. Using photonic networks offers further benefits in this context. Already fiber based optics helps replacing thousands of comparatively heavy copper cables and connectors which link up to hundred electronic boards that can be contained in a modern satellite. To support reducing of electronic cables and to increase bandwidth capabilities we investigated Wavelength Division Multiplexing (WDM) techniques for high-performance computing (HPC) applications. WDM techniques are very attractive in this context since they allow a space multiplexing of several channels in one physical link, realized either as a fibre or as a waveguide structure. Coarse Wavelength Division Multiplexing (CWDM) is also preferable compared to Dense Wavelength Division Multiplexing (DWDM) since the wider distance of used wavelengths in CWDM allows much more tolerance against thermal fluctuations without applying sophisticated cooling techniques.

The technology of a photonic network has to consider the interconnection topology that is already given in a pure electronic system if one decides to replace the electronic network by a photonic network. In current space craft applications the processing devices are often linked with multi-stage Clos networks. Therefore we investigated realization possibilities of a photonic Clos network using optical multiplexing techniques for the background of a HPC application as it is given e.g. in space craft computer systems. We will face the benefits and drawbacks of different realization schemes for CWDM Clos networks considering the use of passive and active optical devices like diffraction gratings and Wavelength Interchange (WI) elements using microring resonators. Also the routing algorithms for Clos networks will be considered because some of them are based on edge-coloring strategies of graphs what can be directly mapped onto WDM hardware.

The rest of the paper is organized as follows. In chapter 2 we will present a specific class of routing algorithms for Clos networks that can be directly mapped onto WDM networks. Chapter 3 describes different realization possibilities for such WDM networks using different state-of-the-art technology. It is distinguished between a short-term realization, e.g. for a space craft solution, using fibres and optoelectronic VCSEL devices for a CWDM on-board network without WI. Furthermore we propose an advanced mid-term realization using nanophotonic devices using WI based on a modified edge-coloring routing algorithm for a NoC solution. Chapter 4 discusses specific requirements for the optical laser sources for WDM architectures. Finally we conclude the paper with a summary of the most important statements.

## 2 Clos Networks

### 2.1 Setup of Clos Networks

Clos networks are multistage interconnection networks, which connect input ports with output ports via the local input/output ports of a number of crossbar stages. A basic Clos network consists of three stages: input, middle and output stage. Each stage contains a number of crossbar switches. In general, three-stage

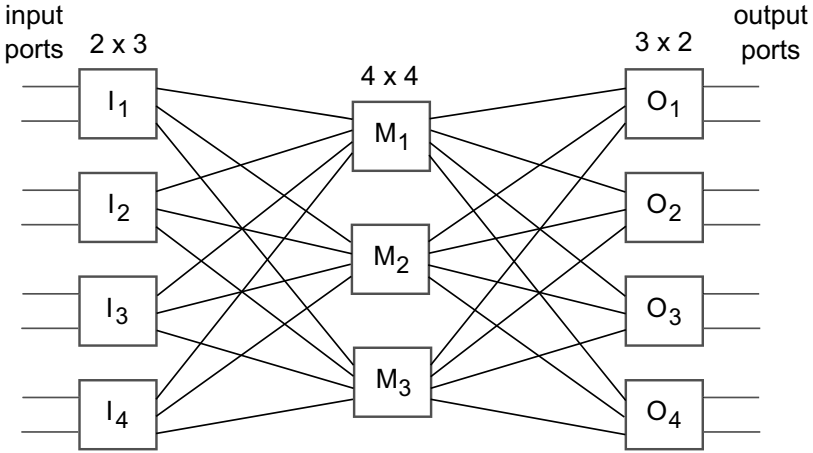


Fig. 1. Set up of a symmetric (2, 3, 4) Clos network

Clos networks are defined by a tuple  $C(n_1, r_1, m, n_2, r_2)$ , in which the first stage is made of  $r_1$  crossbars of size  $n_1 \times m$ , the last stage consists of  $r_2$  crossbars of dimension  $m \times n_2$ , and there are  $m$  crossbar switches of size  $r_1 \times r_2$  in the middle stage. The  $i^{th}$  local output port of an input stage switch  $I_j$  is connected to the  $j^{th}$  local input port of the  $i^{th}$  middle stage switch ( $i = 1, \dots, r_1$ ). The  $j^{th}$  output link of a middle stage switch  $m_k$  is connected to the  $k^{th}$  local input port of the  $j^{th}$  output stage switch ( $j = 1, \dots, r_2$ ). The tuple  $C(n, r, m, n, r)$  defines a symmetric three-stage Clos network  $C(n, m, r)$ . Figure 1 shows a  $C(2, 3, 4)$  Clos network. A three-stage Clos network can be expanded by replacing each of the middle stage switches with another three-stage Clos network leading to five stages. In the following we will restrict our explanation to three-stage networks which present the general form.

Clos networks are non-blocking if some constraints concerning their number of switching elements are fulfilled. If  $m \geq n$  then each request on any input port of an input stage switch can be routed to the relevant output port of any output stage switch. However, in this case it could be possible that another existing connection uses exactly the ports of a middle stage switch we need for the requested link. Then this link has to be rearranged to another available middle stage switch. In this case the Clos network is denoted as *rearrangeable non-blocking*. If  $m \geq 2n - 1$  then each request of any input link of an input stage switch can be routed to the relevant output link of any output stage switch without rearranging another requests. In this case the Clos network is denoted as *strict-sense non-blocking*.

The drawback of a Clos network is that it is not a self-configuring or self-routing network, meaning that the switches are directly adapted according to a header information given in the arriving data bit stream. Instead of that, a central routing algorithm has to be applied which calculates in advance the position



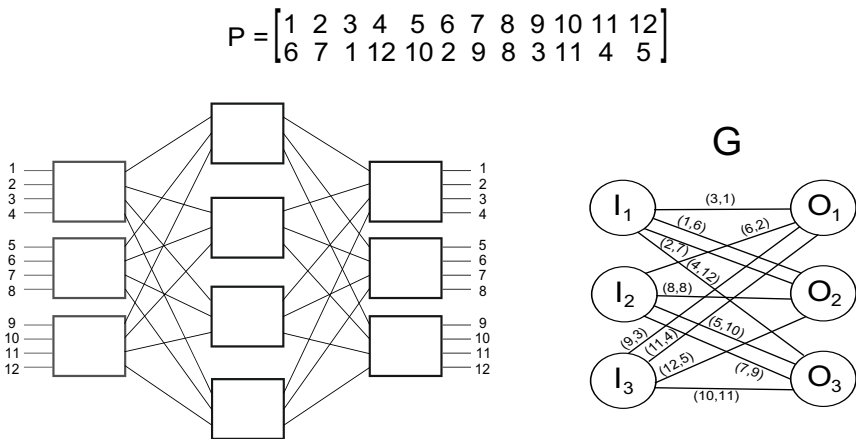
of the switches in the different stages. However, this drawback can be tolerated if the application knows in advance the desired input/output connection.

### 2.2 Routing Algorithms in Clos Networks

Different approaches are known in literature to calculate how the crossbar switches are to set to realize a non-blocking routing. In [1] a procedure based on matrix decomposition is presented, in [2] a method that uses edge-coloring of a graph. In our work we focused on edge-coloring procedures because they can be intuitively mapped onto a WDM network. The mentioned graph presents the desired interconnect links that can be expressed by a permutation  $P : x \rightarrow \pi(x)$  that defines that the input port  $x$  of a Clos network is to connect to the output port  $\pi(x), 1 \leq x, \pi(x) \leq N$ , with  $N = n \cdot r$ . Figure 2 shows the corresponding graph  $G$  for an example of a (4,4,3) Clos network that has to be switched accordingly to 12 desired input-output links defined by a permutation  $P$ . For each input and output stage corresponding nodes  $I_i$  and  $O_j$  are generated in  $G$ . An edge is drawn from  $I_i$  to  $O_j$  for each defined connection in  $P$  which refers to ports belonging to the related input and output stages.

For the three input and output stages  $I_1, I_2 \dots, O_2, O_3$  of the Clos network in figure 2 we receive three nodes in the graph  $G$  labeled with the same identifiers. Two edges are running between  $I_1$  and  $O_2$  since we have two desired connections in  $P, (1 \rightarrow 6)$  and  $(2 \rightarrow 7)$ , which refer input stage  $I_1$  and output stage  $O_2$ . An analogue situation holds for  $I_2$  and  $O_3$ , and for  $I_3$  and  $O_1$ .

The goal is now to separate  $G$  in multi-graphs in such a way, that the union of all multi-graphs together is identical to the graph  $G$  and each of the resultant multi-graphs can directly mapped onto the linking of input and output ports of one middle stage switch. Therefore multiple edges between pairs  $(I_x, O_y)$  in  $G$



**Fig. 2.** A (4,4,3) Clos network and its corresponding graph  $G$  for a desired permutation  $P_4$

have to be eliminated because this leads to a conflict in the middle stage. To achieve that the graph  $G$  is first subdivided in two subgraphs  $G_1$  and  $G_2$  (see figure 3, left) in which no multiple edges are running between an input-output node pair. Furthermore the edges in each graph  $G_1$  and  $G_2$  are colored with the same color.

However, we have to separate the two graphs further on since we need four different colored graphs for the four different middle stages in our Clos network. This is performed by Euler partitioning [3] of  $G_1$  and  $G_2$  as follows. Starting from an arbitrary node in  $G_i$  one selects an edge and moves to the node to which the edge is running. This edge is removed from the graph  $G_i$ . This process is continued until e.g. no edges are given. The removed edges are subsequently inserted in two new subgraphs  $G_{ij} \in (i, j[1, 2])$ . Each edge in  $G_{ij}$  receives the same color, the  $G_{ij}$ 's among each other receive a different one. This procedure halves the number of edges running out of a node and the number of edges in the resulting subgraphs. Euler partitioning can be repeated until the number of edges corresponds to the number of ports in the middle stage of the Clos network and the number of the resultant graphs is equal to the number of middle stage switches. The result for the example is  $G_{11}, G_{12}$  for  $G_1$  and  $G_{21}, G_{22}$  for  $G_2$  (see figure 3, right).

Finally all crossbars in the Clos network can be configured as follows. The resulting Clos network with its set crossbar switches is shown in figure 4. Since each edge in the graphs represents one desired link of  $P$  one can conclude how the crossbars in the three stages have to be set. E.g., the edge running from  $I_1$  to  $O_2$  in the red graph  $G_{12}$  corresponds to the desired link  $(1 \rightarrow 6)$ . Consequently, the input port 1 in input stage  $I_1$  has to be connected to local output port 2 because this port leads to the red middle stage (red corresponds to  $\lambda_2$  in the following). The local port 6 in the output port  $O_2$  must be connected to local input port 2 because this port leads to the red colored middle stage switch. Consequently, the local input 1 has to be connected with local output port 2 in the red middle stage. In the same way all the other edges of the multi-graphs

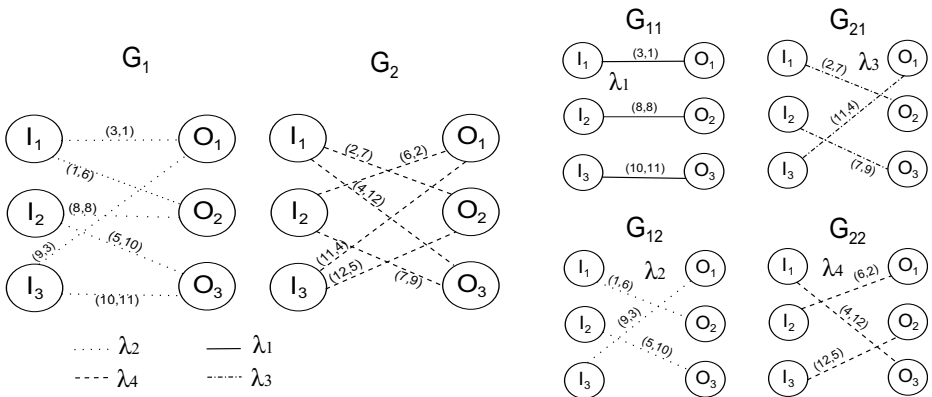


Fig. 3. Euler partitioning of graphs and continuation of edge coloring

are to handle. For more details on the exemplary shown partitioning scheme, e.g. which constraints have to be fulfilled in order to find always an appropriate subdivision of the graph, refer to [2].

### 3 Mapping the Colored Clos Network onto Photonic CWDM Clos Networks

The mapping of the colored Clos network can be mapped straightforward to a CWDM hardware layout. E.g., for the Clos network in figure 4 it is enough to use one optical link leaving each input stage switch and running to the middle stage switches if we can use four different wavelengths in each optical link. In the following we present two different realization possibilities based on different photonic technologies. The first proposal is more orientated on state-of-the-art technology using optical fibres and optoelectronic devices developed in the project MAUI (Multiwavelength Assembly for Ubiquitous Interconnects) [4], [5]. It was driven by the mentioned space craft application. Whereas the solution with those MAUI devices is thought as a network on board solution we also go a step ahead and propose a layout for a photonic NoC solution based on microring resonators to realize a WI function.

#### 3.1 Photonic Clos Networks with Fiber Based Technology

The MAUI device is an optoelectronic module which realizes 48 links with four different wavelengths in a  $12 \times 1$  fibre ribbon to link boards or chips mounted on boards. For sending data there is a sender device in which four columns of

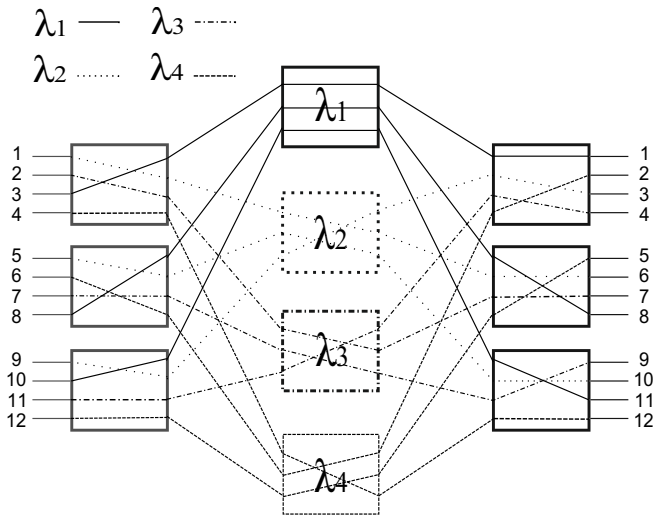


Fig. 4. Clos network as result of the edge-coloring routing algorithm

bottom-emitting laser diodes (LDs) are flip-chip bonded on a circuit containing the driver circuitry for the LDs. Each LD column is emitting light in another wavelength and each LD can be individually and digitally controlled by an external pin. To each sender device belongs a receiver device which contains four columns of 12 PIN photo diodes (PDs). Both devices contain mechanical lid equipment with MT-ferrule alignment pins to plug a  $12 \times 1$  MT fibre connector on top of their device surface. In addition deflection gratings are inserted in this subassembly for multiplexing and de-multiplexing the different wavelengths from each fibre to the LDs, resp. PDs.

Considering these device features we realize a strict non-blocking  $(4, 4, 12)$  Clos network to realize a  $48 \times 48$  connection. Figure 5 shows a conceptual layout for such a  $48 \times 48$  Clos network consisting of four MAUI devices (one sender and receiver pair between input and middle stages, resp. between middle and output stages) and two standard multimode fibre ribbons of size  $12 \times 1$  to connect a sender/receiver pair.

The network consists of four  $12 \times 12$  crossbars in the middle stage and 12 crossbars of size  $4 \times 4$  in the input and in the output stage. This size is exactly adapted to the capacity of the devices which offer 12 optical links with four wavelengths each. The switching in the crossbars shall be realized with electronic hardware. All middle stage switches can be integrated e.g. in one low-cost FPGA which has just to realize the connection of 48 input / output ports with  $4 \times 12^2 = 566$  digital switches, what is easy to meet. The FPGA can be closely connected to the MAUI receiver module on the left side of the middle stage and to the

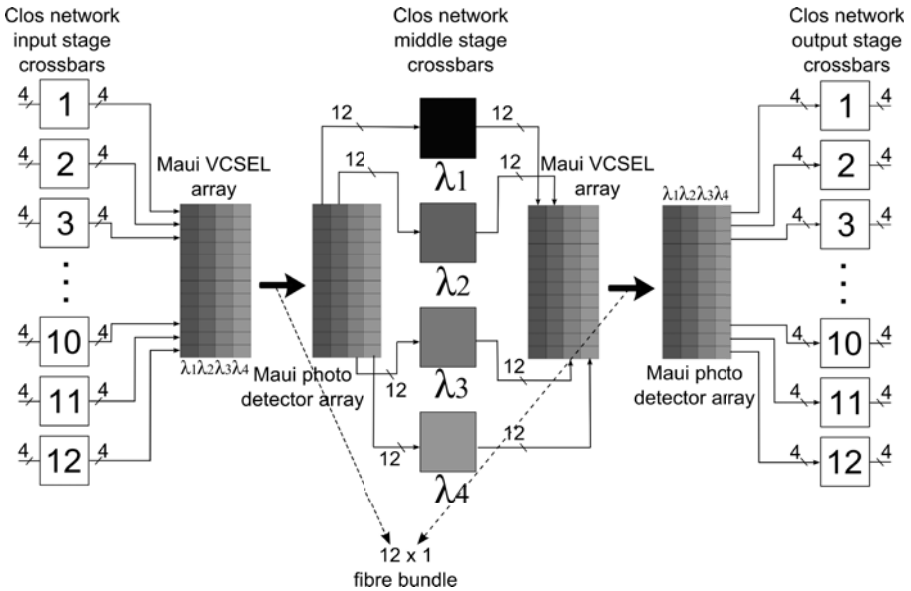


Fig. 5. Scheme for  $48 \times 48$  CWDM Clos network using devices from the MAUI project

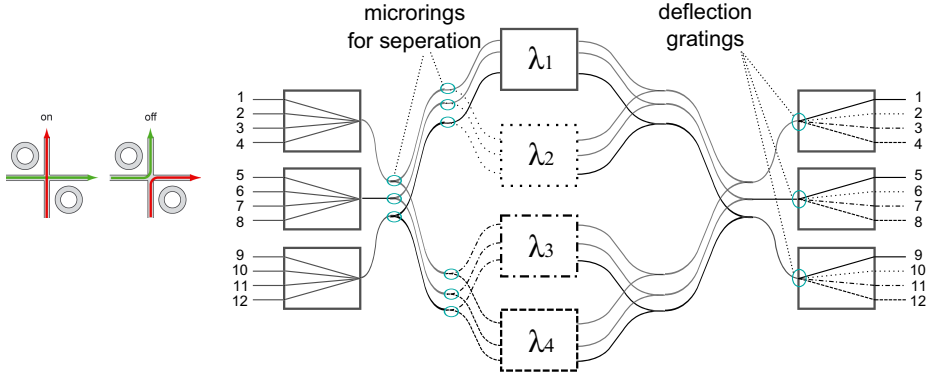
MAUI sender module on the right side of the middle stage. Therefore only very short ranged electronic interconnections are sufficient what allows high cycle times and simplifies board wiring.

It is necessary that the single LDs and PDs are contacted in the right way what can be exactly read out in the Clos network configured by colored edges. The four local output ports of the 12 crossbars in the Clos network's input stage control one row of a MAUI sender module. Since all crossbars in the middle stage are characterized with the same color, each middle stage is directly connected with a specific column of a  $12 \times 4$  MAUI device using the same wavelength for sending and receiving. The ports leaving the first crossbar in the middle stage, to which the color black ( $\lambda_1$ ) is assigned (see figure 5), contact directly all 12 pins of a Maui sender module in the first column controlling the first wavelength. The 12 output ports of the second crossbar in the middle stage device are responsible for the 12 LDs in the second column, and so on. Finally the 12 output rows of the MAUI receiver module located at the Clos network's output stage are connected 1-to-1 to the input ports of the crossbars (i.e. first PD row to first crossbar, second row to second crossbar, and so on).

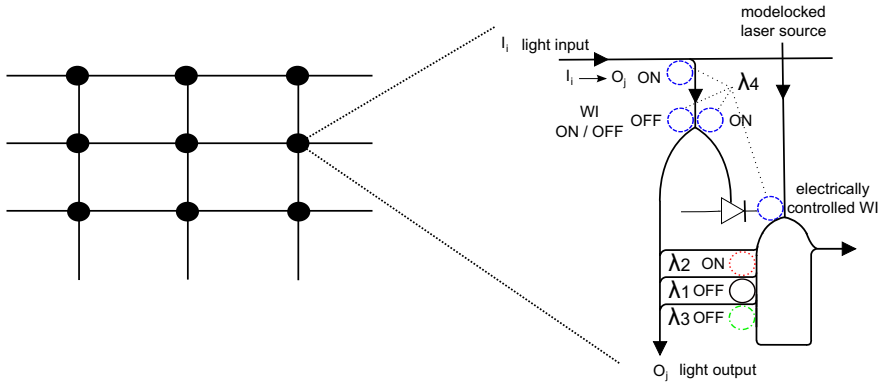
The layout shown in figure 5 can be easily expanded to a  $(4, 4, 24)$  Clos network realizing a  $96 \times 96$  port connection. This requires only four fibre ribbons and four MAUI sender/receiver pairs, one FPGA with 192 pins to realize 2304 digital switches in the middle stage crossbars and short range electronic on-board interconnects. This represents a drastic reduction compared to a pure electronic on-board network or even an electronic Clos network between boards. Connectors with 192 pins and 192 long on-board lines are eliminated leading to reduced wiring because four thin  $1 \times 12$  fibre ribbons do not lead to a spaghetti fibre wiring.

### 3.2 Photonic Clos NoC with WI Elements Based on Nanophotonic Microrings

Figure 6 shows a possible layout for the photonic Clos NoC using passive deflection elements in the output stage, middle stage crossbars that realise a WI and a hierarchical waveguide structure in the input stage routing the input data stream with electronically controlled nanophotonic microrings to the right middle stage crossbars. Using passive deflection gratings in the output stage is possible because we assigned a fix wavelength to each output port. In each port of every input stage module one of the possible wavelengths is injected in one waveguide structure and the mixed wavelengths are propagated to a separation stage at which the wavelengths are switched by microrings to the right middle stage. Such microring switches were recently demonstrated [6], [7] and proposed as switching elements for photonic NoCs [8], [9]. They are controlled by an electronic control circuit which injects an electric field into p-n-contacts surrounding the rings. Then the resonance of the ring can shift such that the transmitted light is in resonance and makes therefore a right angle turn. We propose to use such microrings for the seperating the wavelengths in the input stage to the right middle stages. For that a fix assignment to the microrings is sufficient. In this



**Fig. 6.** Scheme for a photonic Clos NoC using microrings as switching elements for input routing and WI functionality and passive optical routing in the output stage



**Fig. 7.** WI functionality using microrings in the middle stage photonic Clos NoCs

sense also the input stage works as a passive optical system. We first switch by appropriate tuned microrings the colors red ( $\lambda_2$ ) and black ( $\lambda_1$ ) to the upper half of the network and then we separate the two colors to the correct middle stages. The same has to happen for the other two colors in the lower half (6).

The task of the middle stage modules is to couple the required wavelengths in the outgoing wave-guide structures in such a way that they can be separated by the deflection gratings according to the fixed assigned wavelength of the output ports. This can possibly cause a WI. Again we propose to use microrings for that purpose. A possible solution for such a switching is shown in figure 7.

If the incoming light via an input port  $I_i$  has to be directed to the output port  $O_j$  the microring ( $I_j \rightarrow O_j$ ) has to be switched on. If the wavelength has not to be changed the incoming light is directly propagated to the output (at WI ON/OFF, left microring ON, right microring OFF). Else (shown in figure 7) the light is detected via a photo receiver to determine 1s and 0s in the input data. Then the light of a mode-locked laser [10] is correspondingly modulated

via the microring denoted as electrically controlled WI in (7) and the desired wavelength is filtered out by further microrings.

The actual output position for all used microring switches has to be calculated by the electronic control circuit according to the desired interconnections. A central electronic control circuit means no restriction because a non self-configuring network like a Clos network requires anyway a centralized routing algorithm from the algorithmic viewpoint. In order to detect if wavelengths have to be converted and if so in which wavelength we modified the edge-coloring algorithm presented in 2.2.

As in section 2.2 we start with a graph in which an edge is running between each  $(I_i, O_j)$  node pair if there is a desired interconnection between ports belonging to the stages  $I_i$  resp.  $O_j$  (see figure 8). We decompose this graph in a multi-graph according to the class of output ports to which the same color or wavelength is assigned. As result we receive so much partial graphs as there are wavelengths. If not more than one edge is running between the node pairs  $(I_i, O_j)$  in such a partial graph we have no conflict for that wavelength, denoted as  $c_k$  in the following. We assume that each edge is labeled with a tuple  $(x \rightarrow y)$  that contains the desired connection between the global input port  $x$  and the global output port  $y$ . Then the middle switch stage, which is responsible for that wavelength, can route the incoming data stream directly to its corresponding local output port running to the output stage  $O_j$  which serves the global output port  $y$ . At the local input port the wavelength  $c_k$ , that is assigned to the output port  $y$ , has to be injected in the waveguide.

A conflict is given if more than one edge, e.g.  $e$  edges, is leaving a node  $I_i$  in a partial graph  $g_k$  for a certain wavelength  $c_k$ , e.g. see  $I_2$  in the partial graph with the red colored edges. In this case we have to find for each additional edge an alternative wavelength as follows. Let  $I_i$  be the node whose desired interconnections cause a conflict. We are searching through all partial graphs  $g_z (1 \leq z \leq n; z \neq k)$  in a fixed order for the first partial graph in which node  $I_j$  has no outgoing edge. There must be such a partial graph because there are  $n$  partial graphs, one for each of the  $n$  wavelengths, and exactly  $n$  edges leave each node  $I_i$  in all partial graphs together. Consequently, there must be  $e - 1$  partial graphs  $g_z (z \neq k)$  in which  $I_i$  has no leaving edge. The wavelength assigned to the first partial graph, in which we found a node  $I_i$  without edges, can then be used as first alternative wavelength. If we need more free wavelengths then the search has to be continued in the remaining partial graphs. The output data stream is inserted in the optical link that is running to that middle stage which is

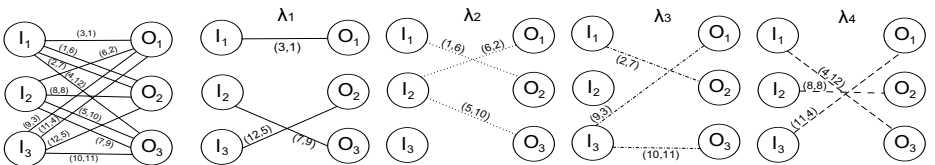


Fig. 8. Edge-coloring algorithm for WI function

responsible for that alternate wavelength. Figure 8 shows two desired connections in  $I_3$  to an output with red colour according to the desired permutation  $P$  given in figure 2. Therefore the first desired connection (6,2) can be selected via the colour red. For the second one (5,10) an alternate wavelength must be found. In the partial graph, which is responsible for the green ( $\lambda_3$ ) connections, no edge is leaving from  $I_2$ . Consequently, we can inject green light in port 5 of the input stage  $I_2$  which is passively routed to the middle stage which is responsible for the green wavelengths. In this middle stage a WI function has to be applied from green ( $\lambda_3$ ) to red ( $\lambda_2$ ) and the output has to be switched to local output port 3 because this local output port is connected to the output stage  $O_3$ . There the light is passively deflected to the output port 10, the desired target address.

### 3.3 Evaluation of the Presented Solutions in Terms of Required Switches

In the following we express depending on the number of used wavelengths,  $\#col$ , and the size of the network,  $N \times N$ , the number of the required switches for the two different photonic Clos networks we investigated in this paper: (i) a fibre based network on board solution as short-term realization, e.g. for a space craft application, and (ii) a NoC proposal using nanophotonic microrings for routing and WI functionality as mid-term solution. We can determine the size ( $n, m, r$ ) of the photonic Clos networks as follows:  $r = N/\#col; n = \#col; m = \#col$ . Consequently, the number of switches in the input, middle and output stage for the fibre based network can be calculated (1).

$$\#Switches_{fibre-based-Clos} = r \times n^2 + m \times r^2 + r \times n^2 = 2N\#col + \frac{N^2}{\#col} \quad (1)$$

For the microring based Clos NoC we have only active switches in the middle stage. As one can see in figure 7 in each of the  $m \times r^2$  switching elements of the photonic crossbar we need  $(4 + \#col - 1)$  microrings which have to be electronically switched on or off. Consequently, (2) is the number of required switches for the NoC network (2).

$$\#Switches_{NoC-based-Clos} = r \times m^2 \times (4 + \#col - 1) = \frac{N^2}{(\#col)} \times (4 + \#col - 1) \quad (2)$$

For the case that the ratio of (2) to (1) is below 1 the NoC solution requires fewer active switches. A longer mathematical transformation yields that this holds if condition (3) is satisfied.

$$N < \frac{2\#col^2}{2 + \#col} \quad (3)$$

The limits according to (3) where the NoC solution requires less switches is for 4 wavelengths  $N = 5.3$ , for 8 wavelengths  $N = 12.8$ , for 16 wavelengths  $N = 28.4$ . The larger  $N$  is the more preferable is a solution without WI and two active stages in the input and output of the photonic Clos network. Therefore



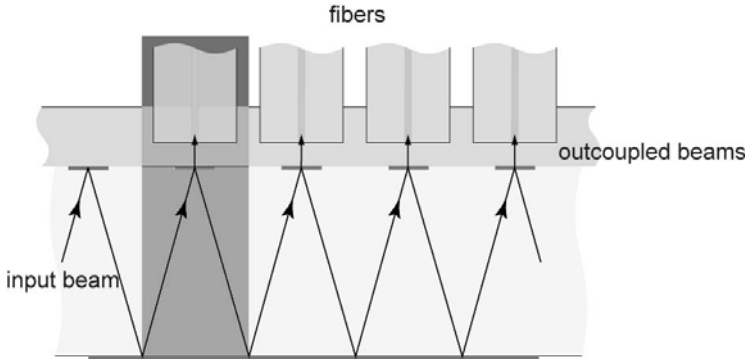
we can conclude as follows. Besides the additional flexibility, it is also preferable to implement the possibility of WI based on microrings for smaller network sizes of  $N$  in terms of the number of realizable elementary switches.

For that NoC solution we assumed the use of a single mode-locked laser source whereas the fibre based solution uses MAUI sender modules containing different stripes of semiconductor VCSEL arrays emitting light with different wavelengths. Mode-locked lasers offer the advantage of an off-chip single broadband laser source for WDM interconnections [11]. For a space craft solution the use of an external single mode-locked laser source discards due to its size. Nevertheless, there are some characteristics making mode-locked lasers ideal as optical supply source for WDM in HPC architectures: (i) generating ultra-short pulses in the  $fs$  range, (ii) thermal stability and (iii) its comparatively broad wavelength spectrum to use several wavelengths that reduce the efforts in the number or required switches for smaller sized networks. However, for a use in a HPC system there is the drawback of the comparatively long distance between the pulses in the MHz range. The use of passive optics can help eliminating this drawback as we discuss in the next chapter.

## 4 Consideration on the Practical Implementation

The schemes for WDM-based interconnection require the use of suitable sources. Most preferable would be multiple-wavelength VCSEL devices. However, practical difficulties may occur since the wavelength of VCSEL emitters is not very well defined due to fabrication tolerances and temperature drifts. Wavelength tolerances in the range of several nanometers may easily occur. In combination with the operating range of the filters, this puts a limit to the number of channels that can be handled.

In order to achieve a large number of channels, it might be an interesting alternative to use short pulse lasers as suggested in [10]. In recent years, mode-locked lasers which emit pulses with durations in the  $ps/fs$ -range have become more and more practical, so that nowadays turn-key systems are available that emit pulses with durations of less than 100  $fs$ . The pulse duration  $\tau$  is related to the spectral width  $\Delta\lambda$  of the optical radiation by  $\Delta\lambda = \lambda^2/c\tau$ . Here,  $c$  denotes the speed of light and  $\lambda$  the center wavelength of the radiation. For example, if  $\lambda = 780nm$ , one has  $\Delta\lambda \approx 100 nm$  for  $\tau = 20ns$  and  $\Delta\lambda \approx 40nm$  for  $\tau = 50ns$ . In this scheme, it is necessary, however, to split up the optical power from a single  $fs$ -laser source to supply an optical signal to many communications channels. Modulator devices are required to generate the data streams. For the modulators similar considerations apply like for VCSEL devices in terms of wavelength range and tolerances. Therefore, there is no clear advantage for either scheme. In  $fs$ -laser scheme, it is attractive to use a single source and distribute the signals with very little skew to the different communication links. Efficient multiple-beam splitting using free-space and waveguide optics has been demonstrated in the past by using various concepts, see e.g. [12]. The concept of a microoptical H-tree for short pulses was demonstrated in ref. [13].



**Fig. 9.** Optical fanout module acting as beam-splitter and delay-line using the scheme of [14]

A less desirable feature of mode-locked laser sources is the fact that the repetition rate of the pulses is typically less than 1 GHz, i.e. lower than the data rates for the communication channels. However, this could be solved by adding tapped-delay lines into the optical distribution scheme [14] (see figure 9). This means, a single optical pulse would not only be split spatially to  $N$  output channels, but also in time to generate virtually a pulse chain of higher repetition rate. The temporal splitting of  $fs$ -pulses was also demonstrated by the use of suitable microoptical devices [15].

## 5 Conclusion

In the paper we investigated optical WDM techniques with and without WI functionality and the use of different technologies levels (fibre based links with VCSELs on one side and nanophotonic microring switches using mode-locked lasers on the other side) for the realization of photonic Clos networks in HPC architectures. In addition we showed the usefulness of edge-coloring routing algorithms for a direct mapping of a Clos network architecture onto WDM hardware. For a space craft solution, which was our originally inducement of the presented investigation, the fibre/VCSEL based solution is to prefer. For a NoC solution with WI functionality that allows realizing the Clos network's input and output stages solely with passive optics, a microring/mode-locked laser technology is to favor. In particular this holds if the number of network ports is smaller. The exact break-even point depending on network size  $N$  and numbers of used wavelengths was mathematically derived. In conclusion, one might say, that WDM-multiplexing appears very attractive in order to achieve high-throughput optical interconnection. However, the practical aspects related to the suitability of the light sources are not completely solved yet. VCSEL-implementation is very attractive, the use of  $fs$ -pulses with suitable modulators might offer an interesting alternative as well.

## References

1. Jayszczyk, A.: A Simple Algorithm for the Control of Rearrangeable Switching Networks. *IEEE Trans on Communication*, 169–171 (1985)
2. Carpinelli, J.D., Oruc, A.Y.: Applications of Matching and Edge-Coloring Algorithms to Routing in Clos Networks. *Int. Journal Networks* (1994)
3. Gabow, H.N.: Using Euler Partitions to Edge Color Bipartite Multigraphs. *Internat. J. Comput. Inform. Sci.* 5, 345–355 (1976)
4. Lemoff, B.E., et al.: Parallel-WDM for multi-Tb/s optical interconnects. In: *Proceedings IEEE 18th Annual Meeting of the Lasers and Electro-Optics Society*, pp. 359–360 (2005)
5. Lemoff, B.E., et al.: MAUI: Enabling Fiber-to-the-Processor with Parallel Multiwavelength Optical Interconnect. *IEEE J. Lightwave Technology* 22, 2043–2054 (2004)
6. Xu, Q., et al.: 12.5 GBit/s carrier-injection-based silicon microring silicon modulators. *Optics Express* 15(2), 430–436 (2007)
7. Xia, F., Sekaric, L., Vlasov, Y.A.: Ultra compact optical bufferes on a silicon chip. *Nature Photonics* 1, 65–71 (2007)
8. Shacham, A., Bergman, K., Carloni, L.P.: The Case for Low-Power Photonic Networks on Chip. In: *44th ACM/IEEE Design Automation Conference, 2007. DAC 2007, June 4-8, 2007*, pp. 132–135 (2007)
9. Small, B.A., Lee, B.G., Bergman, K., Xu, Q., Lipson, M.: Multiple-wavelength integrated photonic networks based on microring resonator devices. *J. Opt. Netw.* 6, 112–120 (2007)
10. Keeler, G.A., Nelson, B.E., Agarwal, D., Debaes, C., Helman, N.C., Bhatnagar, A., Miller, D.A.B.: The benefits of ultrashort optical pulses in optically interconnected systems. In: *IEEE Journal of Selected Topics in Quantum Electronics*, March-April 2003, vol. 9(2), pp. 477–485 (2003)
11. Nelson, B.E., Keeler, G.A., Agarwal, D., Helman, N.C., Miller, D.A.B.: Wave-length division multiplexed optical interconnect using short pulses. *IEEE Journal of Selected Topics in Quantum Electronics* 9(2), 486–491 (2003)
12. Jahns, J.: Free-space optical digital computing and interconnection. In: Wolf, E. (ed.) *Progress in Optics*, vol. XXXVIII. Elsevier, Amsterdam (1998)
13. Knuppertz, H., Bohling, M., Jahns, J.: Optical clocking and interconnection using short pulses and CDM. In: *ICO Top. Meet. on Optoinformatics/Information Photonics 2006*, St. Petersburg, Russia (2006)
14. Gruber, M., Kerssenfischer, R., Jahns, J.: Planar-integrated free-space optical fan-out module for MT-connected fiber-ribbons. *Lightwave Techn.* 22, 2218–2222 (2004)
15. Grunwald, R., Bock, M., Jahns, J.: Femtosecond-laser pulse shaping with microoptical retroreflector arrays. In: *Conf. Lasers and Electro-optics (CLEO) 2008, San Jose, CA* (2008)

# Improvement of a System for Prime Factorization Based on Optical Interferometer

Kouichi Nitta, Nobuto Katsuta, and Osamu Matoba

Department of Computer Science and Systems Engineering,  
Graduate School of Engineering, Kobe University  
Rokkodai 1-1, Nada, Kobe 657-8501, Japan  
nitta@kobe-u.ac.jp, katsuta@cs.brian.cs.kobe-u.ac.jp,  
matoba@kobe-u.ac.jp

**Abstract.** An optical system to execute prime factorization is modified to improve its processing performance. In the improvement, some deletions in interference measurements are permitted. As results, it is experimentally verified that the improved method can provide correct results in factorization of 30bits integer.

**Keywords:** Parallel processing, plane wave, optical interference, modulo operation, prime factorization, spatial parallelism.

## 1 Introduction

Recently, some solutions based on optical signal processing have been proposed for various problems requiring hard computational tasks [1-4]. For example, two different systems for the travelling salesman problem (TSP) are presented Refs. [1] and [2]. In Ref. [1], the TSP is solved with an optical correlator. On the other hand, white light interferometry is utilized for the problem in the system shown in Ref. [2].

In such a situation, we also research an optical method for prime factorization [5]. In the method, modulo multiplication is executed in parallel by a simple Michelson interferometer. Modulo multiplication is an important operation in an algorithm for prime factorization. The characteristics of the optical method are based on spatial parallelism of light.

In our previous works, some advantaged features of the optical method are clarified. Optical hardware for parallel processing is achieved with only a single light source and a single light modulator. Requirement to accuracy of alignment in the optical set up is not so critical in prime factorization. This feature is caused by properties of the algorithm.

We have presented some reports based on the research. Two-dimensional (2D) parallel processing of the method is demonstrated in Ref. [6]. This processing form is considered to be suitable for optical implementation. Also, an improved method has been proposed to treat larger scale targets [7].

In this research, another improvement is reported. This method provides correct results for prime factorization though there are deletions in a data set for postprocessing. It is shown that this method is useful for large scale processing.

## 2 Modulo Operation Based on Optical Interference and Phase Modulation

An algorithm for prime factorization utilizes a specific function shown in Eq. (1).

$$f(x) = a^x \bmod N \quad (1)$$

This function is called modulo exponentiation. In Eq. (1),  $N$  is a target integer of prime factorization and it is given as a product of two prime factors.  $a$  is also an integer which is satisfied with Eqs. (2) and (3), respectively.

$$1 < a < N \quad (2)$$

$$\gcd(a, N) = 1 \quad (3)$$

$f(x)$  is known to be a periodic function and the period is an integer. In case that the period is an even number, elements of prime factors can be extracted with post processing. Details of the algorithm are equivalent to Shor's quantum method presented in Refs. [8, 9].

Because  $f(x)$  is derived with a sequence of parallel processing for modulo multiplication, this processing is an important operation in prime factorization. Modulo multiplication is defined as Eq. (4).

$$g(x) = yx \bmod N \quad (4)$$

An optical method to derive  $g(x)$  is based on phase modulation of optical signals. Considering a light wave represented as Eq. (5),

$$U(\phi) = \exp(i2\pi\phi) \quad (5)$$

The optical field corresponding to  $g(x)$  is obtained by setting  $\phi = yx/N$ . In accordance with the principle, a system for parallel processing is constructed with a Michelson interferometer. Figure 1 shows a schematic diagram of the optical system. In the system, tilt angle of the mirror device is given as Eq. (6).

$$\theta(y) = \frac{1}{2} \sin^{-1} \left( \frac{y\lambda}{DN} \right) \quad (6)$$

In the equation,  $\lambda$  and  $D$  show wavelength of the light source and pixel pitch of sensor array, respectively. As result, desired results of parallel processing can be obtained. Fig. 2 shows relations between pixels and phase of optical signals.

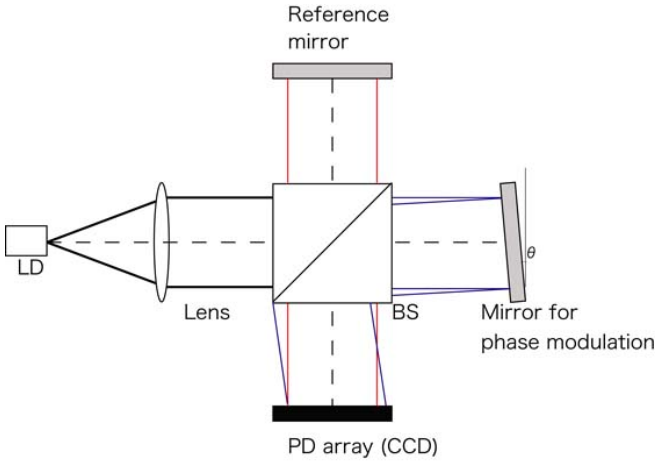


Fig. 1. Schematic diagram of optical set up for parallel modulo multiplication

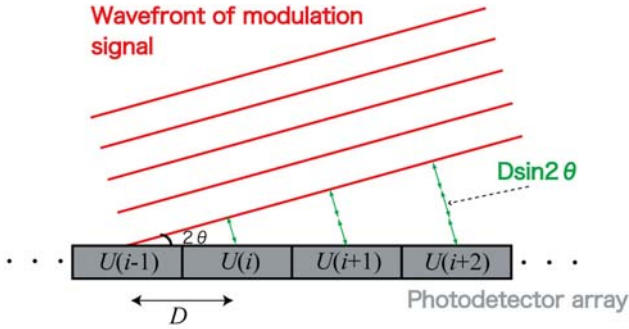


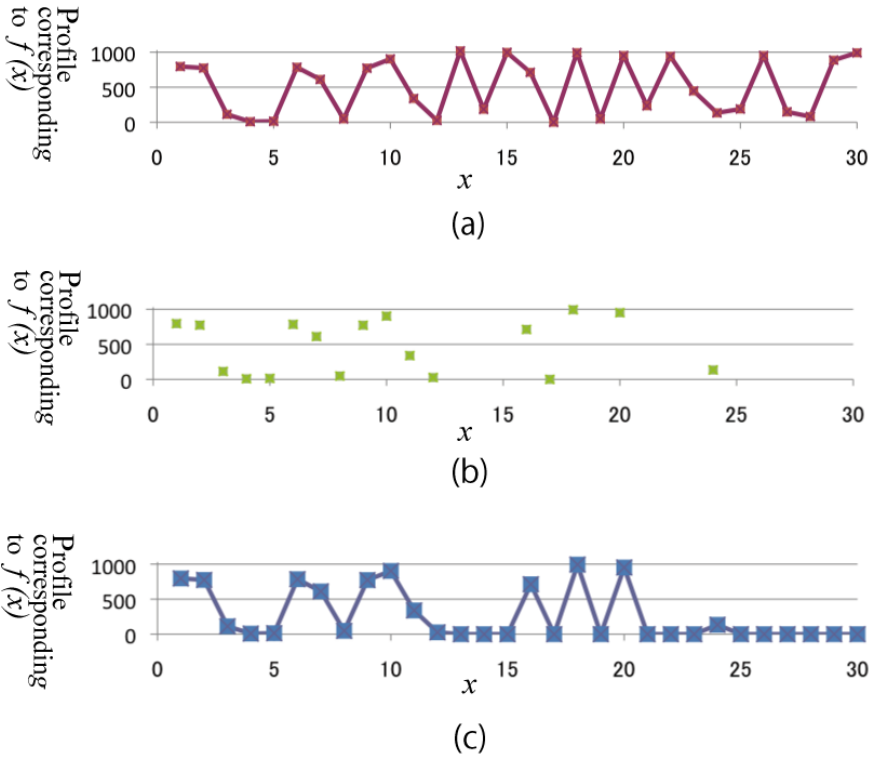
Fig. 2. Diagram to show relations between pixels of detector array and detected optical signals with phase modulation

### 3 Optical Hardware and Improved Solutions

In our method for prime factorization,  $l_i (= a^{2^i} \bmod N)$  is derived from  $i=0$  to  $n-1$  as preprocessing.  $n$  shows a bit length of  $N$ . Next, interference measurements are executed by setting. After  $n$  times measurements, a data set corresponding to  $f(x)$  is extracted for post-processing to obtain the period of  $f(x)$ . In the original method [5], Eq. (7) should be satisfied.

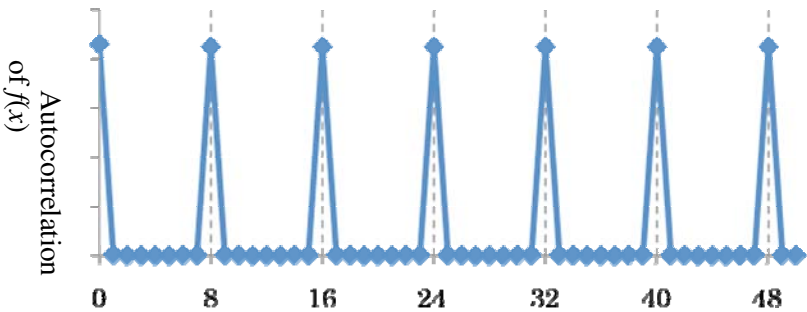
$$l_i \cdot 2^{i+1} - 1 < M \quad (1 \leq i \leq n - 1) \tag{7}$$

Here,  $M$  shows the number of detector array. As a result, two-dimensional parallel system can treat only less than 12 bits integers for factorization.



**Fig. 3.** An example of profile corresponding to  $f(x)$  in cases of (a) the original method, (b) results obtained by optical measurements with some deletions, and (c) data set after interpolation

Therefore, the method described as following is proposed for larger scale processing. In the method, data set corresponding to  $f(x)$  is described in accordance with the same procedure as that of the original method. If the condition shown as Eq. (7) is not satisfied at  $x=x'$ , we set '0' at  $f(x')$ . An example of the data sets obtained by the original and proposed methods is shown Fig. 3. From this procedure, we may achieve prime factorization of larger integer.



**Fig. 4.** Experimental results of verification at  $N=537625733$  and  $a=305208178$

We verify the proposed method experimentally. In the experiment, the optical hardware for 2D parallel processing [6] is used. Figure 4 describes an example of verification. Profile of the figure shows autocorrelation of  $f(x)$  derived with post-processing. In the results of Fig. 3,  $N$  and  $a$  are set to be 537625733 (=23801×23293) and 305208178, respectively. From the profile, it is found that the period is 8. Finally, two correct factors can be obtained from the period. We can demonstrate that the proposed improvement executes prime factorization in 30 bits integer. Note that the improvement is not verified to achieve all integers which are less than 30bits.

## 4 Comments

In terms of optical supercomputing, a feature of our method is to utilize spatial parallelism of light. In 1980's, many methods based on spatial parallelism have been developed in the research field of digital optical computing. In these methods, symbolic substitution [10], perfect shuffle [11], systolic array [12], and so on [13], are implemented on optical systems. Optical array logic has also been proposed as paradigm for general purpose of parallel processing [14]. Our research is much inspired by these methods. We describe essential difference between our method and these previous ones as following.

In the previous methods, at first, many emitters are required to prepare a set of input data for target parallel processing. Additionally, photo-detector array is necessary to obtain output results. On the other hand, our method utilizes only one light source because a set of the input can be generated by collimation of the light beam and tilt of the plane wave obtained by the collimation. Also, large scale parallel processing can be achieved with less number of detectors. This is because the algorithm for prime factorization needs not a set of individual results obtained by optical parallel processing but only characteristics of profile in the set.

Our method permits slight alignment errors whereas previous optical methods generally require highly accurate for alignment. We have estimated and discussed on the robustness of our method against the errors in Ref. [15]. Consequently, spatial parallelism is considered to be useful for optical supercomputing.

## 5 Summary

We have presented an improvement in a system for prime factorization based on optical parallel processing. In the improvement, large scale factorization is executed by permitting some deletions in the profile of  $f(x)$ . We have experimentally verified usefulness of the improved method.

## References

1. Shaked, N.T., Messika, S., Dolev, S., Rosen, J.: Optical solutions for bound NP-complete problems. *Appl. Opt.* 46, 711–724 (2007)
2. Haist, T., Osten, W.: An optical solution for the traveling salesman problem. *Opt. Exp.* 15, 10473–10482 (2007)



3. Oltean, M.: Solving the Hamiltonian path problem with a light-based computer. *Nat. Comput.* 7, 57–70 (2008)
4. Oltean, M.: Solving NP complete problems with delayed signals: an overview of current research directions. In: Dolev, S., Haist, T., Oltean, M. (eds.) *OSC 2008*. LNCS, vol. 5172, pp. 115–128. Springer, Heidelberg (2008)
5. Nitta, K., Matoba, O., Yoshimura, T.: Parallel processing for multiplication modulo by means of phase modulation. *Appl. Opt.* 47, 611–616 (2008)
6. Katsuta, N., Nitta, K., Matoba, O.: Parallel processor for modulo multiplication with optical interference. In: *Technical Digest of The 13th Microoptics Conference*, pp. 84–185 (2007)
7. Nitta, K., Katsuta, N., Matoba, O.: Study on processing performance of optical modulo operations. *Journal of Physics: Conference Series* 139, 12006 (2008)
8. Shor, P.: Algorithms for quantum computation: Discrete logarithms and factoring. In: *Proc. 35th Ann. Symp. on Foundations of Comput. Sci.*, vol. 1898, pp. 124–134 (1994)
9. Vedral, J., Barenco, A., Ekert, A.: Quantum networks for elementary arithmetic operations. *Phys. Rev. A* 54, 147–153 (1996)
10. Brenner, K.H., Huang, A., Streibl, N.: Digital optical computing with symbolic substitution. *Appl. Opt.* 25, 3054–3060 (1986)
11. Lohmann, A.W., Stork, W., Stucke, G.: Optical perfect shuffle. *Appl. Opt.* 25, 1530–1531 (1985)
12. Caulfield, H.J., Rhodes, W.T., Foster, M.J., Horvitz, S.: Optical implementation of systolic array processing. *Opt. Comm.* 40, 86–90 (1981)
13. Yu, F., Jutamulia, S.: *Optical signal processing, computing, and neural networks*. Wiley-Interscience, Hoboken (1992)
14. Tanida, J., Ichioka, Y.: Optical logic array processor using shadowgrams. *J. Opt. Soc. Am.* 73, 800–809 (1983)
15. Nitta, K., Katsuta, N., Matoba, O.: An Optical Interferometer for Parallel Modulo Operation. *The Review of Laser Engineering* 2008, 1327–1330 (2008)

# Combinatorial Optimization Using Electro-Optical Vector by Matrix Multiplication Architecture

Dan E. Tamir<sup>1</sup>, Natan T. Shaked<sup>2</sup>, Wilhelmus J. Geerts<sup>3</sup>, and Shlomi Dolev<sup>4</sup>

<sup>1</sup> Department of Computer Science, Texas State University, San Marcos,  
Texas 78666, USA  
dt19@txstate.edu

<sup>2</sup> Department of Electrical and Computer Engineering, Ben-Gurion University of the Negev,  
P.O. Box 653, Beer-Sheva 84105, Israel  
natis@ee.bgu.ac.il

<sup>3</sup> Department of Physics, Texas State University, San Marcos,  
Texas 78666, USA  
wg06@txstate.edu

<sup>4</sup> Department of Computer Science, Ben-Gurion University of the Negev, P.O. Box 653,  
Beer-Sheva 84105, Israel  
dolev@cs.bgu.ac.il

**Abstract.** A new state space representation of a class of combinatorial optimization problems is introduced. The representation enables efficient implementation of exhaustive search for an optimal solution in bounded NP complete problems such as the traveling salesman problem (TSP) with a relatively small number of cities. Furthermore, it facilitates effective heuristic search for sub optimal solutions for problems with large number of cities. This paper surveys structures for representing solutions to the TSP and the use of these structures in iterative hill climbing (ITHC) and genetic algorithms (GA). The mapping of these structures along with respective operators to a newly proposed electro-optical vector by matrix multiplication (VMM) architecture is detailed. In addition, time space tradeoffs related to using a record keeping mechanism for storing intermediate solutions are presented and the effect of record keeping on the performance of these heuristics in the new architecture is evaluated. Results of running these algorithms on sequential architecture as well as a simulation-based estimation of the speedup obtained are supplied. The results show that the VMM architecture can speedup various variants of the TSP algorithm by a factor of 30x to 50x.

**Keywords:** Optical Computing, Parallel Processing, Combinatorial Optimization, The Traveling Salesman Problem, Heuristic Search, Hill Climbing, Genetic Algorithms.

## 1 Introduction

This paper presents a new weight incidence representation of Hamiltonian cycles along with a set of operations on this representation including mutations and crossovers. The proposed representation facilitates efficient mapping of heuristic search techniques onto a new electro optical matrix by vector multiplication (VMM) architecture and enables fast search for a sub optimal solution to the TSP with a relatively large

number of cities. In addition, the paper outlines efficient mapping of exhaustive search for solutions of TSP with a small number of cities onto the VMM.

The VMM consists of an electrical unit and an optical unit [1] and serves as a co-processor to a controller. Under the proposed implementation the controller is working in parallel with the optical unit in a pipeline mode. The controller prepares 256 vectors which constitute a specific representation of TSP solutions according to a given algorithm and sends them in real time to the VMM. The fact that the controller can prepare the vectors in real time is due to the novel representation of TSP solutions and novel representations of basic operations on TSP solutions. Through the multiplication of a matrix containing solutions and a vector of weights, the optical unit computes the cost of 256 Hamiltonian tours in parallel at a rate 125 million cost evaluations per second. The controller/VMM system can complete 125 million iterations of an algorithm such as hill climbing in one second thereby achieving a speedup of 30x to 50x in various variants of the algorithms. In the current architecture, the role of the optical unit is solely to compute the cost of each solution. In the future, we plan to explore porting additional parts of the search algorithm to the optical unit.

Many combinatorial optimization problems require an exponential amount of resources (time and / or space) with respect to a given parameter of the problem and necessitate NP complete or intractable procedures for finding an optimal solution [2]. A common approach for solving such problems is to define a search space that is an enumeration of potential solutions to the problem or steps toward the solution, and perform heuristic search in that space [3]. A multitude of heuristic search and combinatorial optimization methods is under extensive research. The list of these techniques includes the A\*, Hill Climbing, iterative hill climbing (IHC), genetic algorithms (GA), tabu search, swarm, and simulated annealing [3-10].

The traveling salesman problem is one of the most commonly addressed combinatorial optimization problems and is chosen as the platform of study for this research. In the context of this research, the TSP is stated in the following way: "Given a complete weighted undirected graph, find the minimal Hamiltonian cycle of the graph [11,12]." As a consequence of assuming undirected graph this paper is only concerned with the symmetric TSP, similar results are expected for the asymmetric problem.

Because of the complexity of the TSP, exhaustive solutions are limited to problems with a small number of cities and heuristic search might require a significant amount of computing resources before settling on an acceptable solution. As a consequence of the inherent complexity, multitude of algorithms, heuristics, architectures, and data structures for representing the problem as well as parallel processing procedures for the solution of the TSP have been explored [13-18].

Due to the potential for achieving high speed of computation, optical computing may be an interesting platform for exploring approaches for exhaustive solution for relatively small, bounded, problems and heuristic solutions of large problems. Shaked et al., have developed a new edge-weight based representation for the TSP and certain other NP complete problems [1,11,12]. This representation enables computing the cost of a TSP solution through a dot product operation. Shaked has mapped this representation to an optical vector by matrix multiplication system where TSP solutions are represented in a transparency matrix and the dot product operation is implemented using an optical vector by matrix multiplication [19]. In addition, Shaked has demonstrated an efficient method for electrical and optical construction of the matrix [20].

The papers by Shaked address exhaustive solution for bounded NP complete problems. One advantage of the approach presented in the paper is that the same matrix can be used for solving any problem with up to  $N$  cities and the only element that changes from one instance of a traveling salesman problem to another instance is the weight vector.

Only a few other papers address optical solution to the TSP. Haist et al. presents an optical TSP system that provides a polynomial-time solution for the problem yet requires an exponential amount of photons [21]. As a result, his system is also limited for an exhaustive solution of relatively small instances of the TSP. Collings has demonstrated the use of optical hardware to find local optimal solutions to the TSP using a Hopfield neural network based heuristic [22]. Additional papers on optical systems addressing the TSP and related problems are listed in [23-27].

Recently, Tamir et al., have proposed a new fast electro-optical architecture for vector by matrix multiplication [1]. In the proposed architecture, the VMM consists of a matrix of  $256 \times 256 \times 8$  bits which is multiplied by a vector of  $256 \times 8$  bits. The proposed VMM is capable of performing 16 Tera integer operations per second and completes the multiplication of a  $256 \times 256 \times 8$  matrix by a  $256 \times 8$  vector at a rate of 125 million vector-by-matrix multiplications per second. The paper shows how to map the solution of bounded NP complete problems developed by Shaked et al., into the new proposed VMM. Using the representation proposed by Shaked, the architecture can check 125 million solutions of up to 23 cities in 1 second. In this paper we adopt a new representation for Hamiltonian cycles. Using this representation the VMM, working along with a controller, can efficiently handle heuristic solutions to problems with thousands of cities.

## 2 Strategies for Solving the TSP

### 2.1 Exhaustive Search in the TSP Search Space

Given a representation of a solution, exhaustive search enumerates the entire set of solutions and evaluates the cost of each solution. The best cycle is retained. The complete, undirected, weighted graph with  $N$  vertices ( $C_N$ ) contains  $\frac{(N-1)!}{2}$  solutions. Hence, enumerating all of these solutions is of complexity of the order of  $O(N^N)$ . The complexity is generally related to time complexity. Nevertheless, certain TSP solution strategies trade time complexity by space complexity [6], number of constraints [28], or number of photons required to complete the computation on an optical computing device [21]. Some papers detail methods for efficient implementation of exhaustive search. Nevertheless, due to the high growth rate of the complexity function, exhaustive search is only practical for problems with a relatively small number of cities.

### 2.2 Heuristic Search Procedures

Despite the reduction in problem size, heuristic search algorithms are often very complex and require careful utilization of computer resources such as processing power and storage space. Many heuristic search algorithms are designed for optimal utilization of processing power in order to reduce processing time and do not fully exploit

the storage space or the trade-offs between time and space complexity. Several researchers have studied time/space trade-offs [6,29,30]. A related problem is the problem of anytime and any space algorithm [29,30]. In parallel to the research on mapping heuristic search to the VMM we are performing a research on efficient utilization of time and space resources for addressing NP-complete problems. For this end, we propose novel methods of record keeping using a cache for tracking solutions explored by the heuristic. This method enables an anytime / any space solution to the TSP. The current paper introduces the concept of record keeping along with the mapping of the problem to a parallel execution on the VMM thus enabling a significant speedup over existing approaches.

### **2.2.1 Hill Climbing and Iterative Hill Climbing**

Hill climbing is a steepest descent greedy search algorithm [3-6,31]. There are two parts to the hill climbing algorithm. First, a valid solution, called an initial configuration, is generated. Next, the hill climbing algorithm attempts to improve the current solution by making local changes to the configuration and taking the best new solution that exists in the local search space. Each improvement is referred to as a step. This improvement process continues until the hill climbing algorithm can no longer find a better solution, at which point the procedure returns the last solution found. Iterative Hill Climbing (ITHC) is a variation of hill climbing that addresses the problem of getting trapped at a local minimum. In ITHC, once a local minimum is found, another initial configuration is generated from the global search space and the climbing process restarts. This process, of generating initial configurations and improving them, continues iteratively until the global search space is exhausted or a desired number of iterations are completed.

### **2.2.2 Genetic Algorithm Based Search**

Genetic Algorithms are based on the principle of natural selection in which solutions are represented by chromosomes [7]. Each chromosome contains a series of characteristics which encode the solution at a particular point in a solution space, without ambiguity. For example, in combinatorial optimization problems, such as feature selection, solution chromosomes are represented by bit strings. A *1* bit represents a feature selected, and a *0* bit represents a feature which is not selected. New generations of solutions are produced by elimination of low quality solution chromosomes and addition of solutions through chromosome crossovers and mutations to produce children solutions. Crossovers usually consist of swapping of chromosome bits from two good quality chromosomes, while mutations can be random changes to the chromosomes of individual solutions. Over iterations these processes give rise to solutions which, on average, have a higher fitness than the previous generation [7].

## **2.3 Representing an Hamiltonian Cycle**

The literature on GA for the TSP contains numerous ways for representing Hamiltonian cycle [32,33]. Laranga et al, describe several representation methods including path based, binary, adjacency, ordinal, and matrix, methods, other representations include vector based methods [32]. The path based method is the most natural way to represent a Hamiltonian cycle. It is a vertex based representation obtained by listing

the cities visited in the order of visitation. So the cycle  $1 - 2 - 3 - 4 - 5 - 6 - 1$  is represented as the sequence  $\{1,2,3,4,5,6\}$ . The problem with this and most other representations is that the result of crossover is not necessarily a valid Hamiltonian cycle. Hence, these representations do not enable straight forward implementation of classical crossover.

The path can be represented in an adjacency vector structure where element  $i$  of the vector contains the value  $j$  if vertex  $j$  is located in place  $i$  of the cycle. Several matrix representations have been considered. The first representation is a vertex based representation where a  $N \times N$  matrix is used for a  $N$  vertex graph. The element  $(i, j)$  of the matrix contains 1 if and only if the vertex  $i$  is traversed before the vertex  $j$ . Another matrix representation includes 1 in place  $(i, j)$  if, and only if, in the vertex  $j$  is explored immediately after vertex  $i$  [32].

We consider three additional vector representations. The first representation is due to Shaked [19]. This is a binary edge based vector where 1 in place  $k$  of the vector denotes that edge  $k$  is traversed by the Hamiltonian cycle and the edges are enumerated in a consistent way. For example for the graph  $C_5$  the edges can be enumerated in the following order  $[e_{1,2}, e_{1,3}, e_{1,4}, e_{1,5}, e_{2,3}, e_{2,4}, e_{2,5}, e_{3,4}, e_{3,5}, e_{4,5}]$ . In this example and under this representation, the vector  $B = [1,0,0,1,1,0,0,1,0,1]$  denotes that edges  $e_{1,2}, e_{1,5}, e_{2,3}, e_{3,4}$ , and  $e_{4,5}$  are traversed. Hence, the vector  $B$  represents the cycle  $1 - 2 - 3 - 4 - 5 - 1$ . We refer to this vector as the “binary incident vector.” Note that due to the symmetry the edge  $e_{1,5}$  stands also for the edge  $e_{5,1}$ . Shaked uses another vector which is an edge-weight based vector. The compatible edge-weight vector for  $C_5$  is:

$$W = [w_{1,2}, w_{1,3}, w_{1,4}, w_{1,5}, w_{2,3}, w_{2,4}, w_{2,5}, w_{3,4}, w_{3,4}, w_{4,5}].$$

The novelty of this representation is that it enables calculating the cost (or length) of a specific cycle represented by a binary incidence vector  $B$  through the dot product  $W \cdot B$ .

Tamir et al. presented an electro-optical unit capable of fast vector by matrix multiplication (VMM). For this VMM we are proposing a new vector representation where the weight vector contains the weights of the edges traversed in the order of traversal. So the cycle  $1 - 2 - 3 - 4 - 5 - 1$  is represented by the vector  $W = [w_{1,2}, w_{2,3}, w_{3,4}, w_{4,5}, w_{1,5}]$ . We refer to this vector as the weight incidence vector of the cycle  $1 - 2 - 3 - 4 - 5 - 1$ . In this case a dot product between the vector  $W$  and the vector  $\bar{1} = [1,1,1,1,1]$  yields the cost of a cycle. Note that the weight incidence vector described above can be inferred from the respective cycle. A cycle however is not always uniquely defined by the weight incidence vector. In some of our implementations, a pair of vectors is maintained, the adjacency vector (e.g.,  $[1,2,3,4,5]$ ) and the incidence weight vector ( $[w_{1,2}, w_{2,3}, w_{3,4}, w_{4,5}, w_{1,5}]$ ).

## 2.4 Operations on Hamiltonian Cycle Representations

We divide the operations on Hamiltonian cycles into two types of operations: mutations and crossovers. A mutation on a representation of a cycle alters the representation in a given way. A crossover uses the representation of two cycles to generate a new cycle. In classical genetic algorithms a chromosome is a binary string that

represents a solution. Chromosome mutation is implemented by a permutation on the binary string. In the case of TSP, mutations are a bit more involved. First, some of the representations are not binary. Second, for a non-complete graph an arbitrary permutation of a Hamiltonian cycle representation does not necessary yield an Hamiltonian cycle. Hence, in general, a mutation in the TSP domain has two stages, permutation of the representation and if needed repair of the representation or regeneration of a valid Hamiltonian cycle.

The 2-Opt operation is commonly used in heuristic TSP solution and as a GA mutation. The 2-Opt algorithm removes 2 edges from a Hamiltonian cycle and replaces them with 2 edges whose sum is less than the sum of the edges that were removed, while maintaining the Hamiltonian property of the new cycle [11,12]. This operation is referred to as a “butterfly.” Other mutations include: displacement mutation, exchange mutation, insertion mutation, scramble, and random permutation [32,33].

The classical genetic algorithm of crossover between chromosomes takes two chromosomes split each chromosome into two or more parts and then combines different parts to create one or more chromosomes. Again, in the case of TSP, an arbitrary crossover of the representation of two Hamiltonian cycles does not necessary yield Hamiltonian cycles. Thus, a general TSP crossover involves a stage that resembles classical crossover followed by repair and / or regeneration of a cycle. Some of the commonly used crossover operations include: partially mapped crossover (PMX), ordered crossover (OX), position based crossover, heuristic crossover, neighborhood relationship crossover, meta ordering crossover, and self crossover. A comprehensive list of these and additional mutations, crossovers, and permutations can be found in [32,33].

### 3 The VMM Architecture

The VMM can serve as a co-processor attached to a DSP or a dedicated CPU, referred to as the controller. A high level schema of the VMM is included in Fig. 1. As the figure shows, the VMM is composed of two main components: the optical unit and the electrical driver.

#### 3.1 The VMM Optical Unit

One of the configurations that can be used to implement the optical component of the VMM is based on the Stanford multiplier principle and illustrated in Fig. 2 [1]. As shown in this figure, the input vector of the VMM is represented by a set of light sources, the matrix of the VMM is represented by a slide mask or a real-time SLM and the output (multiplication-product) vector of the VMM is represented by a set of sensitive detectors. The light from each of the sources is spread vertically so that it illuminates a single column of the matrix. Next, each row in the matrix is summed onto a single detector in the detector array. This VMM configuration can be implemented through several optical techniques. One of these techniques uses two sets of lenses each of which contains a cylindrical lens and a spherical lens with focal lengths of  $f$ . A single set of lenses has an equivalent focal length of  $f/2$  in the vertical/horizontal direction and  $f$  in the other direction. As shown in Fig. 2, the first set of

lenses is positioned between the input vector (represented by the light sources) and the matrix (represented by the SLM). This set of lenses is positioned so that the light coming from each of the sources illuminates only a single column in the matrix, which means collimating the light diverging vertically from each of the sources but imaging it in the horizontal direction. The other set of lenses is positioned between the matrix and the output vector (represented by the sensitive detectors) and is rotated by 90 degrees compared to the first set of lenses (see Fig. 2). Therefore, these lenses image a row in the matrix onto a vertical position of a single detector in the detector array and spread the light from a single column of the matrix. Other papers proposed additional versions and applications of the optical VMM. Comprehensive literature reviews in this subject can be found in references [1,34].

### 3.2 The VMM Electrical Driver

The electrical driver is comprised of 256 single electrical driver (SED) units and has two types of inputs: a  $1 \times 256 \times 8$  bit input vector  $A$ , which is the VMM input vector (that is, the VCSEL source array driving signal), and a set of 256 vector inputs  $B_0$  to  $B_{255}$  (total of  $256 \times 256 \times 8$  bit). The output of the VMM is a  $1 \times 256 \times 20$  bit vector  $C$ . The VMM output vector  $C$ , is an aggregation of the set of scalar outputs ( $C_0$  to  $C_{255}$ ), where the output  $C_j$  emerging from the  $j^{\text{th}}$  SED unit is a single 20-bit bus which is generated by the output detector array. Within each SED, the input vector  $B_j$  can be stored in an internal dual-port modular memory buffer/shifter before it is directed to the SLM. The output  $C_j$  is directed to the external output. The electro-optical configuration supports a dot-product operation between the input row vector  $A$  (being converted into light by the VCSELs) and one column of the entire SLM matrix. Each SED unit performs one vector dot-product operation per cycle of 8 ns (the reciprocal of 125 MHz). Combined together, the 256 units perform a vector ( $1 \times 256 \times 8$  bit) by matrix ( $256 \times 256 \times 8$  bit) multiplication operation at a rate of 125 MH.

The proposed system can perform multiplication of a  $1 \times 256 \times 8$  bit vector by a  $256 \times 256 \times 8$  bit matrix at a rate of 125 million vector-by-matrix multiplications per second. If the matrix and vector are smaller than  $256 \times 256$  and  $1 \times 256$ , respectively, then it may be possible to achieve the same rate with multiple small matrices/vectors. If the matrix and / or the vector have more than  $256 \times 256$  ( $256 \times 1$ ) elements, then there is an overhead related to decomposing the matrix into sub matrices. In most of the cases, this overhead is negligible.

## 4 VMM Implementation of Hill Climbing and Genetic Algorithms in the TSP Search Space

The VMM is assumed to be a co-processor attached to a controller. Our current proposal and simulations assume that the controller prepares vectors according to the specific algorithm and sends them to the VMM where the fast matrix multiplication yields the cost of 256 vectors per cycle. In future implementations we will consider using an FPGA, ASIC, or other types of dedicated hardware to implement an electrical unit that is designed for the TSP algorithm. This unit will work directly with the SLM matrix and will supply a direct link for exchanging information between the

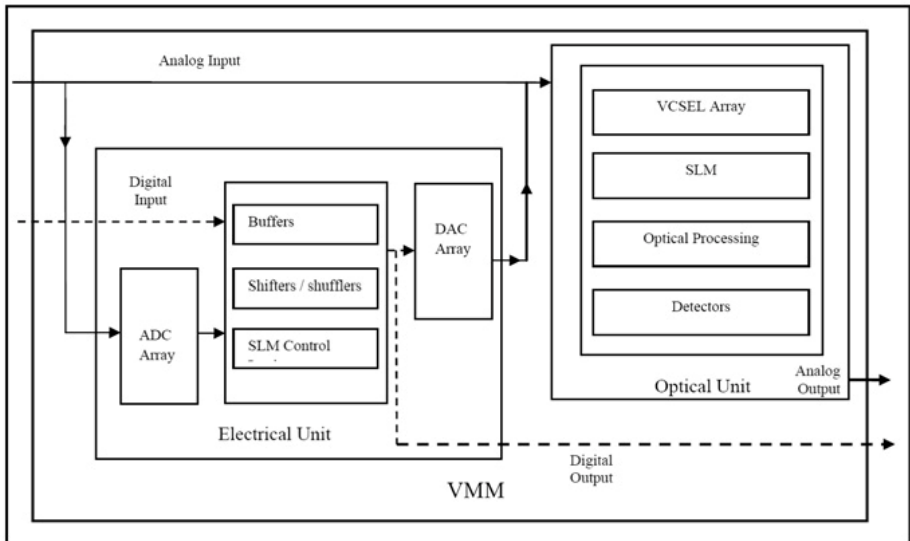


electrical unit and the optical unit. In addition, we consider implementing other parts of the algorithm such as identifying the  $K$  best solutions on the optical unit. We have implemented a simulation of the ITHC algorithm on the VMM. The simulation of the genetic algorithm implementation on the VMM is currently in advanced stages. We report on the actual ITHC simulations in this section.

#### 4.1 VMM Implementation of Iterative Hill Climbing in the TSP Search Space

The ITHC in the TSP search space procedure is implemented through iterations on two execution phases: tour construction and tour improvement. Following extensive experimentation with tour construction algorithms such as the random restart and the greedy randomized adaptive search procedures (GRASP) [6,35], we adopted a deterministic approach which employs a greedy enumeration (GE) of spanning paths according to their weight and converts them into spanning cycles by adding an edge connecting the first and last vertex [6].

The actual implementation of the ITHC using the VMM is done in the following way: First, the controller is generating the initial starting configuration using the modified Kruskal's algorithm [11]. This is called the initial reference cycle. Reference cycles are represented using the adjacency vector representation as well as the weight incidence vector. All the other cycles are represented only by their weight incidence vector. Next, the controller is generating all the 2-Opt butterflies that evolve from the reference cycle. Each butterfly is a permutation which changes the location of two vertices in the reference cycle or a swap of two pairs of edges in the weight incidence vector. Hence, a butterfly implies removing two weights from the reference weight incidence vector and adding two weights to the vector. As the controller prepares these



**Fig. 1.** The electro optical computing system

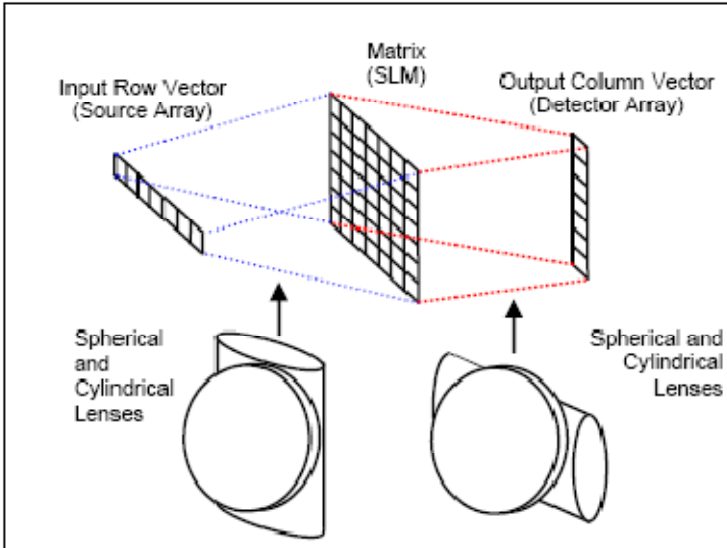


Fig. 2. The VMM optical unit

vectors, they are sent to the VMM. Since the VMM cycle is 8 ns the controller can prepare 256 vectors, and send them to the VMM, in real time. The VMM computes the cost of 256 vectors at a time and returns the results to the controller which retains the best result. After generating all the possible butterflies the best cycle is selected and becomes the reference cycle. This completes the first step of hill climbing. The controller verifies that the current step is not in the cache, places the current step in the cache, prepares the next set of weight incidence vectors, and sends them in real time to the VMM. Again, the best cycle is retained. It becomes the reference cycle and a new step is created. This process is repeated until a restart condition is met. That is, either a local optimum has been achieved or a hit on the cache, denoting that this step has already been explored, occurs. At this point the controller implements the greedy enumeration procedure to generate a new initial reference cycles and a new climber is spawned to climb from this point [6]. The process of generating new climbers repeats until a time limit or a limit on the number of climbers is reached.

#### 4.2 VMM Implementation of Genetic Algorithm Based Search

As in the case of iterative hill climbing the role of the controller is to prepare vectors according to the algorithm and send them for cost evaluation to the VMM. We use the incidence edge-weight vector as the primary representation for chromosomes. Nevertheless, a crossover might require maintaining the adjacency vector. A mutation is a 2-Opt operation as described in the previous section. We are experimenting with several versions of crossovers including PMX and OX [32], in addition, we have developed a new and novel crossover operation which is efficient in computation time and contribution to solution quality. Moreover it has a good fit with the electro-optical architecture, thus it is efficiently implemented on the VMM. The new crossover

operator is an extension of an operator proposed in [13]. It involves the following operations: First, the cycle is split into two distinct paths at an arbitrary point. Each of the paths is going through two different mutations and then the complementary paths are recombined to generate new cycles. The advantage of this method is that it does not require a repair operation after the recombination since the parts of the path that are recombined are mutually exclusive. To further explain, let  $C_1$  be a chromosome. The path represented by  $C_1$  is divided into two mutually exclusive paths. That is, the two paths span the graph vertices and have no common vertices. The two paths are represented by the chromosomes  $C_{11}$  and  $C_{12}$ . Next  $C_{11}$  and  $C_{12}$  are going through two mutations generating  $C'_{11}$ ,  $C''_{11}$ ,  $C'_{12}$ , and  $C''_{12}$ . Finally, the partial paths are recombined to generate two new cycles. The two new cycles are selected arbitrarily from the four valid recombination options. For example, the two new paths can be the cycles which correspond to the recombinations  $C'_1 = C'_{11}||C''_{12}$  and  $C'_2 = C''_{11}||C'_{12}$  (the operator  $||$  stands for concatenation of one chromosome in the internal point of another). Since the two parts of the chromosomes are mutually exclusive with respect to vertices there is no need for a repair operation.

## 5 Simulation Results

At this stage only the ITHC simulation has been completed. The GA based search is in advanced stages of development. With respect to ITHC we have performed experiments with randomly created graphs as well as graphs taken from the TSPLIB set of benchmarks [36]. In this section we show the results of the search as well the computation of the speedup that can be obtained by the VMM.

Figure 3 shows the result of running the ITHC with randomly created graphs and demonstrates a speedup of more than 4x, obtained with GE and caching in a problem with 40 vertices (cities). So far, we have addressed problems with randomly generated graphs of up to 100 cities and obtained a speedup of about 4x. Note that this speedup is due to the greedy enumeration and caching and is not related to the VMM speedup detailed below.

Table 1 shows the results of running the ITHC with TSPLIB benchmarks. The experiments include greedy enumeration without cache. On the other hand an “infinite” memory model is assumed. That is, all the steps of all the climbers are stored in memory. Since the number of climbers is limited (1 million in these experiments) the available memory is sufficient to store the entire set of steps.

The quality of the cycles is good. In several cases the cost of a cycle is the same as the best cost reported in TSPLIB in other cases a degradation of up to 1.5% is observed. This is tolerable given the simplicity and practicality of ITHC. In addition, real applications might include many more climbers. The dedicated memory demonstrates the any-space features of the GE algorithm [29,30]. It also demonstrates the redundancy (%Dup) or the upper limit for improvement with cache (90% in some cases).

### 5.1 The VMM Contribution to the Speed-Up of the ITHC Based TSP Solution

We start with an upper bound on the speedup that can be obtained using the VMM with a problem of 256 cities (which requires a vector of 256 weights), then we show

the results of simulation with 100 cities. For the speedup simulation we are making the following assumptions: 1) the controller is working at 2 GHz or more. 2) The controller bus to memory is operating at 2 GHz, and 3) The VMM is operating at a rate of 125MHz. Note that assumptions 1 and 2 are conservative. The limiting factor is the access rate to the bus and 2 GHz is above the current state of the art. Using a bus with less bandwidth will increase the VMM speedup. Using a processor with higher frequency will have a minor effect on speedup.

In the VMM system a butterfly requires 4 addition or subtraction operations and 4 accesses to memory. Hence, generating 256 butterflies takes about 3 ns. In addition

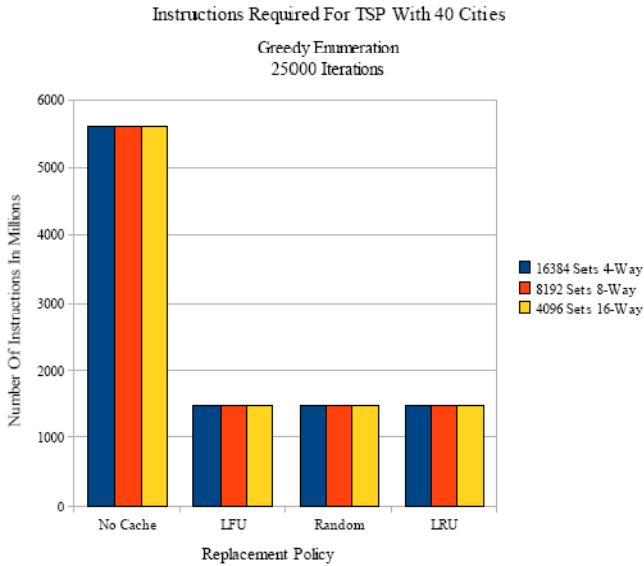


Fig. 3. Number of instructions for a 40-city problem (GE)

Table 1. TSPLIB Benchmarks

	Best	% Dup
<b>ulysses16</b>	100	85.5
<b>ulysses22</b>	100	87.4
<b>gr24</b>	100	86.4
<b>fri26</b>	100	86.9
<b>bays29</b>	100	91.1
<b>att48</b>	100.2	93.6
<b>gr48 1M</b>	101.5	90.1
<b>eil51</b>	100.7	93.2

the controller may need to retain a copy of the best cycle out of 256 cycles; hence 256 comparisons (subtractions) and additional 256 accesses to memory. This will take less than 2 ns. Hence, real time operation is maintained. This means that the controller can generate the vectors for the VMM in real time at a rate of operation of 125 million butterflies per second. Without the VMM, the controller has to calculate the cost of each cycle and maintain the cycle with the best cost. In the worst case, each butterfly requires copying the entire vector. Hence a butterfly involves 5 addition / subtraction operations (one more addition to adjust the final cost) and 260 accesses to memory. Additional overhead would be due to the need to maintain and update pointers to the memory. Under the current assumptions this will take about 160 ns. Thus, a speedup of 20x is obtained with the VMM. In the cases we ran with up to 100 cities, the simulation yields a speedup of about 8x which complies with the calculation for vectors of 256 elements.

## 5.2 The VMM Contribution to the Speed-Up of the GA Based TSP Solution

Each generation (of life of chromosomes) includes a percentage of mutations and a percentage of crossovers thus creating the next generation. Generally, the percentage of mutations is low; sometimes as low as 1%. Additionally, the size of the population within a generation is generally in the order of one hundred hence the fact that the VMM can hold 256 vectors at a time fits well with the population number. In one of our models a population size of 256 is used along with the PMX and OX crossovers. In the second model, the VMM holds up to 128 vectors representing 128 cycles each of which is divided into two mutually exclusive parts. This supports our new crossover operation. Under this model, we can efficiently handle TSP instances with up to 512 cities.

Mutations are implemented as 2-Opt and are identical to the 2-Opt operations in the ITHC. Hence the speedup of the VMM for mutations is expected to be the same. In the worst case a classical crossover operation requires recalculating the cost of a cycle hence the classical crossover may require 256 additions as well as 256 memory writes. We assume that addition operation takes half of the time of memory access operation. Hence, the speedup due to the VMM is expected to be about 30X. The new crossover requires 512 additions and memory writes. Thus, problems with a large number of cities may be subject to a speed-up of 50x or more due to the VMM.

## 6 Conclusions and Proposals for Further Research

We presented a new state space representation which enables efficient implementation of TSP solution algorithms including hill climbing and genetic algorithms with a large number of cities as well as exhaustive search with a relatively small number of cities. The representation uses a weight incidence vector, a data structure that holds the weights of edges that are traversed by a given Hamiltonian cycle. In addition, we have presented the mapping of exhaustive search, ITHC, and GA TSP solution algorithms to a newly proposed electro-optical VMM architecture.

We have performed a set of experiments with a sequential architecture and a simulation of the effect of a proposed parallel implementation where a controller prepares the vectors according to a given algorithm and sends them in real time to the VMM. In addition, the experiments demonstrate the effect of record keeping on the performance of these heuristics [6,37]. The simulation based estimation of the contribution of VMM to improved performance shows that the parallel electro-optical implementation has a

potential speedup of 30x to 50x over sequential implementations in various variants of the TSP algorithms.

In the future, we plan to explore porting additional parts of the search algorithm to the optical unit. In addition, we will consider using an FPGA, ASIC, or other types of dedicated hardware to implement an electrical unit that is designed for the TSP algorithm. This unit will work directly with the SLM matrix and will supply a direct link for exchanging information between the controller and the VMM. In addition, we consider implementing other parts of the algorithm such as identifying the  $K$  best solutions on the optical unit.

**Acknowledgments.** The last author is partially supported by the Rita Altura Trust in Computer Science.

## References

1. Tamir, D.E., Shaked, N.T., Wilson, P.J., Dolev, S.: High-speed and low-power electro-optical DSP coprocessor. *J. Opt. Soc. Am. A* 26, A11–A20 (2009)
2. Garey, M.R., Johnson, D.S.: *Computers and intractability: A guide to the theory of NP-completeness*. W.H. Freeman, New York (1979)
3. Pearl, J.: *Heuristics: Intelligent search strategies for computer problem solving*. Addison-Wesley, Reading (1984)
4. Russell, S.J., Norvig, P.: *Artificial intelligence: A modern approach*. Prentice-Hall, Englewood Cliffs (1995)
5. Xi, B., Liu, Z., Raghavachari, M., Xia, C., Zhang, L.: A smart hill-climbing algorithm for application server configuration. In: *Proceedings of the 13th international conference on world wide web*, pp. 287–296 (2004)
6. Karhi, D., Tamir, D.E.: Caching in the TSP Search Space. In: *Next Generation Applied Intelligence*, Tainan, Taiwan, pp. 221–230 (2009)
7. Vose, M.D.: *The simple genetic algorithm: Foundations and theory*. MIT Press, Cambridge (1999)
8. Glover, F., Laguna, M.: *Tabu Search*. Kluwer Academic Press, Dordrecht (1997)
9. Kennedy, J., Eberhart, R.C.: *Swarm Intelligence*. Academic Press, London (2001)
10. Kirkpatrick, S., Gelatt, C.D., Vecchi, M.P.: Optimization by simulated annealing. *Science* 220, 671–680 (1983)
11. Johnson, D.S., McGeoch, L.A.: The traveling salesman problem: A case study in local optimization. *Local search in combinatorial optimization*, 215–310 (1997)
12. Applegate, D.L., Bixby, R.E., Vasek, C., Cook, W.J.: *The traveling salesman problem: A computational study*. Princeton University Press, Princeton (2007)
13. Wang, L., Maciejewski, A.A., Siegel, H.J., Roychowdhury, V.P.: A comparative study of five parallel genetic algorithms using the traveling salesman problem. In: *Proceedings of the 12th. International Parallel Processing Symposium*, pp. 345–349 (1998)
14. Borovska, P.: Solving the travelling salesman problem in parallel by genetic algorithm on multicomputer cluster. In: *Int. Conf. on Computer Systems and Technologies*, pp. 1–6 (2006)
15. Gang, P., Iimura, I., Nakatsuru, T., Nakayama, S.: Efficiency of local genetic algorithm in parallel processing. In: *Sixth International Conference on Parallel and Distributed Computing, Applications and Technologies*, pp. 620–623 (2005)
16. Langdon, W.B., Banzhaf, W.: A SIMD interpreter for genetic programming on GPU graphics cards. In: O’Neill, M., Vanneschi, L., Gustafson, S., Esparcia Alcázar, A.I., De Falco, I., Della Cioppa, A., Tarantino, E. (eds.) *EuroGP 2008*. LNCS, vol. 4971, pp. 73–85. Springer, Heidelberg (2008)

17. Inoue, T., Sano, M., Takahashi, Y.: Design of a processing element of a SIMD computer for genetic algorithms. In: Proceedings of the High-Performance Computing on the Information Superhighway, pp. 688–691 (1997)
18. Vega-Rodriguez, M.A., Gutierrez-Gil, R., Avila-Roman, J.M., Sanchez-Perez, J.M., Gomez-Pulido, J.A.: Genetic algorithms using parallelism and FPGAs: The TSP as case study. In: International Conference Workshops on Parallel Processing, pp. 573–579 (2005)
19. Shaked, N.T., Messika, S., Dolev, S., Rosen, J.: Optical solution for bounded NP-complete problems. *Applied Optics* 46(5), 711–724 (2007)
20. Shaked, N.T., Tabib, T., Simon, G., Messika, S., Dolev, S., Rosen, J.: Optical binary-matrix synthesis for solving bounded NP-complete combinatorial problems. *Optical Engineering* 46(10), 108201, 1–11 (2007)
21. Haist, T., Osten, W.: An Optical solution for the traveling salesman problem. *Opt. Express* 15, 10473–10482 (2007)
22. Collings, N., Sumi, R., Weible, K.J., Acklin, B., Xue, W.: The use of optical hardware to find good solutions of the travelling salesman problem (TSP). In: Proc. SPIE 1806, pp. 637–641 (1993)
23. Dolev, S., Fitoussi, H.: The traveling beams: Optical solutions for bounded NP-complete problems. In: Crescenzi, P., Prencipe, G., Pucci, G. (eds.) FUN 2007. LNCS, vol. 4475, pp. 120–134. Springer, Heidelberg (2007)
24. Dolev, S., Nir, Y.: Optical implementation of bounded non-deterministic Turing machines. US Patent 7, 130, 093 B2 (January 2005)
25. Anter, A., Dolev, S.: Optical solution for hard in average NP-complete instances (using exponential space for solving instances of the permanent). In: Proc. of the 12th IEEE Meeting on Optical Engineering and Science in Israel (2nd OASIS), Israel (2009)
26. Oltean, M.: Solving the Hamiltonian path problem with a light-based computer. *Natural Computing* 7(1), 57–70 (2008)
27. Oltean, M., Muntean, O.: Solving NP-complete problems with delayed signals: An overview of current research directions. In: Proceedings of 1st international Workshop on Optical Super Computing, pp. 115–128 (2008)
28. Gutfreund, D., Shaltiel, R., Ta-Shma, A.: If NP languages are hard on the worst-case, then it is easy to find their hard instances. *Comput. Complex.* 16(4), 412–441 (2007)
29. Zilberstein, S.: Using anytime algorithms in intelligent systems. *AI Magazine* 17(3), 73–83 (1996)
30. Ramos, T., Cozman, G.: Anytime anyspace probabilistic inference. *International Journal of Approximate Reasoning* 38(1), 53–80 (2005)
31. Aarts, E., Lenstra, J.: *Local Search in Combinatorial Optimization*. Princeton University, Princeton (2003)
32. Larrinaga, P., Kuijpers, C.M.H., Murga: Genetic algorithms for the travelling salesman problem: A review of representations and operators. *Artificial Intelligence Review*, 129–170 (1999)
33. Ursache, L.: Representation models for solving TSP with genetic algorithms. In: Proceedings of CNMI, Bacău, pp. 291–298 (2007)
34. Feitelson, D.G.: *Optical computing: A survey for computer scientists*. MIT Press, Cambridge (1988)
35. Pitsoulis, L., Resende, M.: Greedy randomized adaptive search procedures. *Journal of Global Optimization* 6(2), 109–133 (1995)
36. Reinelt, G.: *TSPLIB -A traveling salesman problem library*. ORSA Journal on Computing 3(4), 376–384 (1991), <http://comopt.ifi.uni-heidelberg.de/software/TSPLIB95/>
37. Lowell, D., El Lababedi, B., Novoa, C., Tamir, D.E.: The locality of reference of genetic algorithms and probabilistic reasoning. In: The International Conference on Artificial Intelligence and Pattern Recognition, Florida, pp. 221–228 (2009)

# Dynamic Optical Circuit Switching Applied to Storage Area Networks

Aharon J. Agranat<sup>1</sup>, Noam Sapiens<sup>1</sup>, and Larry Rudolph<sup>2</sup>

<sup>1</sup> Department of Applied Physics, the School of Engineering and Computer Science,  
the Hebrew University, Jerusalem 91904, ISRAEL

<sup>2</sup> VMWare, Cambridge, MA, USA

**Abstract.** This paper presents a new weight incidence representation of Dynamic wavelength addressing in optical fiber networks utilizing wavelength division multiplexing (WDM) can form the basis for a high-performance, high-bandwidth, low-latency any-to-any interconnection network. WDM optical fiber networks exploit the fact that photons of different wavelengths do not normally interact, thereby enabling the transmission of many channels of data in parallel in the same fiber by using photons of a different wavelength for each channel. Wavelength addressing is a networking concept that utilizes WDM technology to enable direct routing of data. Each node in the network is assigned a specific wavelength that is considered its address. Data transmitted in a certain wavelength on the network is read only by the node that was assigned that wavelength as its address.

We demonstrate the effectiveness of this approach by considering the interconnection needs of a storage area network (SAN). A SAN is a special-purpose interconnection scheme that enables computer systems to view remote storage devices as local. The underlying principle of a dynamic wavelength addressing SAN (WASAN) is to add the existing SAN architecture a dynamic multi-fiber WDM loop with dynamic add/drop capability to each node. A client requesting a data package sends its request to the SAN server to which it is connected. The SAN management then allocates a fiber in the loop, and a wavelength on this fiber to this request. This fiber-wavelength pair now constitutes a circuit that connects the client to the storage device that contains the requested data package. Data can now flow directly and continuously from the storage device to the client. Upon completion of the operation, the fiber-wavelength pair is released to the SAN management to be used for a different task.

The effectiveness of the WASAN is investigated in a series of simulations. Indeed the WASAN performance is superior to the respective SAN of similar sizes and with equal work loads. It is clearly seen that the WASAN performance is significantly less sensitive when the average package size is increased. Furthermore, adding load to the WASAN architecture in the form of extra transmitting nodes does not create the congestion that is formed in the regular SAN architecture, therefore yielding better performance and greater scalability in system size as well as data size.

A straightforward implementation of WASAN would equip each of the nodes in the network with an expensive tunable laser source so that any wavelength can be assigned arbitrarily to each node according to availability by the WASAN management. We investigate an alternative scheme: the laser power grid. The laser power grid is a fiber network adjunct to the circuit switching network that carries raw optical power at the wavelengths that are used by the circuit switching network. The raw optical power is supplied from a battery of single wavelength lasers. Each node is equipped with a special wavelength allocation device that upon request transfers optical power at a prescribed wavelength to the node transmitter. This obviates the need for tunable laser sources at each node, which significantly boosts the cost effectiveness of the WASAN.



# Optical Correlator for Star Identification and Tracking

Jia Hui<sup>1</sup>, Yang Jiankun<sup>1</sup>, Li Xiujian<sup>1</sup>, Hu Wenhua<sup>1</sup>, Yang Juncal<sup>1</sup>, Fan Qingchun<sup>2</sup>,  
and Hao Yuncai<sup>2</sup>

<sup>1</sup> Tech-Physical Research Center of Science College, National University of Defense  
Technology, Changsha, Hunan, 410073, China

<sup>2</sup> National Laboratory of Space Intelligent Control, Beijing 100190, China  
photon\_nudt@126.com

**Abstract.** Star tracker is one of the most important spacecraft attitude sensors which can achieve accuracies within several arc-seconds utilizing star identification and star tracking. The refresh rate and accuracy of star tracker are constrained as there are so many stars in the sky. A novel star identification and tracking method for star tracker using optical correlator is proposed to solve this problem of star map comparing and identification. The proposed optical correlator can optically execute the correlation operation between current star map and the standard star map constructed from the star catalog. The whole sky star identification can be completed within 100ms due to the inherent parallel computing ability of optical correlator. Star map motion can be tracking with an accuracy of up to 1/100 pixel. Computer simulations and experiments indicate that this method has great robustness to small signal-to-noise ratio, and improve the performance of star tracker remarkably.

**Keywords:** Optical computing, Optical correlator, Star tracker, Star identification and tracking.

## 1 Introduction

Star tracker is one of the most important spacecraft attitude sensors which can achieve accuracies within several arc-seconds utilizing star identification and star tracking [1, 2]. It consists of an electronic camera and associated processor. The processor has the capability to calculate the attitude through the approach of star identification between the star map captured by the camera and the internal star catalog, which means that the processor has to find the exactly location of the captured star map in the whole night sky. This is a difficult problem because there are a huge number of stars in the whole sky. For example, there are 45857 stars brighter than magnitude 8.0  $M_v$  from star catalog sky2000 (V4). The traditional star identification algorithms based on the electronic processor have to simplify the problem to some extent as to complete the task within several seconds [3-5]. As a result, the identification rate and accuracy are limited, especially when the SNR of star map is low. To overcome these problems, we proposed a novel star identification method for star tracker utilizing optical correlator.

Optical correlator, one of the most important optical parallel computing devices, can provide fast identification and tracking capabilities. A joint transform correlator

(JTC) is a kind of optical correlator performing correlation between two images at the speed of light [6, 7]. Two digital input images (current and reference images) are entered into the optical system of the JTC by a spatial light modulator (SLM), and the JTC provides the correlation image. If both input images contain identically the same target, the correlation image will contain two symmetric correlation peaks. The shift of these correlation peaks relative to optical axis corresponds to the shift between the current and reference input images. The position of peaks on the correlation image and the corresponding shift value can be measured with sub-pixel accuracy using standard centroid method. The JTC technique has shown a remarkable potential for real-time matching and tracking applications, such as camera motion estimation [8, 9], visual navigation [10], automated rendezvous and docking [11].

We have developed a novel method for star identification and tracking utilizing optical correlator. According to the theory mentioned above, if star map captured by the camera and star map of the catalog are inputted in the JTC, the position of output correlation peaks represents the moving between the two star maps, which can be utilized to calculate the current attitude. Refresh rate of this approach is only limited by the rate of SLM, which can achieve 1000~2000 frames per second [10, 12, 13], and the whole sky identification can be completed in 100ms. As all the stars on the map are used in the correlation, the accuracy and identification rate are improved remarkably. What's more, the noise of detector is not correlated with the stars; as a result, noise can be reduced after the correlation operation.

## 2 Star Identification

Star identification in the sensor field is the main difficulty of attitude estimation for star tracker. Once a correct match is made, there are reliable methods for generating attitude. Hence, for star tracker, star identification is an essential and important part that directly affects the capability of star tracker [4]. The problem is illustrated in Fig. 1 where a star tracker images a small portion of the night sky which it must identify [2]. The image includes uncertainties in the magnitude and in the positions of the stars. Also, false objects may be present in the image. The star tracker is required to solve the problem in a few seconds.

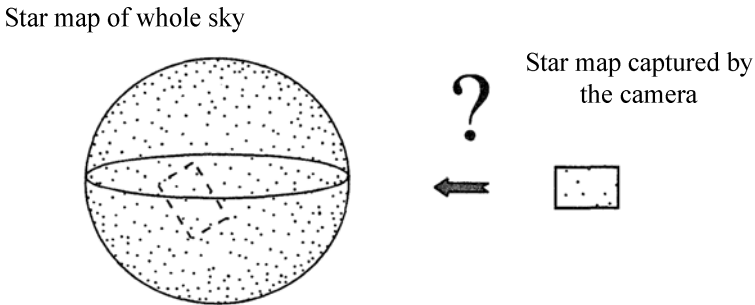


Fig. 1. Whole sky star identification in the sensor field

During the last three decades, a lot of strategies based on the electronic processor had been proposed, such as polygon algorithm, match group algorithm and genetic algorithm [3, 4, 14, 15]. The basic approach can be described as follows: First, establish the internal guide star catalog; Then, extract stars from the current image captured by the camera; Finally, match the captured stars with the guide stars. They all characterize stars relative to their nearest neighboring stars in the image and typically utilize distances, angles and/or brightness.

In principle these identification strategies are serial systems. In those systems, one observation vector is compared with one guidance vector in a match operation, and the best match is made through iterative operation. As a result, if there are  $N$  guidance vectors (stars from catalog) and the number of observation vectors (stars captured by camera) is  $M$ , the number of iteration is  $N^M$  for a complete star identification. Hence, these identification strategies have to reduce the vectors to maintain the iteration in an acceptable time limit, which actually restrains the identification rate and the accuracy.

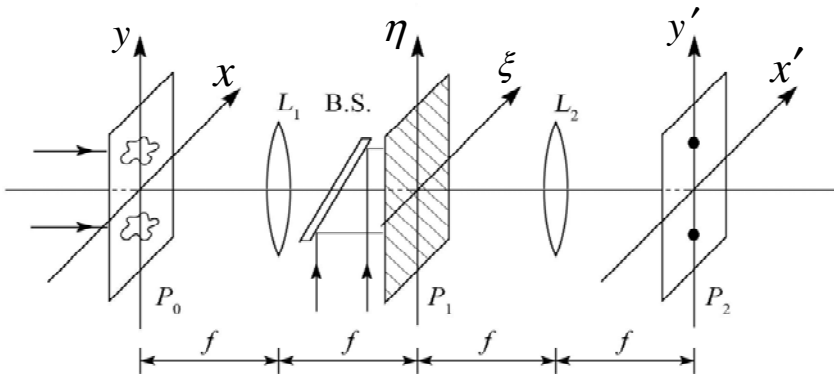
We proposed a novel approach utilizing optical correlator to take advantage of the inherent performance of parallel processing, high speed and vast parallelism in order to realize no reduction whole sky star map identification.

### 3 Optical Correlator for Star Identification

#### 3.1 The Principle of Optical Correlator

The schematic diagram of a joint transform correlator is shown in Fig. 2, in which both the target image function  $t(x, y)$  and the reference image function  $r(x, y)$  are placed side-by-side in the input plane. The amplitude transmittance of plane  $P_0$  is

$$g_i(x, y) = t(x, y - b) + r(x, y + b) \quad (1)$$



**Fig. 2.** Optical joint transform correlator. ( $P_0$ : Input Plane,  $P_1$ : Transform Plane,  $P_2$ : Output Plane, B.S.: Beam splitter,  $L_{1-2}$ : Fourier Transform Lens).

Where the center-to-center separation of the two function is  $2b$ . Fourier transform lens ( $L_1$ ) forms the Fourier transform of  $g_i(x, y)$  at plane  $P_1$ . The intensity of this transform  $|\hat{g}_i(\xi, \eta)|^2$  is recorded by a CCD camera placed on  $P_1$  plane, which is called joint transform spectrum (JPS):

$$\begin{aligned} |\hat{g}_i(\xi, \eta)|^2 &= |\hat{t}(\xi, \eta)|^2 + |\hat{r}(\xi, \eta)|^2 \\ &+ \hat{t}(\xi, \eta)\hat{r}^*(\xi, \eta)\exp(-j4\pi\eta b) \\ &+ \hat{t}^*(\xi, \eta)\hat{r}(\xi, \eta)\exp(-j4\pi\eta b) \end{aligned} \quad (2)$$

Now, the JPS is displayed on  $P_1$  plane and illuminated by a normal plane wave (using the beam splitter BS). The correlation of  $t(x', y')$  and  $r(x', y')$  is obtained on plane  $P_2$  at  $y' = \pm 2b$  by  $L_2$  inverse Fourier transform:

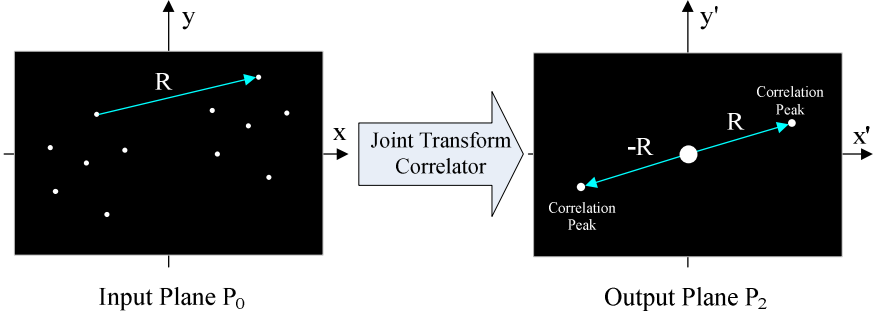
$$\begin{aligned} g_o(x', y') &= t(x', y') \otimes t(x', y') + r(x', y') \otimes r(x', y') \\ &+ t(x', y') \otimes r(x', y') * \delta(x', y' - 2b) \\ &+ r(x', y') \otimes t(x', y') * \delta(x', y' + 2b) \end{aligned} \quad (3)$$

Where functor  $\otimes$  stand for correlation operation,  $*$  stand for convolution operation. The third and fourth item of Eq. (3) denote target image and reference image's cross-correlation, which center respective lie in position  $(0, 2b)$  and  $(0, -2b)$  of  $P_2$  plane. They are a pair conjugated cross-correlation peaks, which corresponding two bright spots in optical experiment if the target image and the reference image was exactly the same one. It is obvious that the shift of these correlation peaks relative to optical axis corresponds to the shift between the current and reference input images. Therefore, the location of target image can be tracked using the position of these correlation peaks.

### 3.2 Star Identification and Tracking Utilizing an Optical Correlator

Star map can be tracked by the JTC. Star map captured by the CCD and standard star map constructed from star catalog are displayed on plane  $P_0$ . If the star map captured by the CCD is identified with the reference star map (or party of the reference star map), correlation peaks are obtained on plane  $P_2$  as shown in Fig. 3. Hence, it's not necessary to identify each star in star catalog as traditional star tracking method does. And the position of the correlation peaks can be calculated with sub-pixel accuracy through standard centroid algorithm. After detecting the correlation peaks, the star map motion is obtained using the difference between the reference correlation peak and the new correlation peak coordinates through Eq. (3).

It can be assumed that the input star map  $t(x, y)$  includes pure star map  $r_s(x, y)$  and noise  $n(x, y)$ . The correlation peak function from Eq. (3) can be written as:



**Fig. 3.** Star tracking utilizing an optical joint transform correlator

$$\begin{aligned}
 g_3(x', y') &= t(x', y') \otimes r(x', y') * \delta(x', y' - 2b) \\
 &= (r_s(x', y') + n(x', y')) \otimes r(x', y') * \delta(x', y' - 2b) \\
 &= r_s(x', y') \otimes r(x', y') * \delta(x', y' - 2b) \\
 &\quad + n(x', y') \otimes r(x', y') * \delta(x', y' - 2b)
 \end{aligned} \tag{4}$$

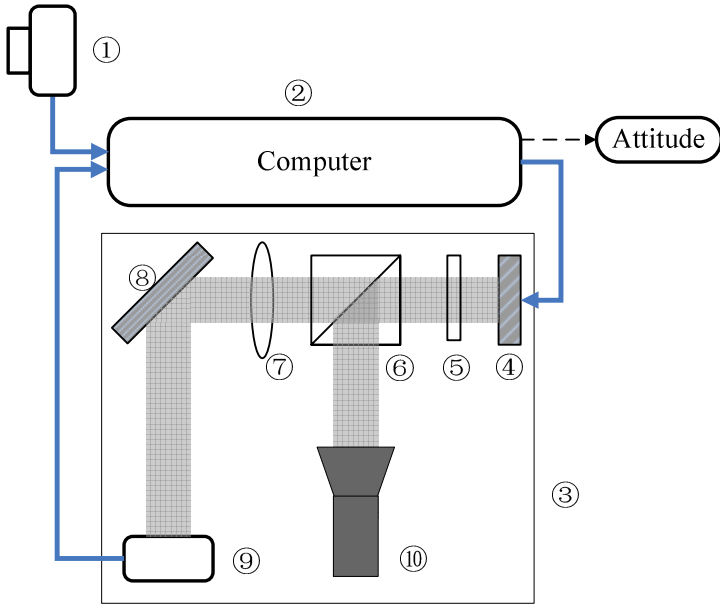
Because noise  $n(x, y)$  is not correlated with reference image  $r(x, y)$ , the second item of Eq. (4) can be ignored. Hence the SNR is improved and the accuracy is increased accordingly.

### 3.3 Whole Sky Star Identification

In fact, only a small portion of the star map of the whole sky star catalog can be displayed in the input plane mentioned in section 3.2 due to the physical scale of the SLM and optical system. Therefore, we construct a spherical triangulation [16] of the whole sky star map, dividing the whole sky star map into 100 patches. When the SLM of 1000 frame per second is applied, the whole sky identification can be completed within 100ms.

## 4 Simulation and Experimental Results

Fig. 4 illustrates the prototype to evaluate the performance of the joint transform optical correlator for star tracker. In the prototype, the input image (including the current star map and the standard star map, as shown in Fig. 5(a) will be inputted and displayed by an electrically addressed spatial light modulator (SLM). The joint transform power spectrum will be detected by a CCD camera and then be inputted again to the SLM. And the correlation output will be detected by the camera. The joint transform power spectrum detected by the CCD camera is shown in Fig. 5(b), and the correlation output of the optical joint transform correlator is shown in Fig. 5(c).

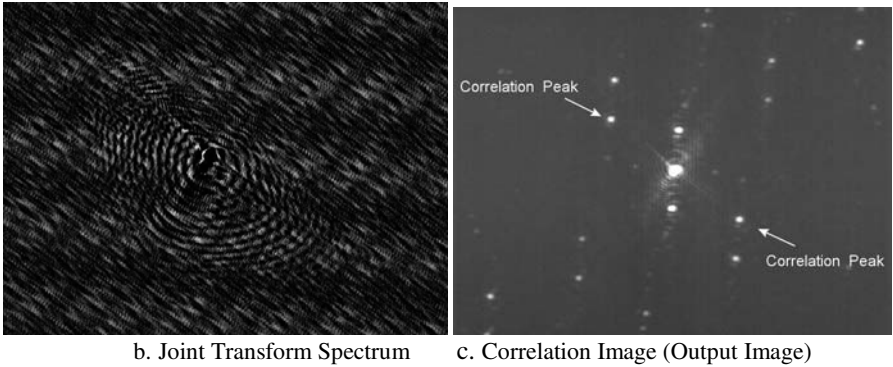


**Fig. 4.** The prototypes of joint transform optical correlator for star tracker. (1.Camera of star tracker 2.Computer 3.Optical correlator 4.Spatial light modulator (SLM) 5.Wave plate 6. Polarizing beam splitter (PBS) 7.Fourier transform lens 8.Mirror 9.CCD camera 10.Laser).



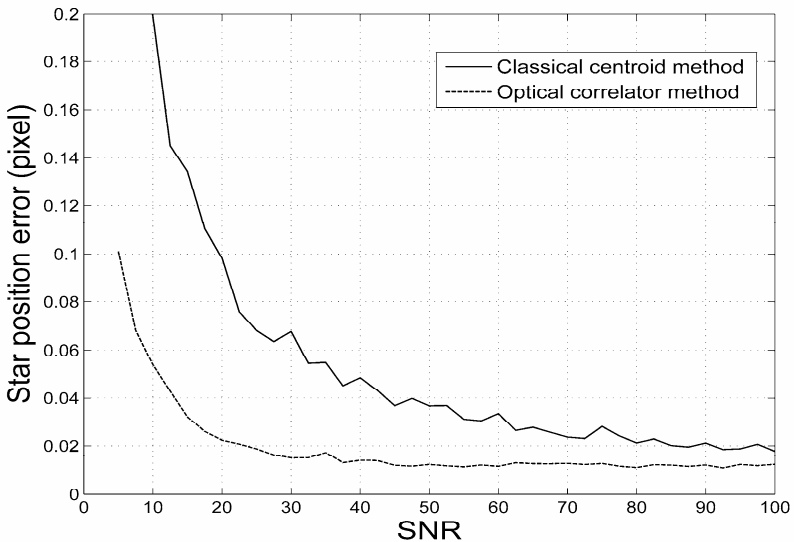
a. Input image (left: star map captured by the camera, right: standard star map)

**Fig. 5.** Experiment results



**Fig. 5.** (continued)

It's obvious that the position of the correlation peaks can be calculated easily from the correlation image. Hence, star tracking can be completed by tracking the correlation peaks without star identification. The simulated star position errors under different SNR of classical centroid method and optical correlator method are shown in Fig. 6. Obviously, the method using optical correlator strongly improves the accuracy performance, which means that shorter expose time is needed using optical correlator method to achieve the same accuracy level.



**Fig. 6.** The star position errors under different SNR of classical centroid method and optical correlator method

## 5 Discussion and Conclusion

A novel star identification and tracking method for star tracker utilizing optical correlator is reported. The optical correlator can optically execute the correlation operation between the star map captured by the camera and the standard star map constructed from the star catalog. The proposed system can reduce the time consume of no reduction whole sky star identification to about 100ms due to the vast parallel operation of the optical correlator. The star map position can be calculated from the correlation peaks exactly. Computer simulations and experiments indicate that the tracking method using optical joint transform correlator has great robustness to small signal-to-noise ratio, and improve the accuracy performance of star tracker remarkably. There are still some problems such as the noise introduced by the optical system itself and the rotation map identification. For future on board application, much attention should also be paid to the system size and mass.

**Acknowledgments.** This work was partially supported by NSFC/China (project No. 60673147).

## References

1. Liebe, C.C.: Accuracy Performance of Star Trackers -A Tutorial. *IEEE T. Aero. Elec. Sys.* 38, 587–599 (2002)
2. Eisenman, A.R., Liebe, C.C.: Advancing State-of-the-Art in Second Generation Star Trackers. In: 1998 IEEE Aerospace Conference, vol. 1, pp. 111–118. IEEE, Los Alamitos (1998)
3. Liebe, C.C.: Pattern Recognition of Star Constellations for Spacecraft Applications. *IEEE Aero. El. Sys. Mag.* 8, 31–39 (1993)
4. Meng, N., Peifa, J.: A Survey of All-sky Autonomous Star Identification Algorithms. In: 1st International Symposium on Systems and Control in Aerospace and Astronautics, Harbin, China, pp. 896–901. IEEE, Los Alamitos (2006)
5. Samaan, M.A., Mortari, D., Junkins, J.L.: Recursive Mode Star Identification Algorithms. *IEEE T. Aero. Elec. Sys.* 41, 1246–1254 (2005)
6. VanderLugt: Signal Detection by Complex Spatial Filtering. *IEEE Trans. Inf. Theory IT-10*, 139–145 (1964)
7. Weaver, C.S., Goodman, J.W.: A Technique for Optically Convolution Two Functions. *Appl. Opt.* 5, 1248–1249 (1966)
8. Janschek, K., Tchernykh, V., Dyblenko, S.: Performance Analysis of Opto-Mechatronic Image Stabilization for a Compact Space Camera. *Control Eng. Pract.* 15, 333–347 (2007)
9. Alam, M.S., Bal, A.: Improved Multiple Target Tracking via Global Motion Compensation and Optoelectronic Correlation. *IEEE T. Ind. Electron* 54, 522–529 (2007)
10. Tchernykh, V., Beck, M., Janschek, K.: An Embedded Optical Flow Processor for Visual Navigation using Optical Correlator Technology. In: 2006 IEEE/RSJ IROS 2006, Beijing, China, pp. 67–72. IEEE, Los Alamitos (2006)
11. Bergeron, A., Bourqui, P., Harnisch, B.: Lightweight Compact Optical Correlator for Spacecraft Docking. In: *Electro-Optical Remote Sensing, Detection, and Photonic Technologies and Their Applications*, vol. 6739, p. 67390. SPIE, Florence (2007)



12. Chao, T.H., Lu, T.: System Issues of Developing Grayscale Optical Correlator for ATR Applications. In: Proceedings of SPIE, vol. 6574, p. 657405 (2007)
13. Chao, T.H., Lu, T., Zhou, H.: Recent Progress on Grayscale Optical Correlator for Automatic Target Recognition. In: Proceedings of SPIE, vol. 6245, p. 624503 (2006)
14. Padgett, C., Kreutz-Delgado, K.: A Grid Algorithm for Autonomous Star Identification. IEEE T. Aero. Elec. Sys. 33, 202–212 (1997)
15. Silani, E., Lovera, M.: Star Identification Algorithms: Novel Approach and Comparison Study. IEEE T. Aero. Elec. Sys. 42, 1275–1288 (2006)
16. Akkiraju, N.: Approximating Spheres and Sphere Patches. Comput. Aided Geom. D. 15, 739–756 (1998)

# Author Index

- Agranat, Aharon J. 144  
Berrettini, Gianluca 5  
Bogoni, Antonella 5  
Caulfield, H. John 1, 30  
Dolev, Shlomi 47, 130  
Dong, Jianji 19  
Fainman, Yeshaiahu 2  
Ferraro, Pietro 86  
Fey, Dietmar 110  
Geerts, Wilhelmus J. 130  
Goliaei, Sama 77  
Haist, Tobias 99  
Hasan, Md. Raqibul 70  
Hou, Xiaoguang 102  
Hu, Wenhua 102  
Huang, Dexiu 19  
Hui, Jia 145  
Ikeda, Kazuhiro 2  
Jahns, Jürgen 110  
Jalili, Saeed 77  
Jiankun, Yang 145  
Juncai, Yang 145  
Katsuta, Nobuto 124  
Knuppertz, Hans 110  
Li, Xiujian 102  
Matoba, Osamu 95, 124  
Meloni, Gianluca 5  
Muntean, Oana 56  
Nie, Yongming 102  
Nir, Yuval 47  
Nitta, Kouichi 95, 124  
Oltean, Mihai 56  
Osten, Wolfgang 99  
Paturzo, Melania 86  
Potì, Luca 5  
Qingchun, Fan 145  
Rahman, M. Sohel 70  
Rudolph, Larry 144  
Sapiens, Noam 144  
Schneider, Max 110  
Shaked, Natan T. 130  
Shamir, Joseph 37  
Tamir, Dan E. 130  
Tan, D.T.H. 2  
Wang, Jing 5  
Wenhua, Hu 145  
Xiujian, Li 145  
Xu, Jing 19  
Yang, Jiankun 102  
Yang, Junbo 102  
Yuncai, Hao 145  
Zalevsky, Zeev 86  
Zhang, Xinliang 19  
Zlotnik, Alexander 86